Mem. Fac. Educ. Ehime Univ.,Nat. Sci., Vol. 12, No. 1 1~118 (1991)

Petrogenesis of the Red Hills Peridotite in the Dun Mountain Ophiolite Belt

Sakae SANO

Science Education Laboratory, Faculty of Education,
Ehime University, Matsuyama, Ehime, 790 Japan.

(Received April 25, 1991)

ABSTRACT

Based on major and trace element chemistry and Sr isotope ratios of rocks and minerals, together with detailed geological and petrological data, constitution of the Red Hills peridotite in the Dun Mountain ophiolite belt, New Zealand, genetical relationships among various facies of the rock and generation and evolution of the magma have been discussed.

The Red Hills peridotite body consists of vertically separated two distinct zones. The large part of the lower zone is composed of homogeneous harzburgite. Small masses of dunite are distributed in the upper part of the lower zone and grade into harzburgite. Often, in this part, plagioclase is included in harzburgite. The porphyroclastic texture, modal composition, chemistry of minerals and rocks indicate that the harzburgite in this zone is the residual mantle peridotite which extracted the melt phase. Clinopyroxene in the harzburgite is distinctly depleted in light REE and the model calculation suggests that the harzburgite would be the residual of 12~20% fractional melting of light REE-depleted, MORB-type source mantle. The invariable Fo=91 of olivine in the harzburgite suggests that the initial melt should be a picritic magma containing 12.5~15wt% MgO.

The upper part of the Red Hills peridotite body, 3km in thickness, is composed mainly of medium- to coarse-grained, equigranular dunite, in which often clinopyroxene and plagioclase are irregularly distributed. Medium- to coarse-grained, protogranular harzburgite occurs as small blocks and flakes in dunite matrix and is infiltrated by dunite 'dike'. The occurrence of spinel anf chemistry of constituent minerals revealed that a part of the upper zone is occupied by the cumulate of olivine from the melt phase. Reaction between harzburgite of the upper zone and the melt, however, is indicated by infiltration of dunite and recrystallization of constituent minerals. The melt incorporated in the reaction should be the magma evolved by crystallization and extraction of olivine, because the harzburgite has lower Al_2O_3 and CaO contents than the 'residual' harzburgite of the lower zone has and because chemically different two groups of olivine occur in the dunite: cumulative olivine without zoning in Ca and recrystallized olivine with Ca-zoning. Thus, the dunite-predominant upper zone represents the 'mantle-crust transition zone', consisted of complex of cumulative and recrystallized olivines (=dunite) and residual blocks of harzburgite.

The Cr# of spinel (<0.6) and $^{87}Sr/^{86}Sr$ ratios of minerals (0.7019～0.7027) are well in the range of variation in mid-ocean ridge basalts and distinctly different from those in basalts occurring in other geological settings such as marginal basins, island arcs and forearc basins. Magma genesis beneath a mid-ocean ridge may be inferred from this study: the initial picritic magma evolved to quartz tholeiitic one by olivine dominant differentiation and reaction with residual harzburgite, forming the 'mantle-crust transition zone' predominantly composed of dunite.

CONTENTS

1. INTRODUCTION

Ophiolite regarded as fragment of oceanic crust and uppermost mantle has thick dunite at the boundary zone of the mantle and crust. This dunite is referred to as the *mantle-crust transition zone* or more briefly, the *transition zone.* Ophiolitic peridotite includes residual uppermost mantle and the magmatic products. Therefore, ophiolitic peridotite is an important clue to investigate the partial melting phenomena on oceanic uppermost mantle. The dunite in the transition zone has essentially been attributed either to crystal accumulation (e.g., Greenbaum, 1972; Elthon et al., 1982) or to residual (e.g., Dick, 1977; Nicolas & Prinzhofer, 1983). Although the direct observation of the transition zone at the recent oceanic ridge, is impossible, the study of ophiolite representing ancient oceanic crust and the uppermost mantle is useful for understanding of the phenomena at the mantle-crust transition zone. Furthermore, study of the transition zone will be able to make clear the behaviors of magma at mantle-crust boundary, and is applicable to the petrogenesis of the primary melt of mid-ocean ridge basalts (MORBs).

In this study the Red Hills peridotite body in the Dun Mountain ophiolite, New Zealand, regarded as ancient oceanic crust and uppermost mantle is dealt as a model field, with detailed field study, petrology with mineral chemistry and Sr isotope geochemistry. The Red Hills peridotite body in the Dun Mountain ophiolite belt includes the large discordant dunite. Based on results of Sr isotopic compositions and some trace element concentrations Davis et al. (1980) has reported that basalts from the Lee River Group regarded as a member of the Dun Mountain ophiolite showed affinities to the MORBs. The present study also support the possibility that the Red Hills peridotite represents the tectonic setting of a mid-ocean ridge system.

Main purposes of this study are as follows :

1) Estimation of original tectonic environment of the Red Hills peridotite.
2) Implication of magmatic processes of the Red Hills peridotite.
3) Application of the magmatic processes as the Red Hills peridotite to a mid-ocean ridge system.

Chapter 2 outlines the geologic relationships between the Red Hills peridotite body and surrounding country rocks, and also deals with the constituent members of the Dun Mountain ophiolite, based on results of previous works.

Chapter 3 deals with the field occurrences of each rock type of the peridotite body and also refers to distribution of the constituent rocks based on field survey. The details of the field research are reported herein.

Chapter 4 describes microscopic textures of the each rock type and chemical compositions of minerals.

Chapter 5 deals with characters of major and trace element abundances and isotopic

compositions of the Red Hills peridotite and the related basalts and diabases in the Lee River Group.

Chapter 6 presents discussions as follows based on geological, mineralogical and geochemical descriptions from chapter 2 to 5: At first, original tectonic environment of the Red Hills peridotite will be discussed from mineralogical and geochemical approaches. Secondary, suitable origin of harzburgite in lower zone of the peridotite is argued from mineral compositions and concentrations of rare earth elements (REEs) of clinopyroxenes and an adequate melting model is also considered. Thirdly, implications on origin of discordant dunite in the transition zone in the peridotite will be argued. Fourthly, from discussions of section 6−1 to 6−3, a petrogenetic model will be proposed for the Red Hills peridotite. Finally, in section 6−5, the suitable petrogenetic model of the Red Hills peridotite will be applied for a magma genesis at a mid-ocean ridge system.

2. GENERAL GEOLOGY AROUND THE RED HILLS PERIDOTITE

The Dun Mountain Ophiolite Belt (Blake & Landis, 1973; Coombs et al., 1973) in the South Island, New Zealand (**Fig. 1**) lies on the western side of the Alpine Fault at the Nelson area (e.g. Coombs et al., 1976; Johnston, 1983). On the contrary to most of other terrestrial ultramafic rocks occur as knockers or blocks in melange, the Red Hills, Dun Mountain and Red Mountain peridotite bodies are outcropped as relatively large masses and are

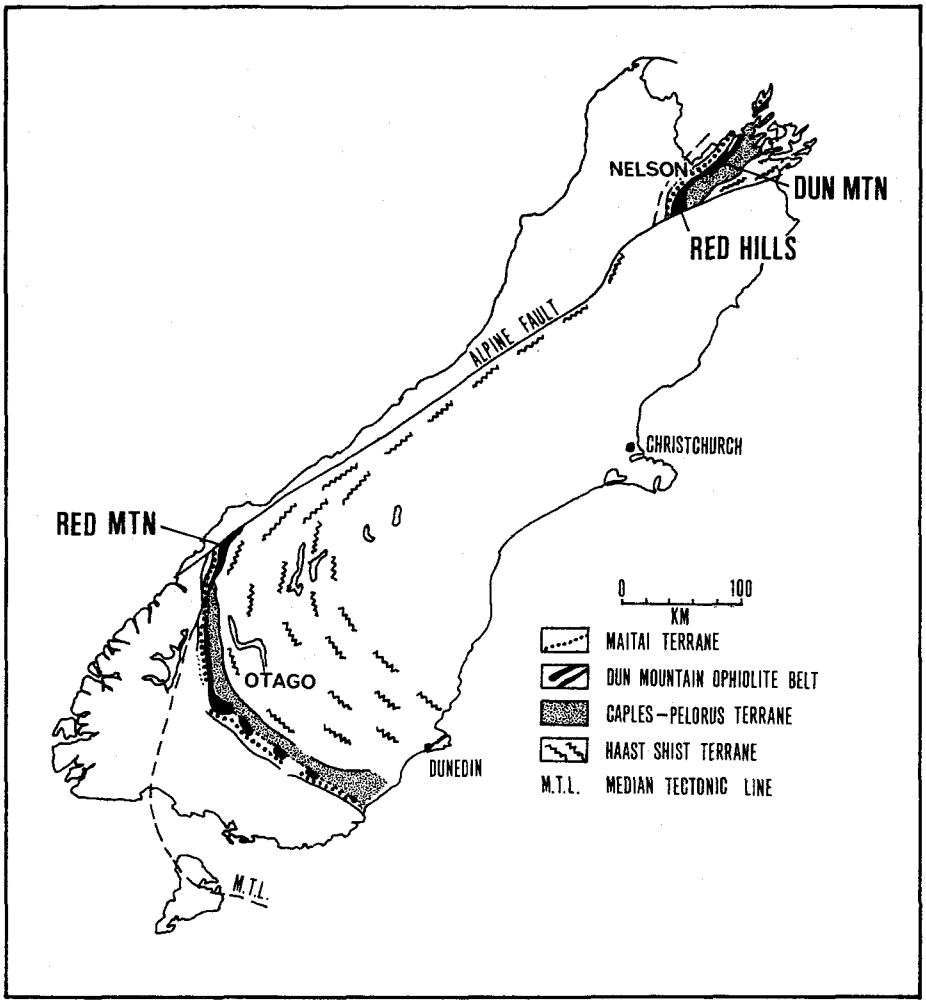

Fig. 1. South Island, New Zealand, showing the location of the Dun Mountain ophiolite belt and other main geologic provinces (simplified from Coombs et al., 1976). Red Hills is in south Nelson, near the southern limit of the portion of the ophiolite belt north of the Alpine Fault.

avoided from mechanical deformations during subduction or accretion events. The Red Hills peridotite body outcrops over an area of about 150km^2 in the northern part of the South Island, and has the length of about 15km and the width of 8km. The Red Hills peridotite body at the western border is fault contact with basalts and gabbros of the Lee River Group (Waterhouse, 1964) which are considered as the extrusive and intrusive members of the Dun Mountain Ophiolite. The Lee River Group is subdivided into the Tinline Formation of gabbros and the Glennie Formation of diabases and basalts. The Glennie Formation in the group is uncomformably overlain by sediments of upper Permian Maitai Group. The eastern border of the body is fault contact with metamorphosed sandstones and mudstones of the Pelorus Group (Bell, 1909; Johnston, 1981) that is Permian to lower Mesozoic in age. Walcott (1969) and Johnston (1983) has proposed the geologic maps of this area. Walcott (1969) classified fhis peridotite body into three parts, upper part of the upper zone, lower part of the upper zone and the basal zone. Upper part of the upper zone is predominated by dunite, and lower part of this zone is composed of harzburgite and dunite. The basal zone is composed of harzburgite (characterized by "protoclastic texture"). Furthermore, he pointed out that the dunite in upper part of the upper zone often accompanies pyroxenite vein and plagioclase peridotite layers. Period of igneous activity of the Dun Mountain ophiolite is about 260Ma, that age is determined by zircon U–Pb method for plagiogranites and clastic rocks in the Red Hills area and the associates (Kimbrough et al., in prep.).

3. GEOLOGY OF THE RED HILLS PERIDOTITE

3−1. Field Observations

Outline of geology of the Red Hills peridotite body is shown in **Figure 2**. The body is roughly divided into two parts, dunite and harzburgite zones. Dunite is mainly exposed in the western area, and harzburgite is exposed in the eastern area of the body. The investigation has been focused to the geological relationships between harzburgite and dunite, and on occurrences of clinopyroxene grains (wehrlitic to olivine clinopyroxenitic composition) scattered in dunite of the western part. Typical columnar sections are displayed in **Figures 4**, **5** and **6**. Occurrences of harzburgite blocks in dunite matrix are restricted within limited levels from 0−1080m of the upper part of the body (**Figs. 7** and **8**).

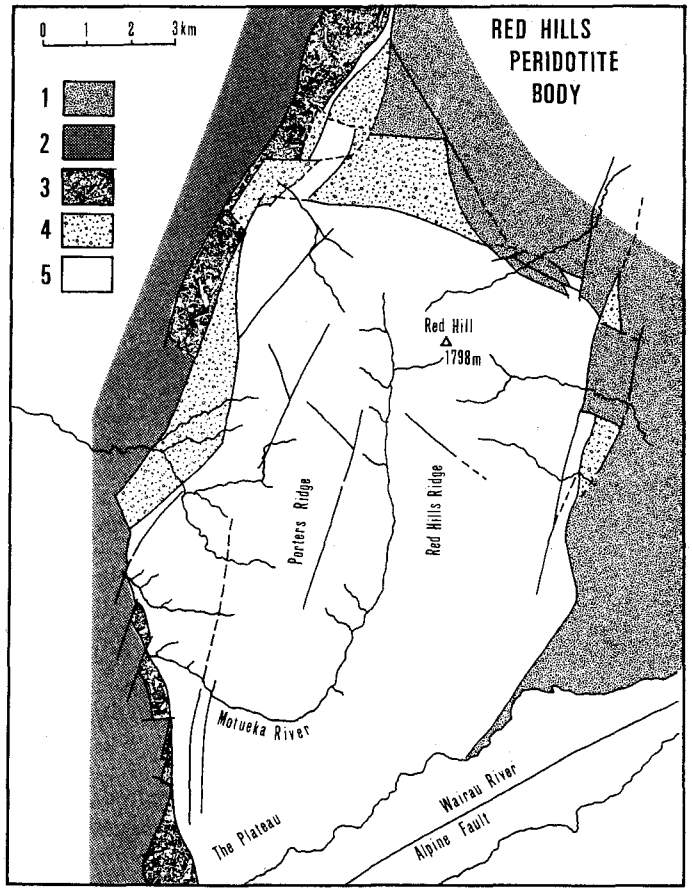

Fig.2. Geologic map of the Red Hills area (modified from Walcott, 1969, and Johnston, 1983). **1** Pelorus Group (Permian to lower Mesozoic), **2** Maitai Group (upper Permian), **3** Lee River Group (upper Permian), and **4** and **5** Dun Mountain Ultramafics (**4** Melanges and **5** Peridotites).

Because the modes and occurrences of clinopyroxene grains on outcrops in the Red Hills peridotite are extremely various and clinopyroxene bearing rocks is not massive to call *wehrlite*, author defines the dominant facies of the upper zone as the *clinopyroxene bearing dunite*. Correlation berween rock nomenclature defined in this study and those used normally (IUGS Subcommission on the Systematics of Igneous Rocks, 1973) is shown in **Figure 9**. The term of *clinopyroxene bearing dunite* instead of *wehrlite* will use from now. In this manner the term of *plagioclase bearing dunite* for *troctolitic rocks* will also use.

The Red Hills peridotite is composed of dunite unit in the upper zone and Harzburgite unit in the lower zone (**Fig. 7**). The rocks of the Red Hills peridotite body are common harzburgite, plagioclase bearing harzburgite, olivine clinopyroxenite, plagioclase bearing dunite, clinopyroxene bearing dunite, common dunite and gabbro (**Table 1**). In addition to these rocks, there are some dikes of plagiogranites and diabases. "Layering" is one of the characteristic features of the whole body, which is clearly shown by the coincidence of directions of strike of dykes of gabbro, and "layering" of olivine-clinopyroxenite and arrangement of clinopyroxene grains. Directions of dikes of plagiogranites and diabases also accord with the general trend of the "layering" of the body.

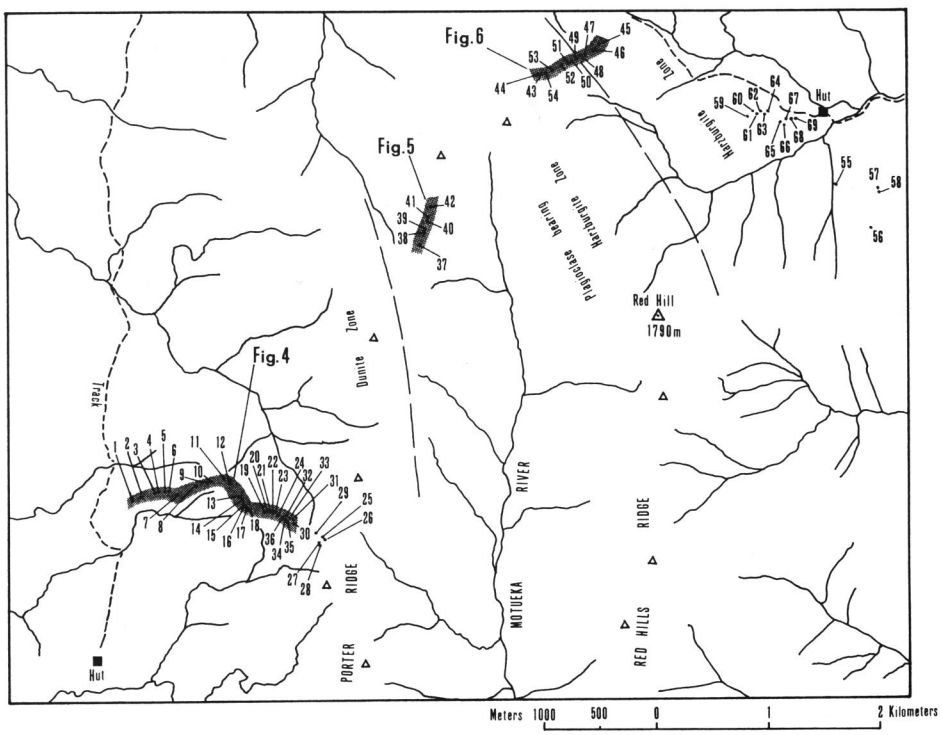

Fig.3. Sampling localities and locations of columnar sections of **Figs.4~6.** Numbers represent RH sample name (**RH**–symbols are omitted). This peridotite is mainly divided into two parts, dunite predominated zone and harzburgite zone from west to east. Furthermore, the harzburgite is subdivided into plagioclase bearing and free harzburgites.

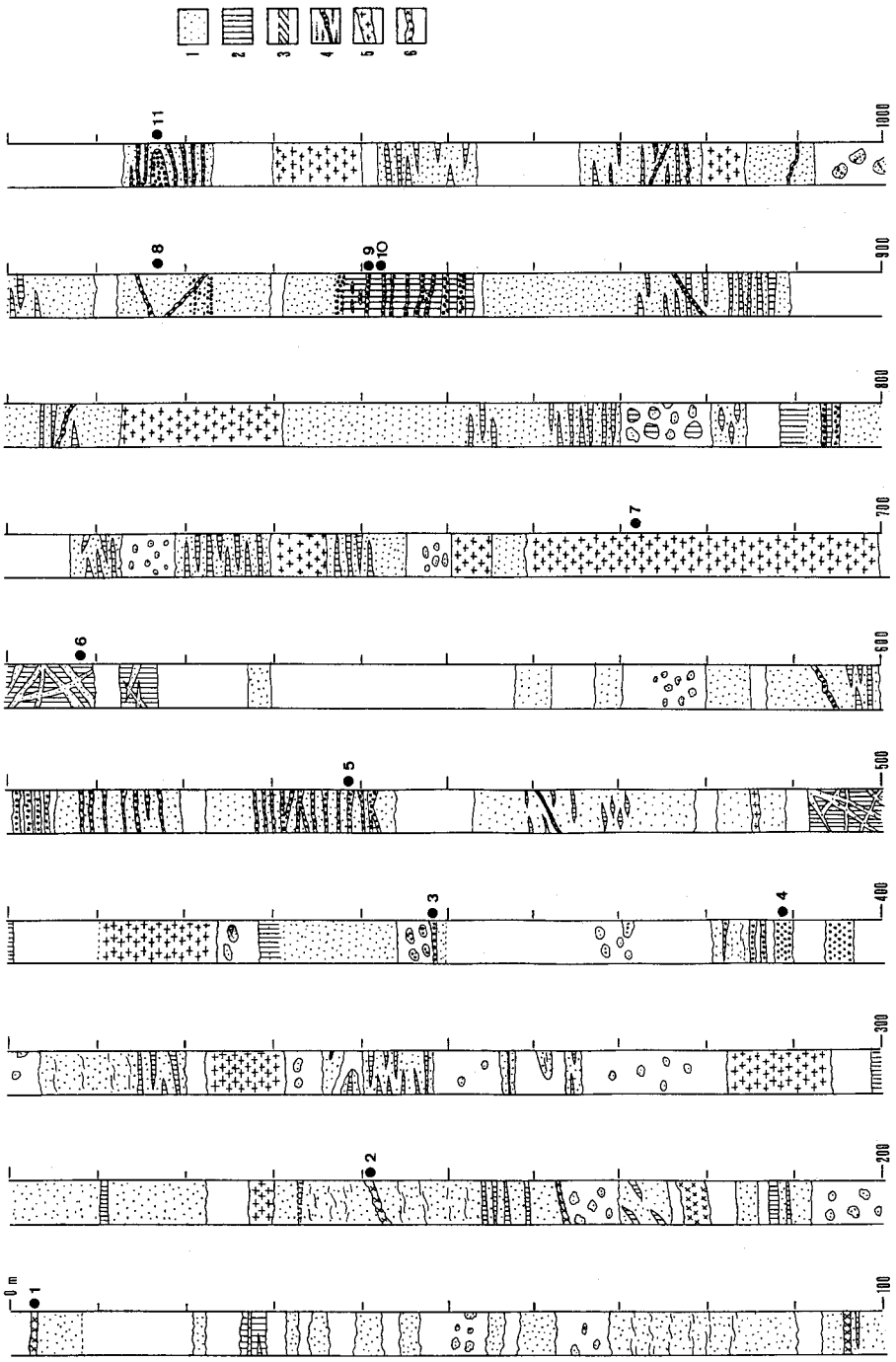

Fig.4. Columnar section of a part of the upper zone. The locality is displayed on **Fig.3.** Numbers with solid circle show RH-sample numbers. **1** common dunite, **2** harzburgite, **3** plagioclase bearing dunite, **4** clinopyroxene rich parts, **5** diabase dike, and **6** plagiogranite dike.

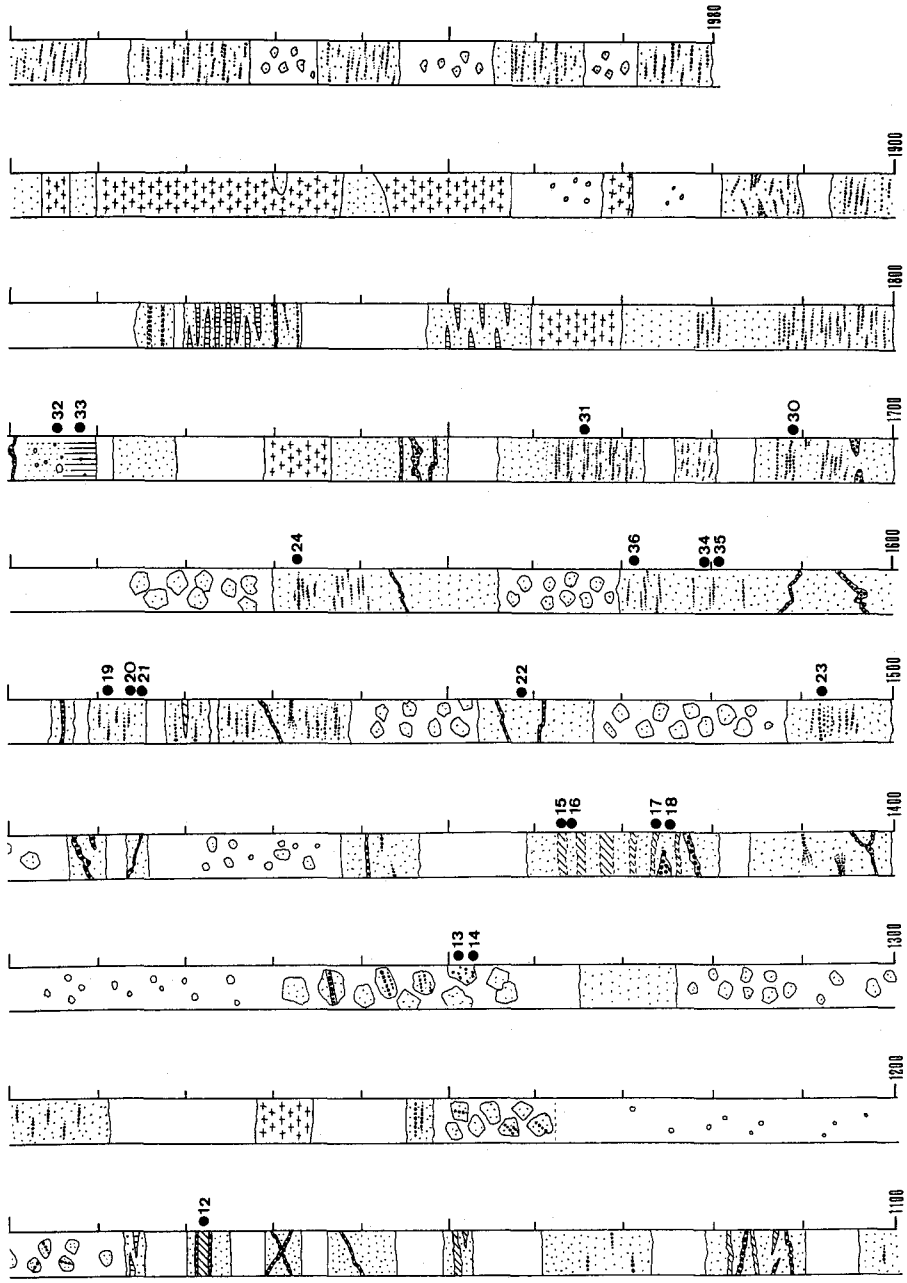

Fig.4. (continued)

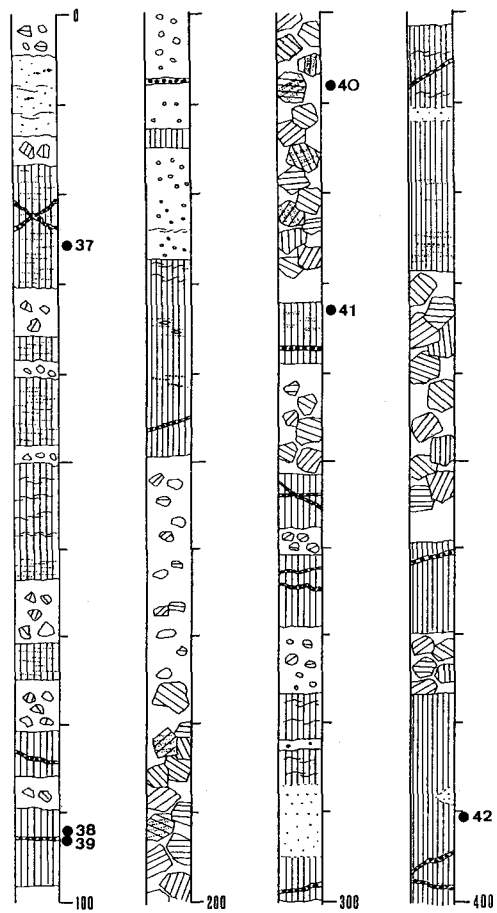

Fig.5. Columnar section of a part of the upper part of the harzburgite zone. The locality is shown in **Fig.3.** Symbols are the same as in **Fig.4** excepting plagioclase bearing harzburgite that is represented by thin dots.

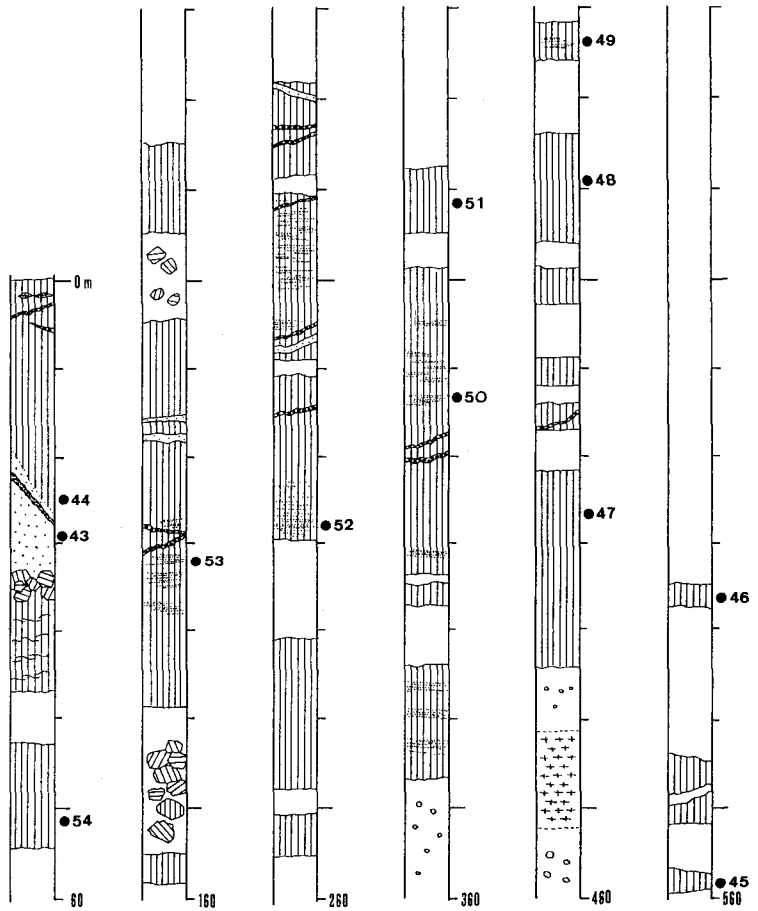

Fig.6. Columnar section of a part of the lower part of the harzburgite zone. The locality is also shown in **Fig.3.** Symbols are the same as in **Fig.5**.

Typical Columnar Section of the Red Hills Peridotite

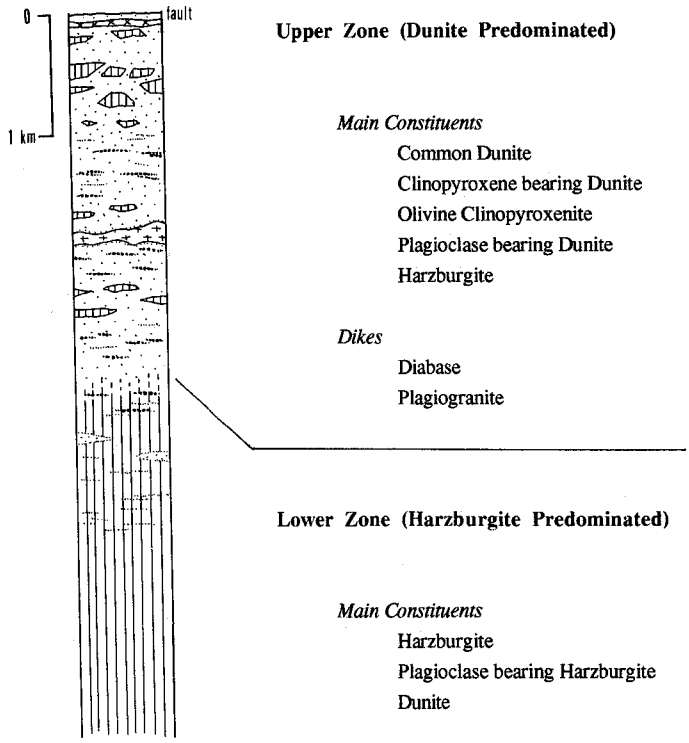

Fig.7. Typical columnar section of the Red Hills peridotite. Symbols are the same as in **Fig.4** excepting plagioclase domains that represented by thin dots.

Table 1. Reference table for rock types and sample numbers

Rock name	Code	Sample number (RH−)
Upper zone (Transiton zone)		
Olivine clinopyroxenite	CPX	4,9,10p,11,23,29,31
Clinopyroxene bearing dunite	CPD	13,14,16,18,19,25,34,35
Plagioclase bearing dunite	PLD	12,15,17,24,28,36
Dunite	UZD	10d,20,21,22,32,26
Harzburgite	UZH	6,8,27,30,33
Gabbro	GAB	3
Lower zone (Harzburgite zone)		
Harzburgite	LZH	38,41,42,44−48,51,55−58,60−68
Plagioclase bearing harzburgite	PLH	37,40,49,50,52,53,54
Dunite	LZD	43,59,69

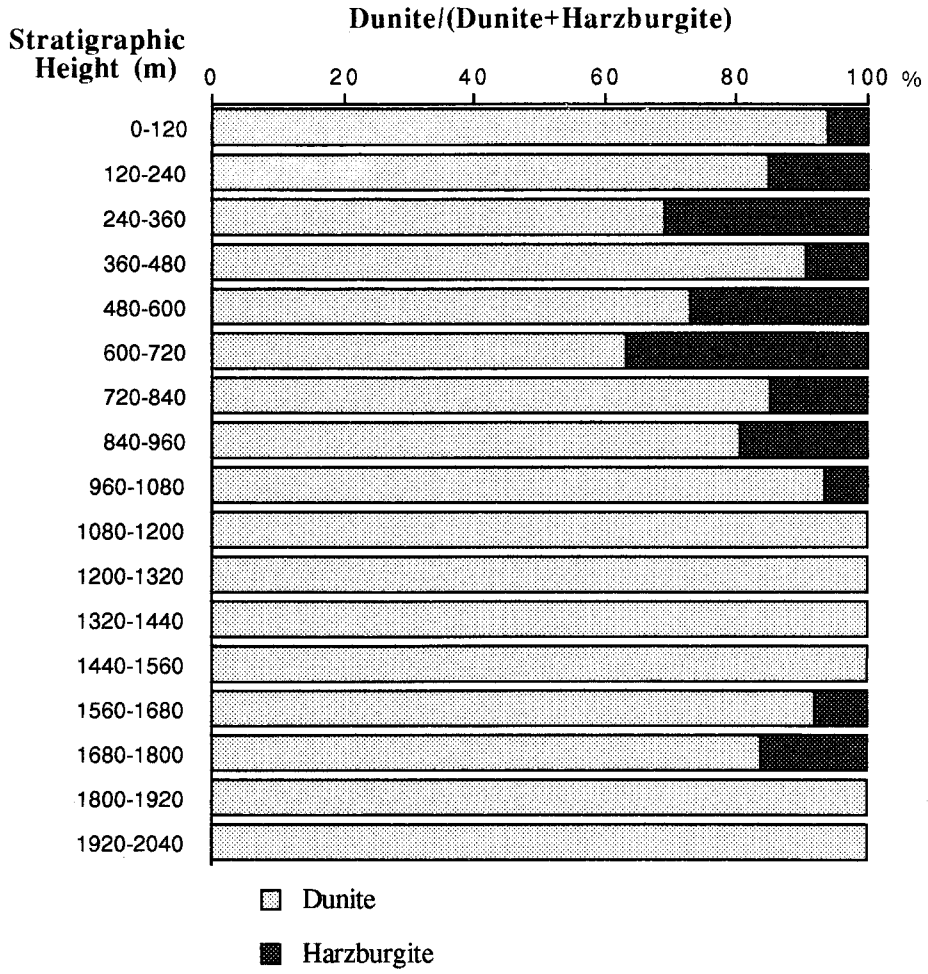

Fig.8. Modal ratios between dunite and harzburgite at the upper zone. The statigraphic levels correspond to that of columnar section (**Fig.4**). Note that the blocky harzburgites concentrate in the upper level of the zone.

3−1−1. Upper Zone of the Body

Comment

Rocks in the upper zone are constituted of olivine clinopyroxenite, clinopyroxene bearing dunite, plagioclase bearing dunite, harzburgite and gabbro in dunite matrix. Derivation of either olivine clinopyroxenite and clinopyroxene bearing dunite or common dunite depends on the degree of concentration of clinopyroxene in dunite matrix, and boundaries among them are gradational (**Fig. 10**).

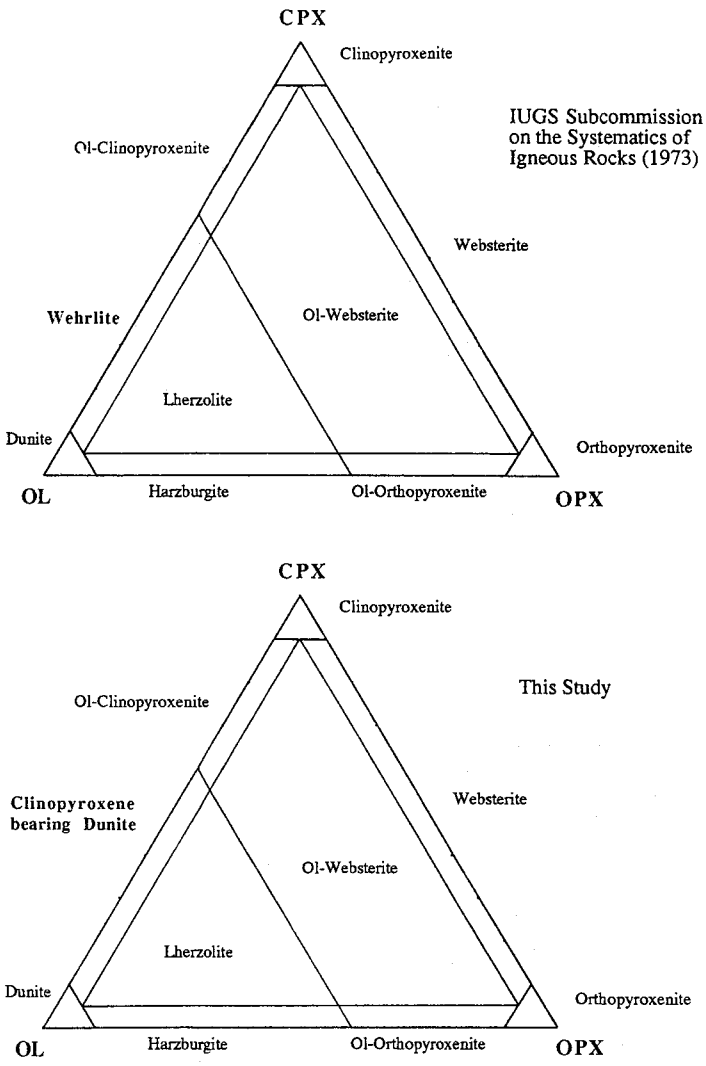

Fig.9. Rock nomenclature of peridotite. In this study, *clinopyroxene bearing dunite* is adopted instead of *wehrlite*.

Thin dike of dunite infiltrates into harzburgite in the harzburgite-predominated part of this zone. At dunite predominated part, harzburgite occurs as lenticular blocks. In part almost composed of common dunite, harzburgite occurs as small flakes which are formed by parallel arrangement of orthopyroxene-grains of a few centimeter in length in olivine matrix (**Fig. 11**). Chromian clinopyroxenes are dispersed only in dunite matrix, and not included in harzburgite. Plagioclase is also accidentally scattered in the dunite. There is no significant relationship of the occurrences between plagioclase and clinopyroxene. Dunite of the upper zone can be divided into three types as follows: 1) Almost pure dunite composed

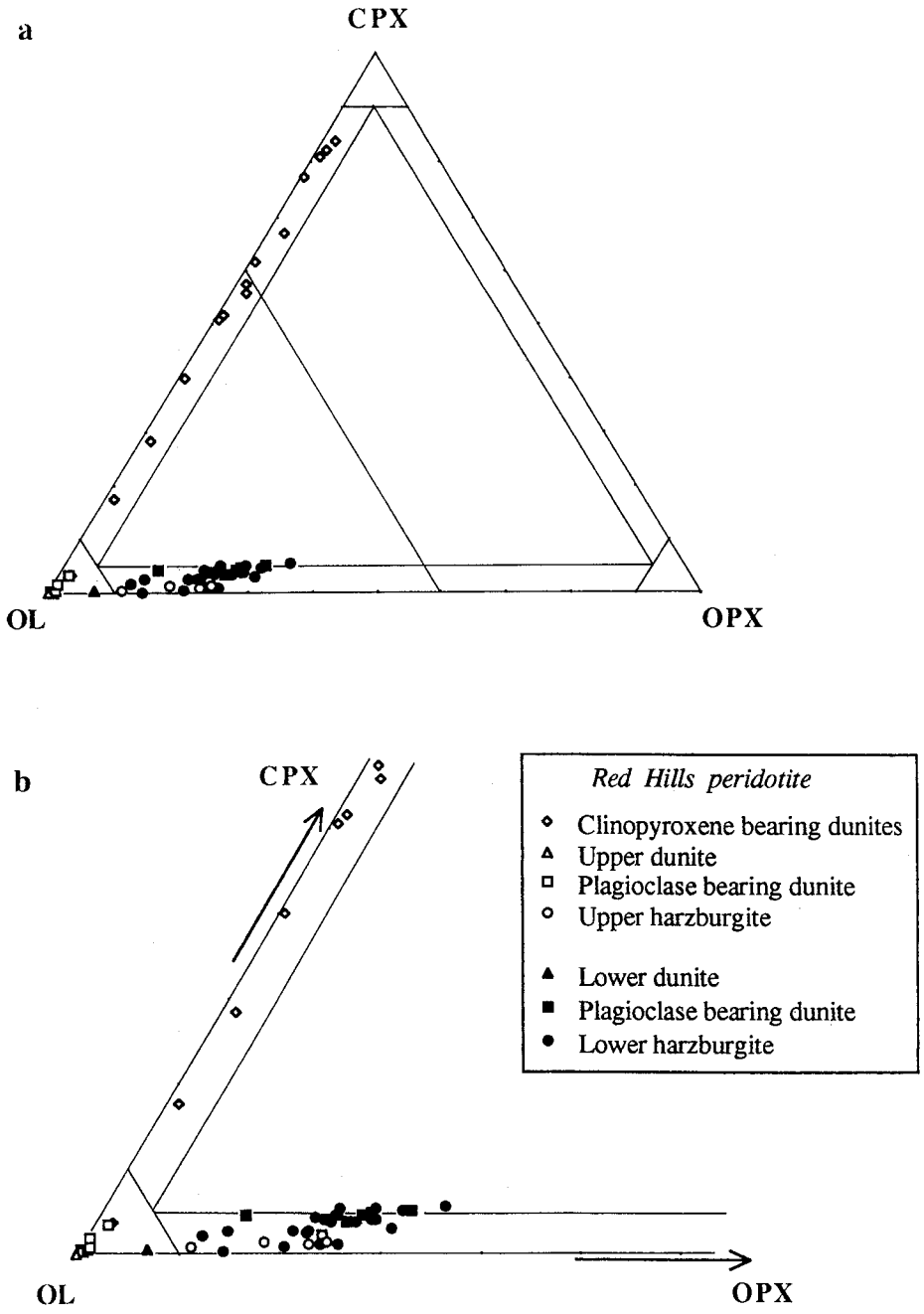

Fig. 10. Modal compositions of peridotites in the Red Hills. Samples from the upper zone (*open* symbols) make a trend of dunite to olivine-clinopyroxenite excepting blocky harzburgite. *Solid* symbols represent the samples of the lower zone. Harzburgites crowd on small compositional range.

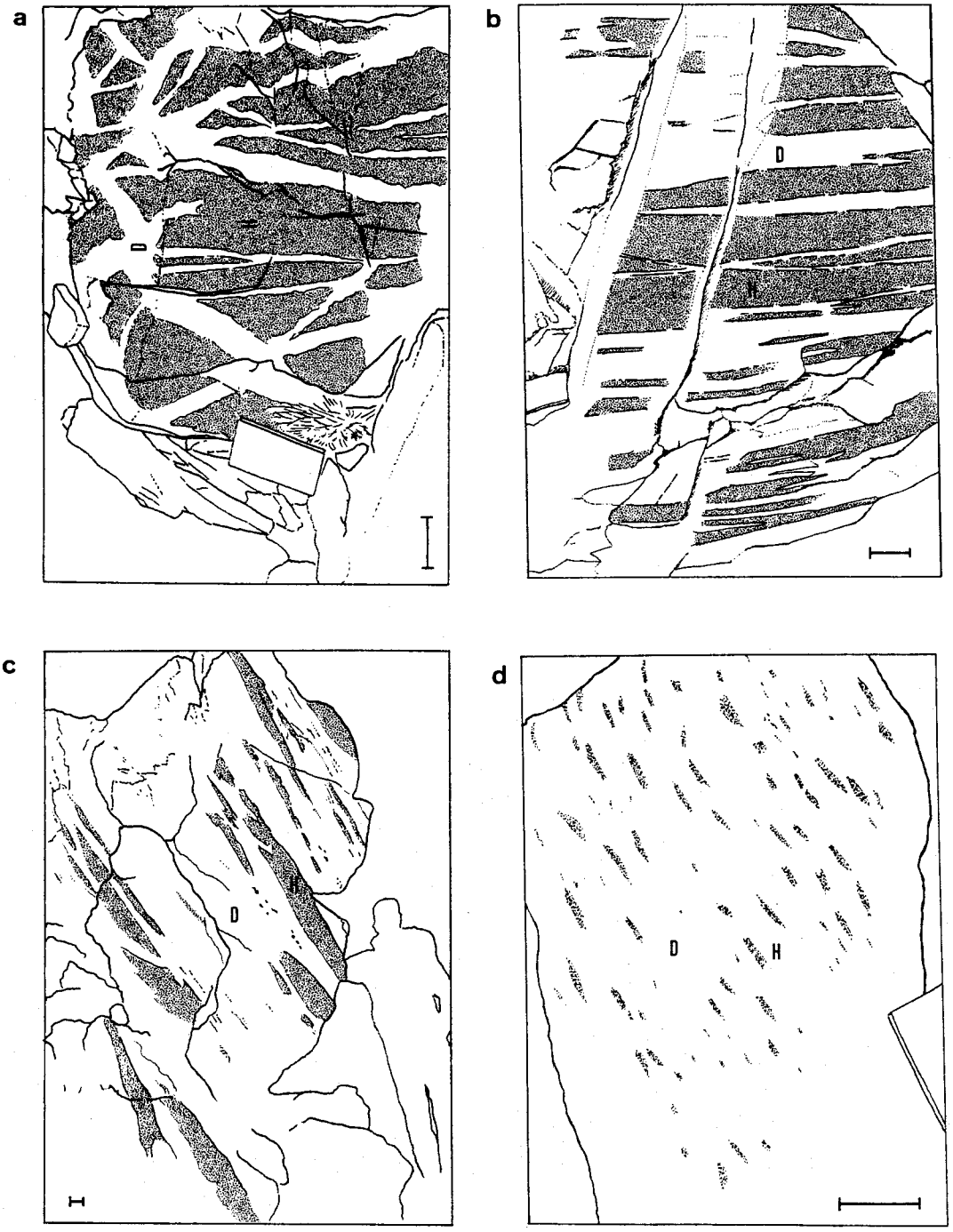

Fig.11. Representative field relationships between dunite (**D**) and harzburgite (**H**) in the upper zone. Scale bars are 10cm in each case.

a: Dunite infiltrates into harzburgite.

b: Parallel occurrence of dunite and harzburgite, this is so called "layering".

c: Harzburgite occurs as lenses or blocks in dunite matrix.

d: Flaky occurrenced of harzburgite in dunite matrix.

of olivine+spinel. 2) Clinopyroxene bearing dunite composed of olivine+spinel+clinopyroxene (various proportion). 3) Plagioclase bearing dunite composed of olivine+spinel+plagioclase (various proportion) ± clinopyroxene.

Olivine clinopyroxenite

Olivine clinopyroxenite shows blocky (?) occurrences (**Fig. 12 a, c** and **h**). Clinopyroxene grains make patches and forms "layers" (or dikes) in dunite matrix. Olivine clinopyroxenite blocks show rounded shape (**Fig. 12 a, c** and **h**). The sizes of blocks are about 2m in diameter. Frequency of the occurrence is quite rare. Though maximum thickness of the "layer" is 1~2m, they are commonly a few cm order. The "layered" olivine clinopyroxenite often shows occurrence that the clinopyroxene grains delaminate into dunite matrix. Namely, modal abundance of the clinopyroxene in the dunite is remarkably not uniform.

Clinopyroxene bearing Dunite

Clinopyroxene grains in clinopyroxene bearing dunite scatter in olivine matrix. The clinopyroxene occurs as lamination (or schlieren) and diffused crystals in olivine matrix (**Fig. 12 b, d, g, h, i** and **j**). The contacts between common dunite and clinopyroxene bearing dunite are sharp (**Fig. 12 d** and **g**) or gradual (**Fig. 12 b, i** and **j**). The lamination of the clinopyroxene grains also find in the uppermost harzburgite of the lower zone of the body.

Dunite

Dunite is main rock type in the upper zone of the Red Hills peridotite body, and forms a matrix of other rocks. Dunite is composed of medium~fine grained equigranular olivine and spinel, and rarely includes fine grained interstitial clinopyroxene. Orthopyroxene is not found. The dunite is partly including some pods and seams of spinel or pegmatitic clinopyroxene crystals.

Plagioclase bearing Dunite

Plagioclase bearing dunite shows the schlieren or lamination of plagioclase like case of clinopyroxene bearing dunite. Modal abundance of plagioclase shows wide variation ranging from 4% to 24%. That is generally heterogeneous. Mode of clinopyroxene is low (up to 3%). Relations of boundary with common dunite is gradual in many case, but rarely show sharp contact.

Harzburgite

Harzburgite shows rough surface by pyroxene crystals in field, while dunite is characterized by smooth surface. Harzburgites in the upper zone mainly occur as blocks in dunite matrix. The shapes of blocky harzburgite are often angular and lenticular cut by dunite (**Fig. 12 e, f, i** and **j**). In general, the boundary of blocky harzburgite and dunite is

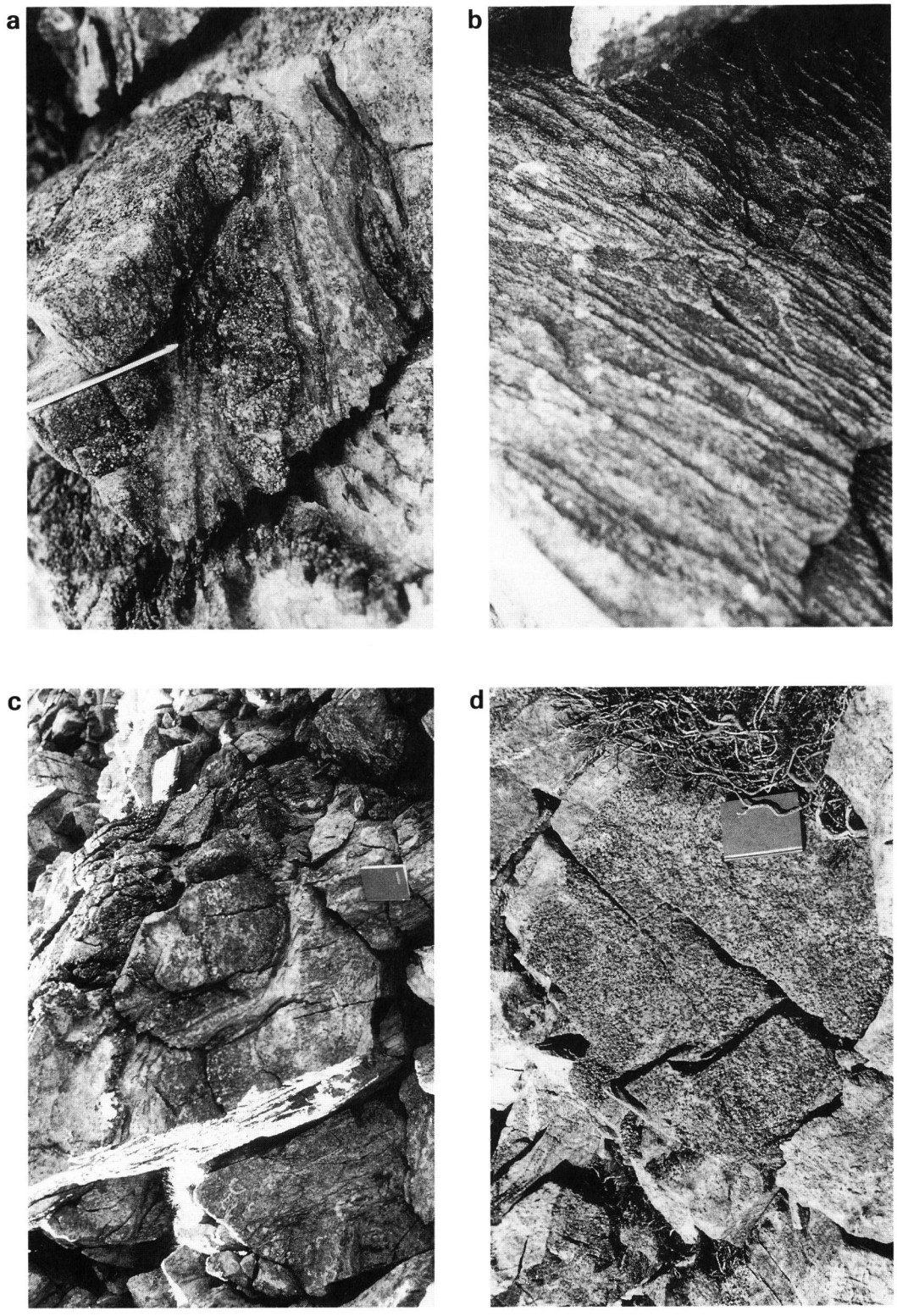
a
b
c
d

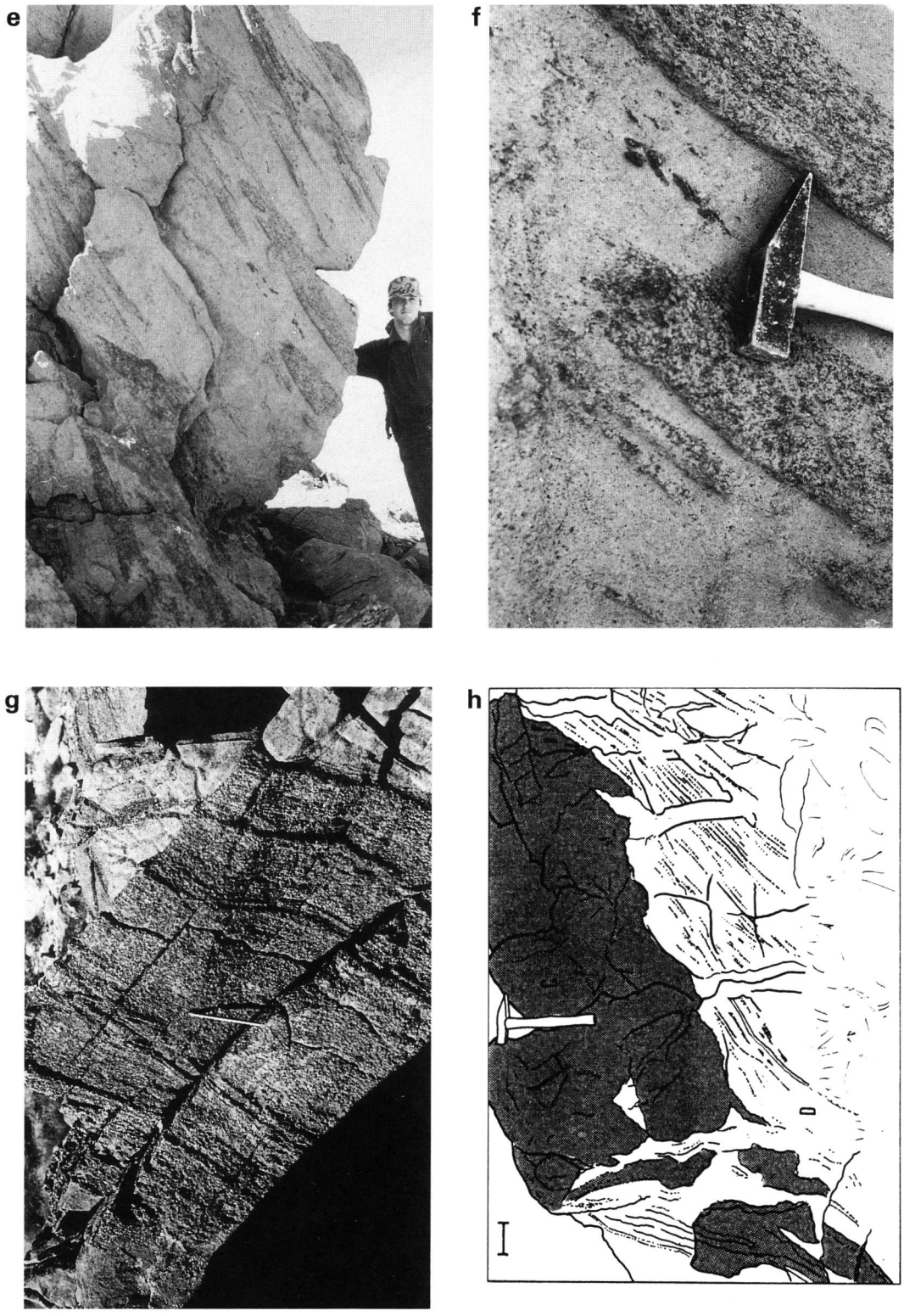
e
f
g
h

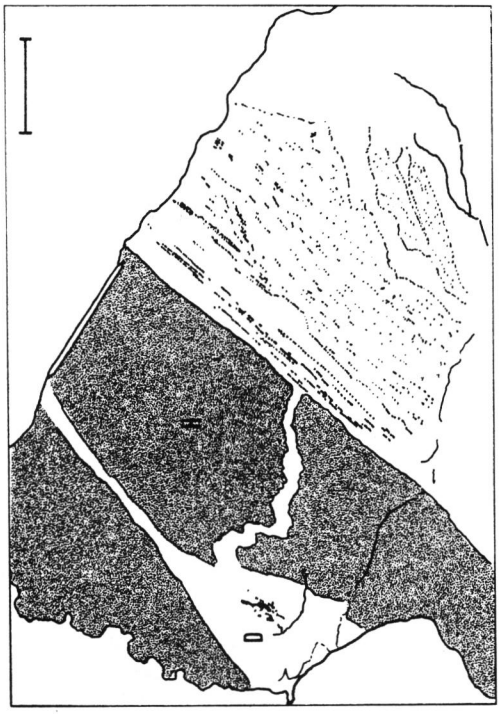

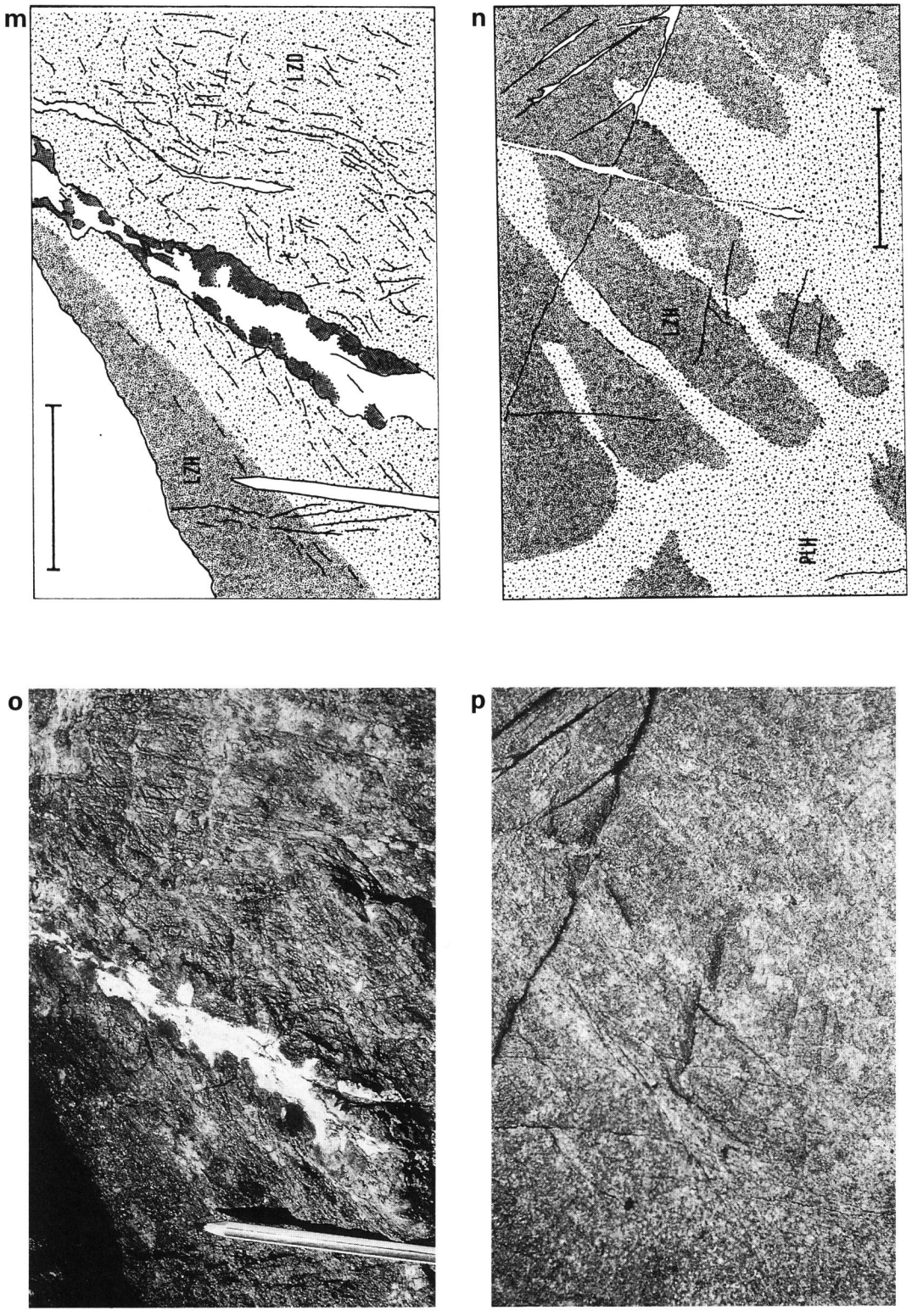
m
LZD
LZH
n
LZH
PLH
o
p

Fig. 12. (p. 20~23) Field occurrences of rocks in the Red Hills peridotite. Scale bars in sketches are 10cm in each case.

a~**j**: Occurrences in the upper zone. **a**~**d**, **g** and **h** show relations between clinopyroxene bearing dunite (or olivine-clinopyroxenite) and dunite, **e**, **f**, **i and j**: relations between harzburgite and dunite.

a and **c**: Olivine-clinopyroxenite (RH-29) and the surrounding dunite.
b: Lamination or schrielen of clinopyroxene grains (RH-13) in dunite matrix. Clinopyroxene grains are represented by salient parts.
d: Clinopyroxene bearing dunite (RH-25) contacts with dunite (RH-26) by sharp boundaries.
g: Clinopyroxene *layering* in dunite matrix. The *layering* is by complex modal distribution of clinopyroxene.
h: Blocky (?) olivine-clinopyroxenite (**C**; RH-11) in dunite with lamination of clinopyroxene (**D**).
e: Harzburgite lenses in dunite matrix (same as in **Fig. 11c**).
f: Part of **e**. Note that position and arrangement of the spinel aggregates (black) in dunite.
i and **j**: Dunite (**D**) infiltrates into harzburgite (**H**; RH-27). Clinopyroxene bearing dunite (**C**) randomly distributes in dunite.

k~**p**: Occurrences in the lower zone.

k and **l**: Typical occurrences of plagioclasses in harzburgite. Plagioclases occurs as band, and cut the harzbugite foliations.
m and **o**: Dunite (**LZD**; RH-43) gradually changes to harzburgite (**LZH**; RH-44). Pegmatitic composite dikes (opx + pl) occur in the dunite.
n and **p**: A relation between harzburgite (**LZH**) and plagioclase bearing harzburgite (**PLH**). PLH probably intrudes into LZH. The boundaries are not clear.

sharp, but harzburgite is rarely grading into dunite. Though many blocky harzburgites expose in the upper zone of the Red Hills peridotite body, they are mostly suffered the serpentinization. The harzburgite blocks are mostly found in upper part of the upper zone.

Gabbro

Gabbro is locally distributed in the upper part of the upper zone. The occurrence looks like "layering" in dunite matrix. However, the gabbro is contact with dunite at sharp boundary, and probably intrudes into dunite. The direction of the dike of the gabbro is parallel to general foliation of the body. Significant chilled margin of the dike is not found.

3-1-2. Lower Zone of the Body

The lower zone of the Red Hills peridotites are composed of common harzburgite, plagioclase bearing harzburgite and dunite (**Figs. 5** and **6**). The uppermost part of the lower zone is characterized by plagioclase bearing harzburgite. This part simultaneously include remarkable lamination of clinopyroxene grains. The occurrence of clinopyroxene is similar to the case of lamination of clinopyroxene in the dunite of the upper zone. The transition from the lowermost part of the upper zone to the uppermost part of the lower zone is not clear.

Harzburgite

Harzburgite is the main constituent in the lower zone, and is quite homogeneous. Porphyroclasts of the coarse grained orthopyroxenes show rough surface on outcrops. Harzburgite of upper part of the lower zone shows "layering" by arrangement of plagioclase grains (**Figs. 5** and **6**). Accidental large clinopyroxene crystals in harzburgite can be detected at the top of the lower zone (**Fig. 14 c**). Irregular infiltration of plagioclase bearing harzburgite is rarely found in the upper part of this zone (**Fig. 12n** and **p**).

Plagioclase bearing Harzburgite

Plagioclase bearing harzburgites are often recognized in upper part of the lower zone. The plagioclase haphazardly occurs as thin seam (**Fig. 12 k** and **l**) and also scatters in harzburgite matrix. The mode of occurrences of plagioclase is decreased to downward. The occurrence of plagioclase bearing harzburgite shows that the plagioclase is formed at later stage than formation of the harzburgite.

Dunite

Dunite in the lower zone forms small pocket in harzburgite (**Fig. 12 m** and **o**). The harzburgite adjacent to dunite shows the most depleted nature. Namely, the modal pyroxene is low. Boundary of the both is gradual. The grain size of olivine in the dunite is larger than that in dunite of the upper zone, and is about 2cm at the maximun. Pegmatitic composite dikes of gabbroic composition are recognized in the dunite (**Fig. 12 m** and **o**). The gabbroic rocks are composed of plagioclase and orthopyroxene.

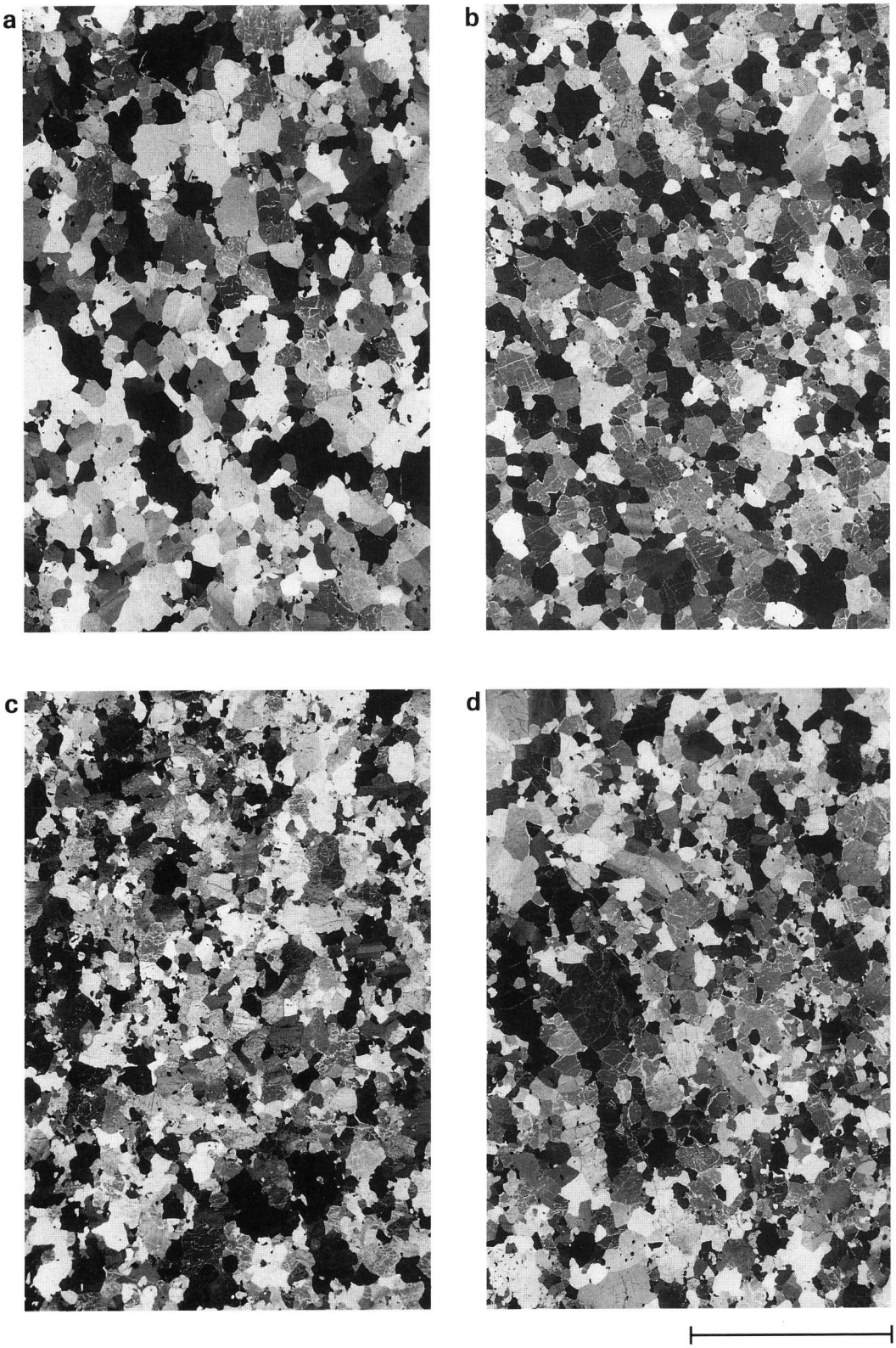
a
b
c
d

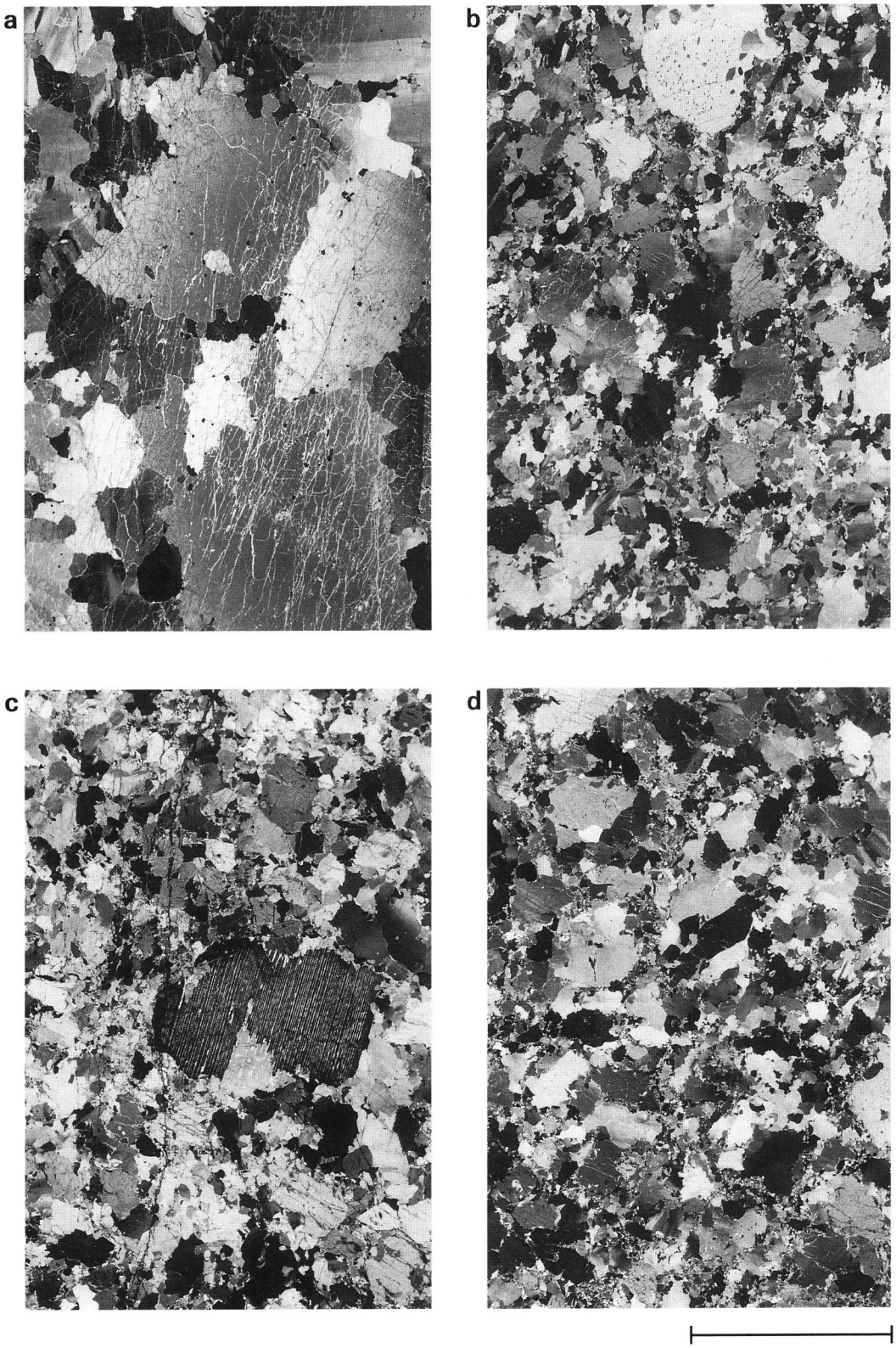
a
b
c
d

Fig.13. (p. 26) Representative rock textures in the upper zone. Scale is 1cm in all cases.
a: Coarse grained xenomorphic equigranular texture in plagioclase bearing dunite (RH-28).
b: Coarse to medium grained hypidiomorphic equigranular texture in common dunite (RH-20).
c: Coarse to medium grained xenomorphic equigranular texture in harzburgite (RH-33), that is similar to secondary protogranular texture of Mercier & Nicolas (1975).
d: Xenomorphic equigranular texture in clinopyroxene bearing dunite (RH-13).

Fig.14. (p. 27) Representative rock textures in the lower zone. Scale is 1cm in all cases.
a: Coarse grained porphyroclastic (suture) texture in dunite (RH-43).
b: Porphyroclastic texture in harzburgite (RH-63).
c: Accidental clinopyroxene crystals in porphyroclastic textured harzburgite (RH-38).
d: Porphyroclastic texture in plagioclase bearing harzburgite (RH-50).

4. PETROLOGY AND MINERALOGY OF THE RED HILLS PERIDOTITE

4−1. Petrography

4−1−1. Upper Zone of the Body

Olivine clinopyroxenite

Olivine clinopyroxenite shows poikilitic and alotoriomorphic equigranular textures. Olivine clinopyroxenite showing poikilitic texture is coarse grained and includes clinopyroxene well developed lamellae of orthopyroxene. Olivine shows kink band. On the other hand, grain size of clinopyroxene in olivine clinopyroxenite showing alotoriomorphic equigranular texture is medium to coarse, and is coarser than that of olivine. The crystal shapes of both olivine and clinopyroxene are anhedral. The grain boundaries are irregular. Spinel disseminates as small grains of rectangular shape.

Clinopyroxene bearing dunite

Clinopyroxene bearing dunite has medium to coarse grained xenomorphic equigranular texture (**Fig. 13 d**). The modal abundance of olivine and clinopyroxene show wide variation in one thin section. Namely, the rock is very heterogeneous. Olivine shows two types of relation of grain boundary, that is, one is predominated by 120° triple grain junction and another is not. In general, the grain shape is irregular on the clinopyroxene predominating domain, and domain predominated by olivine is characterized by 120° triple grain junction. Clinopyroxene displays irregular shape, and the grain size is larger than olivine. Clinopyroxene is well developed by lamellae of orthopyroxene, but the lamellae do not achieve till the rim. Magmatic twin (augite twin) in clinopyroxene is infrequently found (**Fig. 15 c**). Spinel disseminates as small grains of euhedral or rectangular shape in coarse clinopyroxene and olivine crystals, and along these grain boundaries. Phlogopite rarely occurs as interstitial mineral in grain boundary (**Fig. 15 a**). Clinopyroxene rich rock has a tendency that the olivine shape becomes to irregular.

Dunite

Dunite in the upper zone has medium grained hypidiomorphic equigranular texture (**Fig. 13 b**). Olivine forms polygonal shape with straight grain boundaries, and has a predominance of 120° triple grain junction (**Fig. 15 d**). Clinopyroxene rarely occurs as interstitial mineral (**Fig. 15 f** and **h**). Spinel disseminates as small grains in shape of rectangular and euhedral in olivine and along the grain boundaries.

Plagioclase bearing dunite

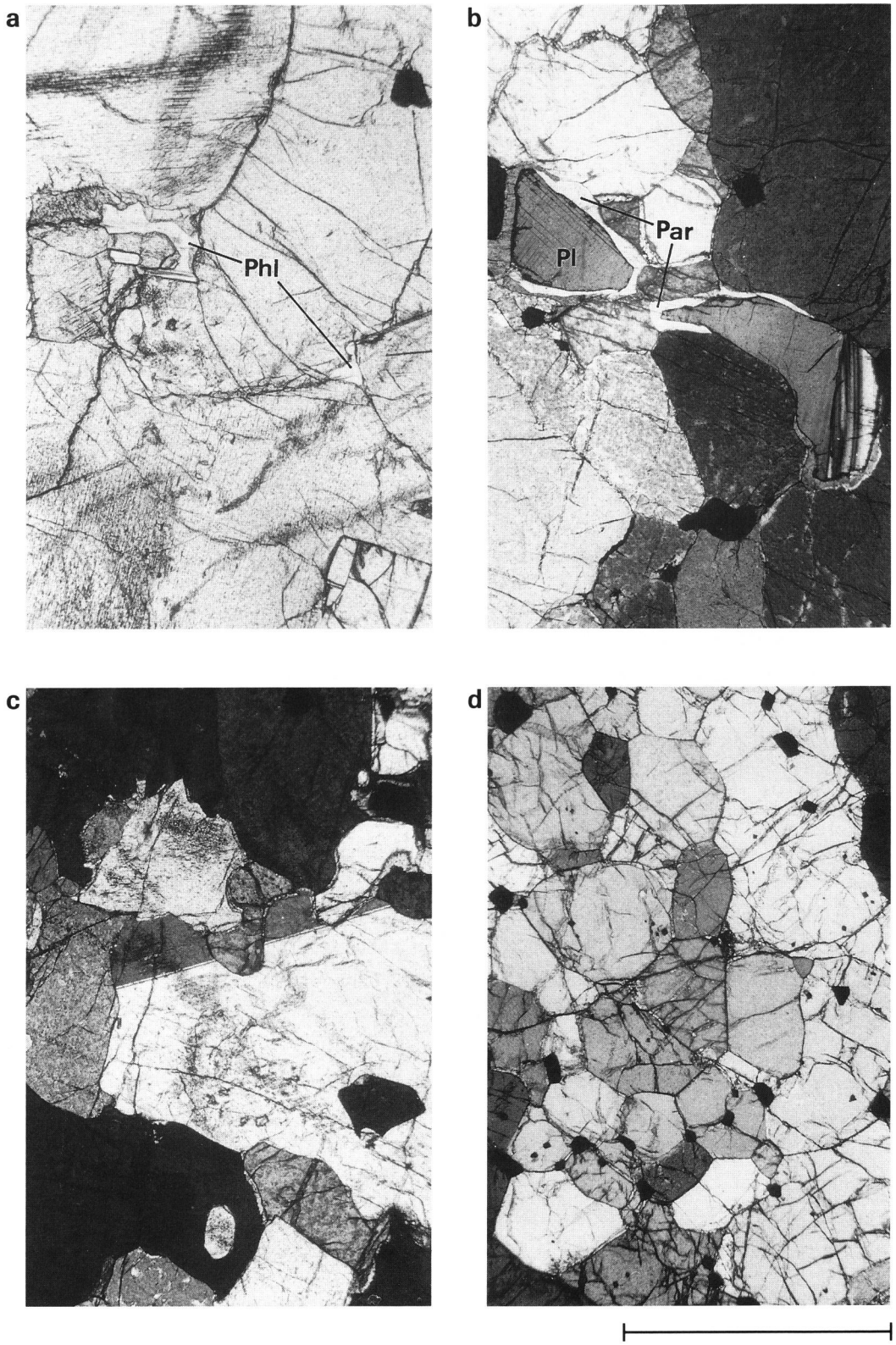
a
Phl
b
Pl
Par
c
d

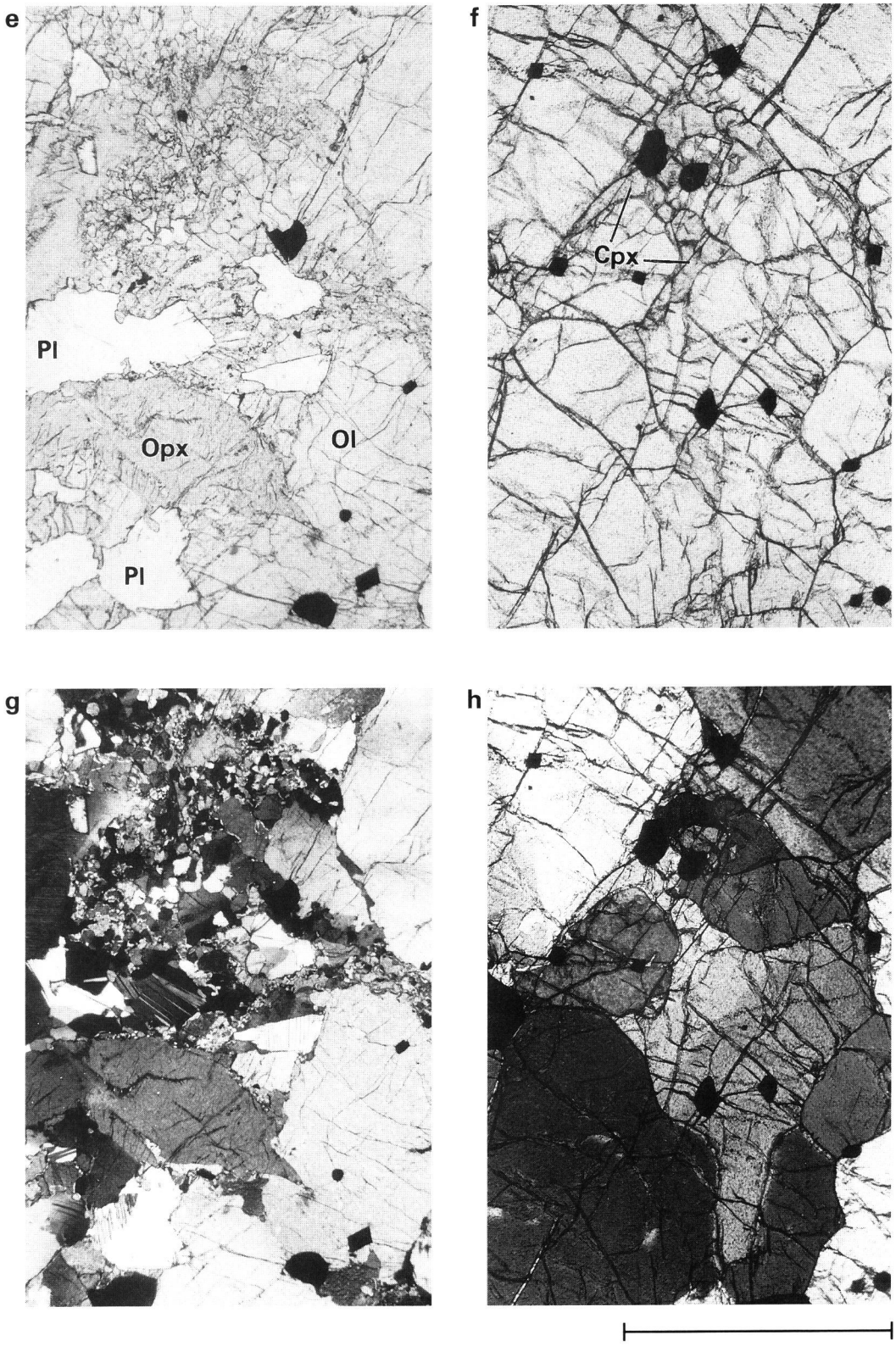
e
Pl
Opx
Ol
Pl
f
Cpx
g
h

Fig. 15. (p. 30~31) Microscopic textures. Scale bars are 2mm in each case.
a~**d**, **f** and **h**: textures in peridotites of the upper zone.

a: Interstitial phlogopites (**Phl**) in clinopyroxene bearing dunite (RH-18) in the upper zone. The occurrences are quite rare.
b: Drop or oval shaped plagioclases in plagioclase bearing dunite (RH-28). The plagioclases are sometimes surrounded by pargasite (**Par**).
c: Magmatic twin (center) of clinopyroxene in clinopyroxene bearing dunite (RH-18).
d: 120° triple grain boundaries in dunite (RH-20).
f: Interstitial clinopyroxene (**Cpx**) in dunite (RH-20).
h: Crossed polarized one of **f**.

e and **g**: textures in peridotites of the lower zone.

e: Typical occurrence of plagioclase (**Pl**) in plagioclase bearing harzburgite (RH-50). **Opx**: orthopyroxene, **Ol**: olivine
g: Crossed polarized one of **e**.

Plagioclase bearing dunite shows medium to coarse grained xenomorphic equigranular texture (**Fig. 13 a**). Grain boundaries of olivine are straight, and are 120° triple grain junction. Olivine shows irregular crystal shape at the clinopyroxene rich domains, like in case of clinopyroxene bearing dunite. Spinel scatters as euhedral to rectangular small grain. Clinopyroxene occurs as interlocking with olivine. Plagioclase fills up the domains of oval or drop shapes, and is often developes by twin (**Fig. 15 b**). The domains are well arranged. On the rims of the domains filled by plagioclase, pargasite is formed as reaction products with orthopyroxene (**Fig. 15 b**). It suggest that the pargasite is formed by reaction between clinopyroxene in dunite and a hydrous magma. The occurrences of pargasites are rare.

Harzburgite

Harzburgite in the upper zone displays medium to coarse grained xenomorphic equigranular texture (**Fig. 13 c**). The texture of the harzburgite is also similar to secondary protogranular texture of Mercier & Nicolas (1975). At domains predominating olivine the olivine makes much straight grain boundary and the grain size is large, while at domains predominating pyroxenes the texture is much porphyroclastic. Orthopyroxene has well developed exsolution lamellae of clinopyroxene. Spinel occurs as aggregates, and forms rectangular and spherical shapes. The harzburgites suffer serpentinization along grain boundaries.

Gabbro

Gabbro dike in upper part of the upper zone shows xenomorphic equigranular texture. Main constituents are plagioclase, clinopyroxene and olivine. There is a variation of modal clinopyroxene / plagioclase ratio in microscopic order. Plagioclase shows twins. Occurrence of spinel is very rare.

4-1-2. Lower Zone of the Body

Harzburgite

The harzburgite shows typical porphyroclastic texture (**Fig. 14 b** and **c**). Size of porphyroclasts of olivine and pyroxenes are 7~8mm. Porphyroclast of orthopyroxene is developed by notable exsolution lamellae of clinopyroxene. Both olivine and orthopyroxene are developed kink bands. These porphyroclasts are surrounded by fine grained matrix of olivine, orthopyroxene and clinopyroxene. Spinel forms "holly-leaf" shape, and exists along the silicate minerals. Small spinel shows rectangular and spherical shape, and is enclosed in silicate minerals. At the upper most part of the lower zone, accidental large clinopyroxene grains that sizes are about 1cm are shown (**Fig. 14 c**).

Plagioclase bearing Harzburgite

Plagioclase bearing harzburgite also has porphyroclastic texture (**Fig. 14 d**). The texture is basically the same as common harzburgite in this zone. Spinel forms "holly-leaf" shape. There is no evidence of reaction between spinel and plagioclase or is no evidence of breakdown of spinel to plagioclase. As discussed below, chemical composition of spinel does not have any evidence for the reaction or the breakdown. Plagioclase occurs as drop or irregular shapes (**Fig. 15 e** and **g**), and forms rock foliation. Twins of plagioclases develop. Plagioclase domain infrequently displays elongated shape. Kink bands in olivine and orthopyroxene porphyroclasts are remarkably developed. The smaller domain filled by plagioclase makes rounded shape. The disseminations of plagioclase domains in and along the other silicate minerals are irrelevant to the basic texture of harzburgite. Though occurrences of plagioclase in the harzburgite are well similar to that of plagioclase bearing dunite in the upper zone, the reaction rim of pargasite around plagioclase does not recognize in this harzburgite. Textures and occurrences of the plagioclase bearing harzburgite suggest that the plagioclase is not formed from breakdown of spinel but probably derived from any trapped melt.

Dunite

Dunite in the lower zone displays coarse grained prophyroclastic texture. Grain boundaries are mainly characterized by sutures and are sometimes shown as curved line (**Fig. 14 a**). Grain size of olivine is about 2cm at the maximum. In general, 120° triple grain junction is not developed. Spinel shows as euhedral crystal, and makes rectangular to spherical grains and often forms aggregates. Small interstitial domains of orthopyroxene and clinopyroxene are rarely recognized.

4-2. Mineral Compositions

Olivine (Table 2)

Compositional variation of olivine as a function of stratigraphic level that is from the up-

Table 2. Representative electron microprobe analyses of olivines in the Red Hills peridotite

Sample	Point	SiO_2	FeO	MnO	MgO	NiO*	Total	Si	Fe	Mn	Mg	Ni	Total Cation	Fo
					Upper dunite predominated zone									
RH−03	P−16	40.16	10.53	0.15	48.47	0.21	99.52	0.994	0.218	0.003	1.788	0.004	3.006	89.14
RH−04	P−2	40.44	10.87	0.08	48.21	0.23	99.83	0.998	0.224	0.002	1.773	0.005	3.002	88.77
RH−06	P−10	40.58	9.31	0.09	49.75	0.22	99.95	0.994	0.191	0.002	1.816	0.004	3.006	90.50
RH−10d	1	40.57	9.99	0.19	48.42	0.08	99.25	1.002	0.206	0.004	1.783	0.002	2.998	89.63
RH−10p	5	40.50	11.13	0.19	47.59	0.24	99.65	1.002	0.230	0.004	1.756	0.005	2.998	88.40
RH−11	P−5	40.10	12.44	0.10	46.76	0.21	99.61	0.999	0.259	0.002	1.737	0.004	3.001	87.01
RH−12	3	40.58	10.01	0.16	48.73	0.19	99.67	0.999	0.206	0.003	1.789	0.004	3.001	89.67
RH−15	P−30	40.76	10.60	0.12	48.62	0.24	100.34	0.999	0.217	0.002	1.777	0.005	3.001	89.10
RH−17	P−27	40.39	10.51	0.17	49.08	0.21	100.36	0.991	0.216	0.004	1.795	0.004	3.009	89.27
RH−18	P−10	40.32	11.31	0.10	48.04	0.16	99.93	0.996	0.234	0.002	1.769	0.003	3.004	88.33
RH−19	P−3	40.56	10.03	0.12	48.92	0.10	99.73	0.998	0.206	0.003	1.794	0.002	3.002	89.68
RH−21	P−24	40.52	9.89	0.07	49.61	0.24	100.33	0.991	0.202	0.001	1.809	0.005	3.009	89.94
RH−22	3	41.05	8.03	0.05	50.55	0.31	99.99	0.998	0.163	0.001	1.833	0.006	3.002	91.82
RH−23	P−27	40.32	11.46	0.06	47.35	0.15	99.34	1.002	0.238	0.001	1.754	0.003	2.998	88.04
RH−24	5	41.10	10.07	0.03	49.68	0.19	101.07	0.997	0.204	0.001	1.797	0.004	3.003	89.79
RH−25	P−8	40.23	10.59	0.18	48.54	0.31	99.85	0.993	0.219	0.004	1.786	0.006	3.007	89.09
RH−26	P−12	40.22	10.55	0.11	48.01	0.15	99.04	0.999	0.219	0.002	1.778	0.003	3.001	89.02
RH−27	P−7	40.52	9.64	0.10	48.40	0.40	99.06	1.003	0.199	0.002	1.785	0.008	2.997	89.95
RH−28	3	40.69	10.18	0.00	49.17	0.18	100.22	0.996	0.208	0.000	1.795	0.004	3.004	89.59
RH−29	P−2	40.45	11.30	0.19	48.16	0.28	100.38	0.996	0.233	0.004	1.767	0.006	3.004	88.37
RH−31	P−2	40.80	10.68	0.16	48.47	0.08	100.19	1.001	0.219	0.003	1.773	0.002	2.999	89.00
RH−33	P−16	41.08	8.71	0.12	49.93	0.35	100.19	1.000	0.177	0.002	1.813	0.007	3.000	91.09
RH−34	P−16	40.59	10.16	0.07	49.38	0.12	100.32	0.993	0.208	0.001	1.801	0.002	3.007	89.65
RH−35	3	41.01	10.26	0.02	49.32	0.17	100.78	0.999	0.209	0.000	1.790	0.003	3.001	89.55
RH−36	5	40.87	10.56	0.00	48.73	0.11	100.27	1.001	0.216	0.000	1.779	0.002	2.999	89.16

Table 2. (continued)

Sample	Point	SiO_2	FeO	MnO	MgO	NiO	Total	Si	Fe	Mn	Mg	Ni	Total Cation	Fo
					Lower harzburgite zone									
RH−37	5	40.96	8.15	0.01	50.51	0.15	99.78	0.998	0.166	0.000	1.835	0.003	3.002	91.70
RH−38	p−2	40.93	8.71	0.09	50.20	0.25	100.18	0.997	0.177	0.002	1.822	0.005	3.003	91.13
RH−39	p−12	41.10	8.66	0.15	49.99	0.43	100.33	1.000	0.176	0.003	1.813	0.008	3.000	91.14
RH−40	p−7	41.37	8.73	0.13	50.49	0.43	101.15	0.998	0.176	0.003	1.816	0.008	3.002	91.16
RH−42	p−23	40.76	8.58	0.12	49.92	0.28	99.66	0.998	0.176	0.002	1.821	0.006	3.002	91.21
RH−43	p−1	41.51	6.75	0.05	51.34	0.30	99.95	1.003	0.136	0.001	1.850	0.006	2.997	93.13
RH−44	p−19	40.95	8.61	0.08	49.96	0.25	99.85	1.000	0.176	0.002	1.818	0.005	3.000	91.18
RH−45	p−9	41.22	7.93	0.07	50.60	0.38	100.20	1.000	0.161	0.001	1.830	0.007	3.000	91.92
RH−46	p−15	40.82	8.53	0.17	49.74	0.34	99.63	1.000	0.175	0.004	1.815	0.007	3.000	91.22
RH−47	p−5	41.22	8.20	0.11	50.28	0.40	100.21	1.001	0.167	0.002	1.821	0.008	2.999	91.62
RH−48	p−5	41.12	8.90	0.14	50.08	0.35	100.59	0.998	0.181	0.003	1.813	0.007	3.002	90.93
RH−49	p−14	40.95	9.08	0.15	49.52	0.26	99.96	1.001	0.186	0.003	1.804	0.005	2.999	90.67
RH−50	4	41.01	9.00	0.11	49.76	0.25	100.13	1.000	0.184	0.002	1.809	0.005	3.000	90.79
RH−51	p−4	41.11	8.65	0.07	50.09	0.37	100.29	1.000	0.176	0.001	1.816	0.007	3.000	91.17
RH−52	p−1	41.54	8.61	0.14	49.63	0.37	100.29	1.009	0.175	0.003	1.797	0.007	2.991	91.13
RH−53	p−9	41.30	8.81	0.09	49.80	0.38	100.38	1.004	0.179	0.002	1.804	0.007	2.996	90.97
RH−54	p−37	41.15	8.83	0.15	50.35	0.32	100.80	0.997	0.179	0.003	1.818	0.006	3.003	91.04
RH−55	4	40.86	8.36	0.00	49.98	0.12	99.32	1.001	0.171	0.000	1.825	0.002	2.999	91.42
RH−59	p−22	41.25	7.87	0.12	50.55	0.40	100.19	1.001	0.160	0.002	1.828	0.008	2.999	91.97
RH−63	p−30	41.04	7.98	0.12	49.58	0.28	99.00	1.007	0.164	0.002	1.814	0.006	2.993	91.72
RH−66	p−3	40.85	8.69	0.01	50.38	0.00	99.93	0.996	0.177	0.000	1.831	0.000	3.004	91.18
RH−65	p−15	40.88	8.78	0.00	50.41	0.09	100.16	0.995	0.179	0.000	1.829	0.002	3.005	91.10
RH−68	p−5−4	41.12	8.67	0.05	50.23	0.15	100.22	1.000	0.176	0.001	1.820	0.003	3.000	91.17
RH−69	p−20	41.52	7.66	0.09	51.26	0.37	100.90	0.999	0.154	0.002	1.839	0.007	3.001	92.26

* : NiO values are unreliable.

per zone to the lower zone (about 8km thickness) is shown in **Figure 16 a**. The Fo (100* Mg/(Mg+Fe) ratio) compositions of the lower harzburgite are very constant, and the average is Fo=91.4. The dunite in the lower zone has higher Fo contents ($Fo_{92\sim93}$) than that of the lower harzburgite. On the other hand, compositions of olivines in the peridotites in the upper zone are characterized by lower Fo contents, and shows wide range ($Fo_{87\sim92}$). Olivine clinopyroxenite has the lowest Fo content in the upper zone. Dunite in the upper

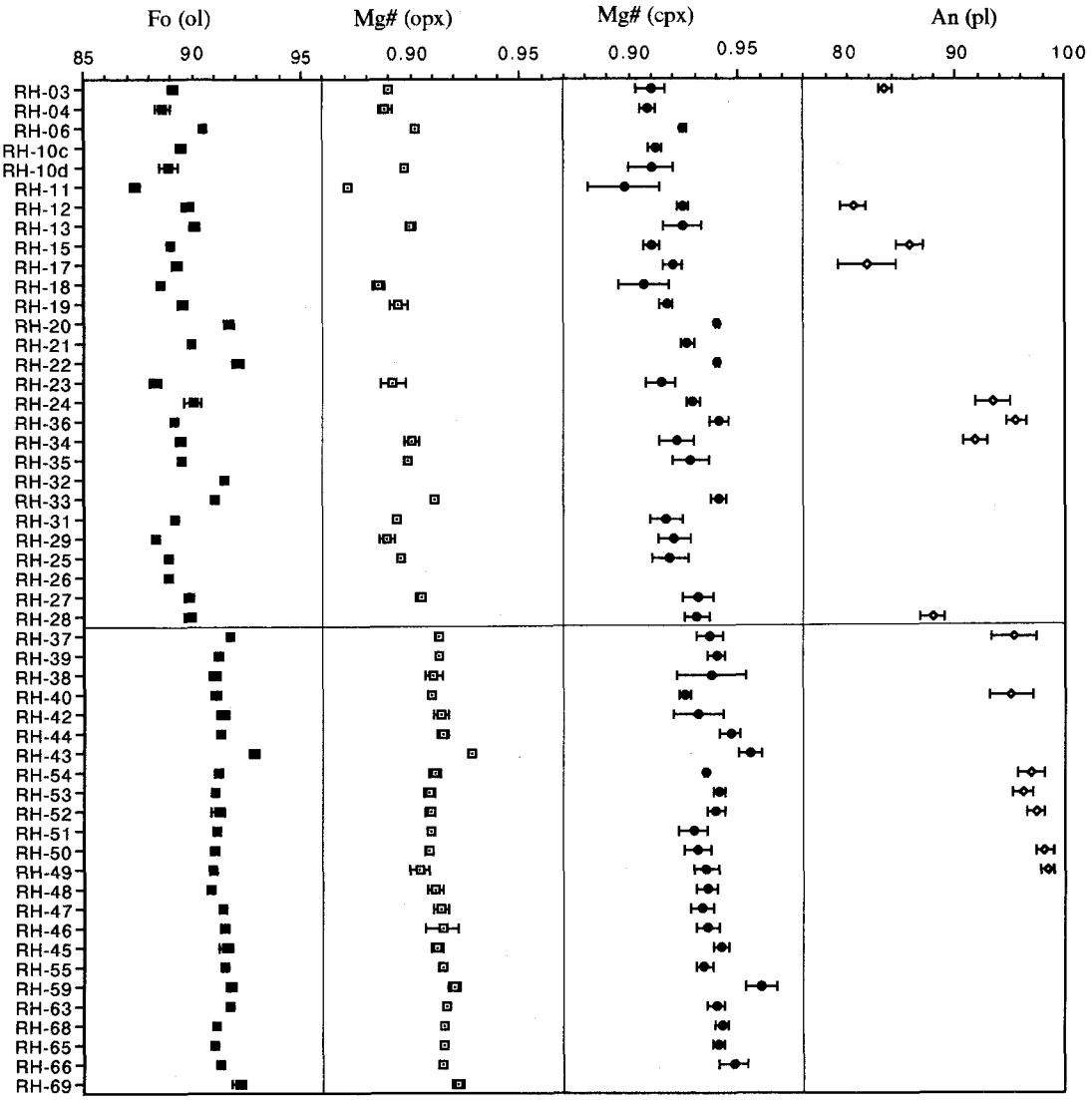

Fig. 16. Compositional variations of minerals against the stratigraphic heights. RH-03~RH-28: the upper zone, RH-37~RH-69: the lower zone. Each point on this figure represents average analytical result of each rock sample.

a: Variations of Fo contents in olivine, Mg# in orthopyroxene and clinopyroxene, and An contents in plagioclase. Error bars represent the standard deviations of mineral analysis in each sample.

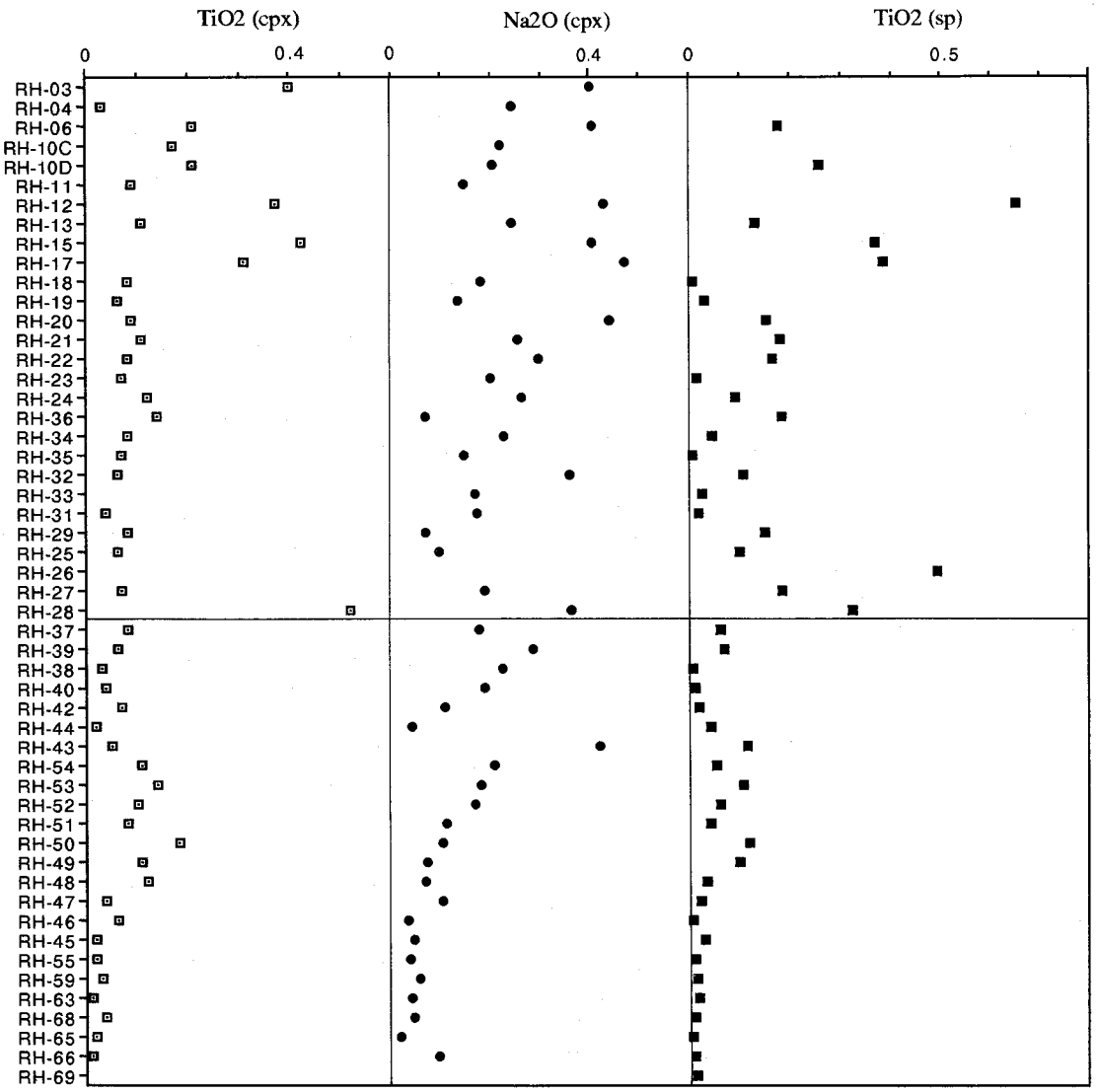

Fig.16. **b**: Variations of TiO_2 in clinopyroxene and spinel, and Na_2O in clinopyroxene.

zone generally has high Fo olivine. Olivine in harzburgite (blocky occurrence) in the upper zone shows lower Fo content than that in harzburgite in the lower zone. It is clear that the Fo contents of olivine in peridotites in the upper zone is characterized by lower than that of olivine in peridotites in the lower zone, and the compositional variation of olivine as a function of stratigraphic level is not cryptic but depends on the rock types.

Spinel (Table 3)

Table 3. Representative electron microprobe analyses of spinels in the Red Hills peridotite

Sample	Point	Al_2O_3	TiO_2	FeO	Fe_2O_3	MnO	MgO	Cr_2O_3	Total	Al	Ti	Fe^{2+}	Fe^{3+}	Mn	Mg	Cr	Total Cation	Mg#	Cr#
Upper dunite predominated zone																			
RH−06	2	28.76	0.17	15.92	2.05	0.08	13.46	39.14	99.58	1.017	0.004	0.400	0.046	0.002	0.602	0.929	3.000	0.601	0.466
RH−10d	2	31.32	0.22	18.60	2.19	0.14	11.97	35.17	99.61	1.107	0.005	0.466	0.049	0.004	0.535	0.834	3.000	0.534	0.419
RH−12	1	27.98	0.66	19.20	3.32	0.14	11.72	37.76	100.78	0.995	0.015	0.484	0.075	0.004	0.527	0.900	3.000	0.521	0.457
RH−13	3	29.46	0.19	17.86	2.16	0.12	12.33	37.85	99.97	1.043	0.004	0.449	0.049	0.003	0.552	0.899	3.000	0.552	0.452
RH−15	2	29.29	0.33	19.18	3.00	0.24	11.30	35.93	99.27	1.051	0.008	0.488	0.069	0.006	0.513	0.865	3.000	0.512	0.436
RH−17	1	29.75	0.42	20.84	3.89	0.02	10.65	34.64	100.21	1.062	0.010	0.528	0.089	0.001	0.481	0.830	3.000	0.477	0.419
RH−18	2	39.02	0.00	16.88	2.59	0.04	13.83	27.32	99.68	1.323	0.000	0.406	0.056	0.001	0.593	0.621	3.000	0.594	0.311
RH−19	2	32.92	0.03	17.40	2.56	0.05	12.87	33.72	99.55	1.150	0.001	0.431	0.057	0.001	0.569	0.790	3.000	0.569	0.396
RH−20	4	20.11	0.18	17.40	4.66	0.14	11.23	44.39	98.11	0.758	0.004	0.465	0.112	0.004	0.535	1.122	3.000	0.535	0.563
RH−21	2	24.63	0.15	17.58	6.79	0.16	11.71	37.96	98.98	0.902	0.004	0.457	0.159	0.004	0.542	0.932	3.000	0.543	0.468
RH−22	2	22.46	0.17	18.95	3.97	0.28	10.84	43.66	100.33	0.824	0.004	0.493	0.093	0.007	0.503	1.075	3.000	0.505	0.540
RH−23	2	41.33	0.01	17.36	1.04	0.03	13.86	26.42	100.05	1.384	0.000	0.412	0.022	0.001	0.587	0.593	3.000	0.587	0.297
RH−24	1	34.02	0.14	17.22	3.26	0.21	13.11	31.96	99.92	1.179	0.003	0.423	0.072	0.005	0.575	0.743	3.000	0.576	0.373
RH−25	1	31.32	0.07	17.85	3.87	0.00	12.50	34.26	99.87	1.102	0.002	0.445	0.087	0.000	0.556	0.808	3.000	0.555	0.405
RH−26	1	29.58	0.50	19.18	8.34	0.20	11.55	30.65	100.00	1.055	0.011	0.485	0.190	0.005	0.521	0.733	3.000	0.518	0.371
RH−27	3	25.51	0.10	18.19	3.46	0.20	11.60	40.97	100.03	0.922	0.002	0.467	0.080	0.005	0.530	0.993	3.000	0.532	0.498
RH−28	3	36.22	0.35	16.03	1.32	0.19	14.24	31.47	99.82	1.236	0.008	0.388	0.029	0.005	0.615	0.720	3.000	0.613	0.363
RH−29	1	25.40	0.22	19.95	5.22	0.08	10.56	38.53	99.96	0.926	0.005	0.516	0.122	0.002	0.487	0.942	3.000	0.485	0.474
RH−31	4	37.08	0.05	16.71	2.18	0.18	13.64	29.65	99.49	1.269	0.001	0.406	0.048	0.004	0.591	0.681	3.000	0.593	0.341
RH−32	4	21.14	0.12	17.40	7.66	0.09	11.76	42.11	100.28	0.777	0.003	0.454	0.180	0.002	0.547	1.038	3.000	0.546	0.520
RH−33	2	23.50	0.01	17.86	1.33	0.02	11.70	45.64	100.06	0.855	0.000	0.461	0.031	0.001	0.538	1.114	3.000	0.539	0.557
RH−34	1	29.97	0.08	19.00	2.00	0.22	11.51	37.19	99.97	1.065	0.002	0.479	0.045	0.006	0.517	0.886	3.000	0.519	0.444
RH−35	3	44.26	0.00	14.80	1.80	0.07	15.69	22.96	99.58	1.456	0.000	0.345	0.038	0.002	0.653	0.507	3.000	0.654	0.253
RH−36	1	32.03	0.16	19.94	2.83	0.08	11.34	34.08	100.46	1.126	0.004	0.497	0.064	0.002	0.504	0.804	3.000	0.503	0.403

Table 3. (continued)

Sample	Point	Al_2O_3	TiO_2	FeO	Fe_2O_3	MnO	MgO	Cr_2O_3	Total	Al	Ti	Fe^{2+}	Fe^{3+}	Mn	Mg	Cr	Total Cation	Mg#	Cr#
							Lower harzburgite zone												
RH−37	2	34.03	0.06	14.93	1.32	0.16	14.62	34.87	99.99	1.167	0.001	0.363	0.029	0.004	0.634	0.802	3.000	0.636	0.401
RH−38	2	30.68	0.00	16.06	1.60	0.13	13.40	37.56	99.43	1.079	0.000	0.401	0.036	0.003	0.596	0.886	3.000	0.598	0.443
RH−39	3	26.89	0.08	17.83	1.57	0.11	11.97	41.21	99.66	0.967	0.002	0.455	0.036	0.003	0.544	0.994	3.000	0.545	0.498
RH−40	1	32.52	0.01	15.81	1.32	0.13	13.72	35.70	99.21	1.135	0.000	0.391	0.029	0.003	0.605	0.836	3.000	0.607	0.418
RH−42	3	44.50	0.03	13.22	1.08	0.13	16.82	24.21	99.99	1.448	0.001	0.305	0.022	0.003	0.692	0.528	3.000	0.694	0.264
RH−43	1	12.52	0.15	16.96	2.51	0.20	10.99	56.13	99.46	0.482	0.004	0.463	0.062	0.006	0.535	1.449	3.000	0.536	0.727
RH−44	2	24.70	0.03	18.04	2.41	0.22	11.75	43.73	100.88	0.888	0.001	0.460	0.055	0.006	0.534	1.055	3.000	0.537	0.528
RH−45	2	25.04	0.07	17.48	1.32	0.14	12.28	44.76	101.09	0.894	0.002	0.443	0.030	0.004	0.555	1.072	3.000	0.556	0.537
RH−46	3	40.91	0.00	14.21	0.82	0.04	15.82	28.05	99.85	1.358	0.000	0.335	0.017	0.001	0.664	0.625	3.000	0.665	0.312
RH−47	1	30.26	0.00	16.21	2.24	0.10	13.55	38.37	100.73	1.054	0.000	0.401	0.050	0.003	0.597	0.896	3.000	0.598	0.448
RH−48	3	45.82	0.03	13.59	0.27	0.00	16.72	23.15	99.58	1.489	0.001	0.313	0.006	0.000	0.687	0.505	3.000	0.687	0.252
RH−49	1	35.40	0.09	16.01	1.03	0.12	14.11	33.23	99.99	1.211	0.002	0.389	0.022	0.003	0.610	0.763	3.000	0.611	0.382
RH−50	2	34.06	0.10	15.60	2.28	0.08	14.34	33.93	100.39	1.166	0.002	0.379	0.050	0.002	0.621	0.779	3.000	0.621	0.391
RH−51	3	44.18	0.06	12.40	1.51	0.05	17.36	24.28	99.84	1.437	0.001	0.286	0.031	0.001	0.714	0.530	3.000	0.714	0.265
RH−52	3	35.32	0.05	15.99	0.86	0.07	14.26	34.08	100.63	1.201	0.001	0.386	0.019	0.002	0.613	0.778	3.000	0.614	0.389
RH−53	3	32.49	0.12	14.76	1.96	0.08	14.54	35.50	99.45	1.126	0.003	0.363	0.043	0.002	0.637	0.825	3.000	0.637	0.414
RH−54	2	33.22	0.06	15.08	0.81	0.08	14.50	36.24	99.99	1.143	0.001	0.368	0.018	0.002	0.631	0.837	3.000	0.632	0.419
RH−55	3	36.72	0.02	14.40	0.69	0.16	15.19	32.62	99.80	1.243	0.000	0.346	0.015	0.004	0.650	0.741	3.000	0.653	0.371
RH−59	3	13.99	0.02	19.19	2.07	0.12	9.73	54.67	99.79	0.538	0.000	0.524	0.051	0.003	0.473	1.410	3.000	0.475	0.705
RH−63	2	31.23	0.03	15.31	2.21	0.08	14.15	37.16	100.17	1.084	0.001	0.377	0.049	0.002	0.621	0.865	3.000	0.622	0.433
RH−66	2	36.17	0.03	14.40	0.37	0.05	15.26	33.73	100.01	1.225	0.001	0.346	0.008	0.001	0.653	0.766	3.000	0.654	0.383
RH−65	3	30.85	0.02	15.65	0.66	0.09	14.06	39.64	100.97	1.066	0.000	0.384	0.015	0.002	0.614	0.919	3.000	0.616	0.460
RH−68	3	36.57	0.02	13.53	0.44	0.01	15.85	33.42	99.84	1.234	0.000	0.324	0.009	0.000	0.676	0.756	3.000	0.676	0.378
RH−69	3	11.74	0.00	18.60	0.46	0.19	9.81	58.81	99.61	0.456	0.000	0.513	0.011	0.005	0.482	1.533	3.000	0.485	0.766

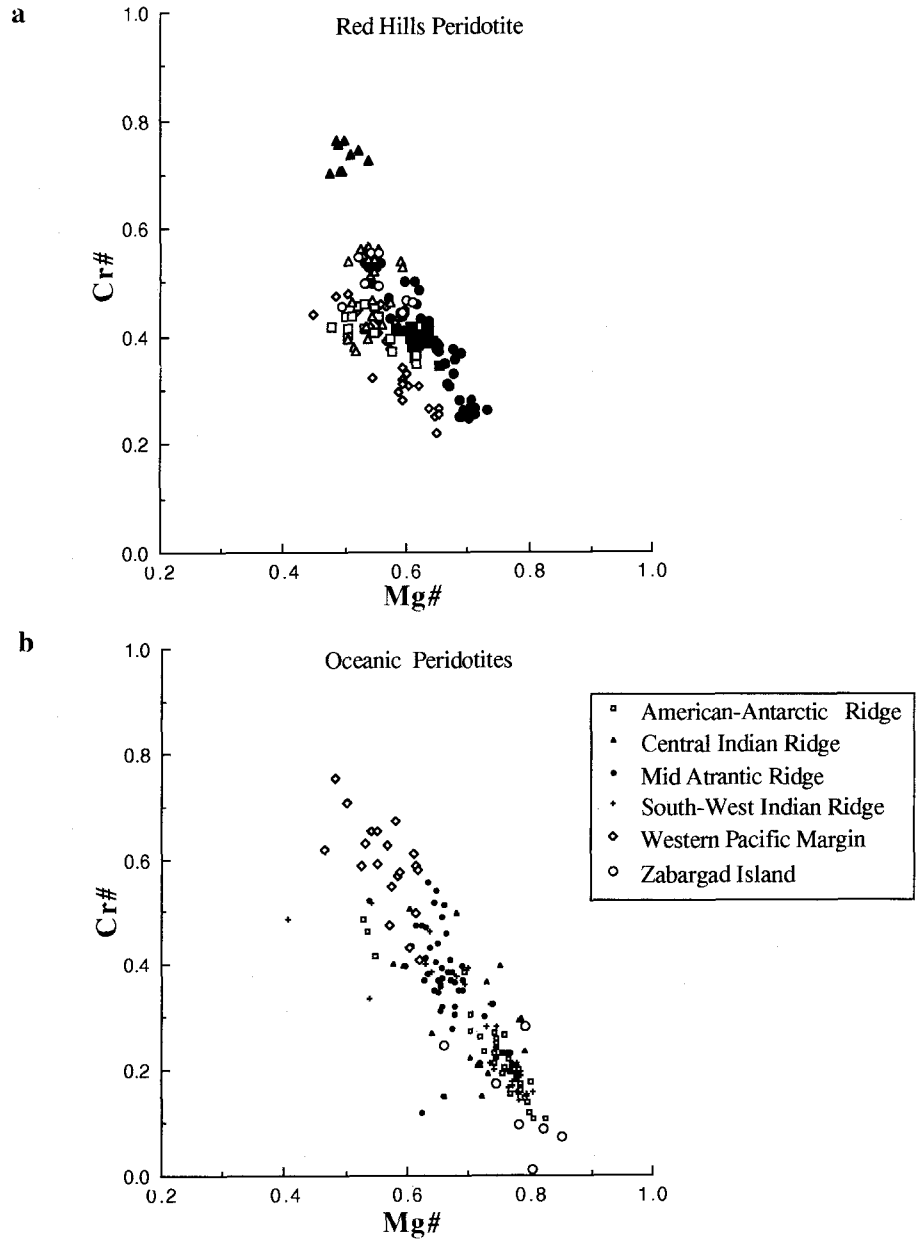

Fig.17. Mg# versus Cr# in peridotite spinels. **a**: Spinels from the Red Hills peridotite. Solid symbols are data from the upper zone, and open symbols are from the lower zone. **b**: Spinels from oceanic peridotites. Data are from Prinz et al.(1976), Bonatti & Hamlyn (1978), Arai & Fujii (1979), Sinton (1979), Hamlyn & Bonatti (1980), Bonatti et al.(1981), Dick & Bullen (1984), Roden et al. (1984), Ishii (1985), Shibata & Thompson (1986), Piccardo et al.(1988) and Dick (1989).

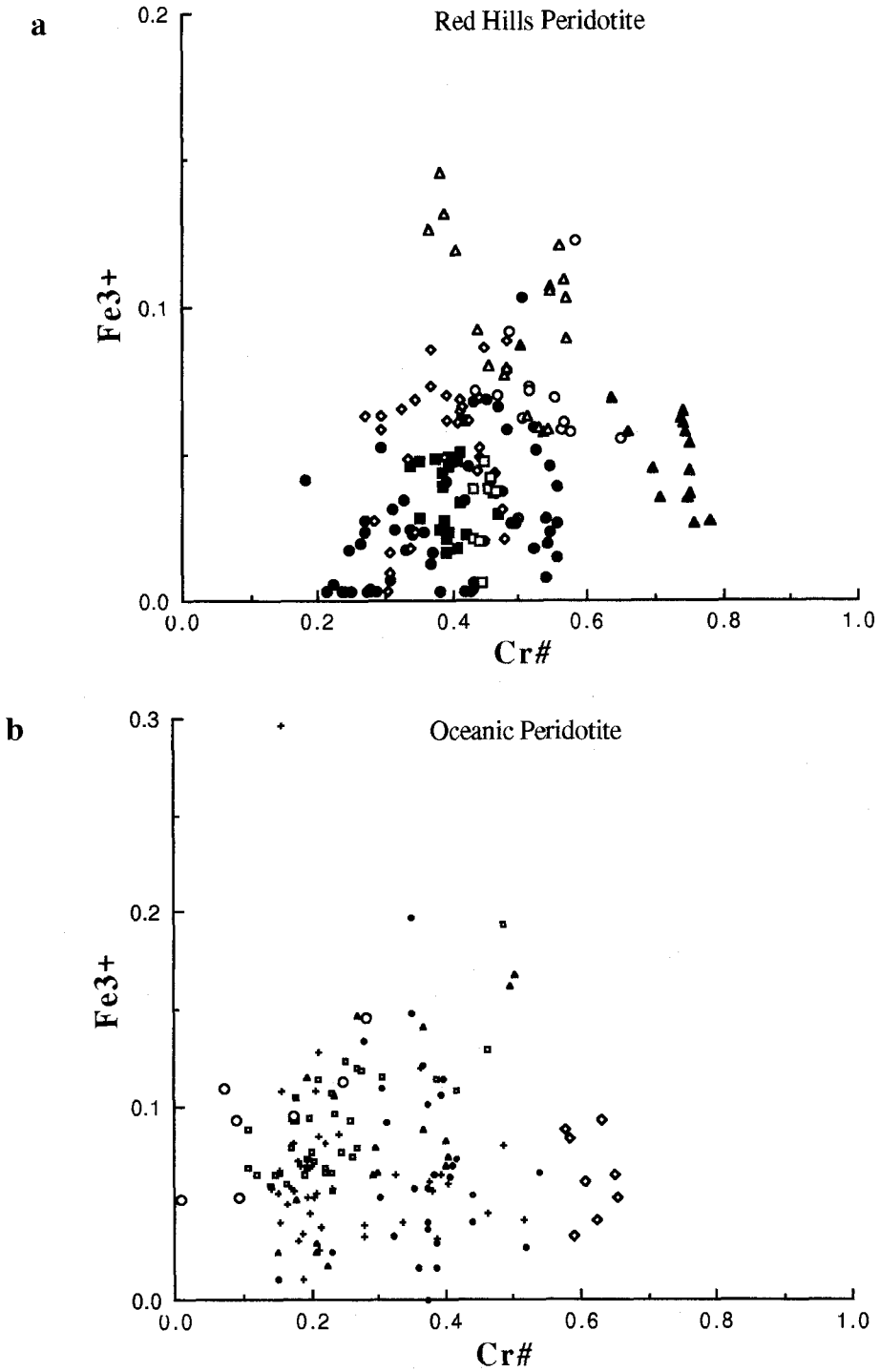

Fig.18. Fe^{3+} versus Cr# in peridotite spinels. **a**: Spinels from the Red Hills peridotite. Symbols are the same as in **Fig.17.** Spinels from the upper zone, especially dunite, show relatively high Fe^{3+}. **b**: Spinels from oceanic peridotites. Data sources are the same as in **Fig.17**.

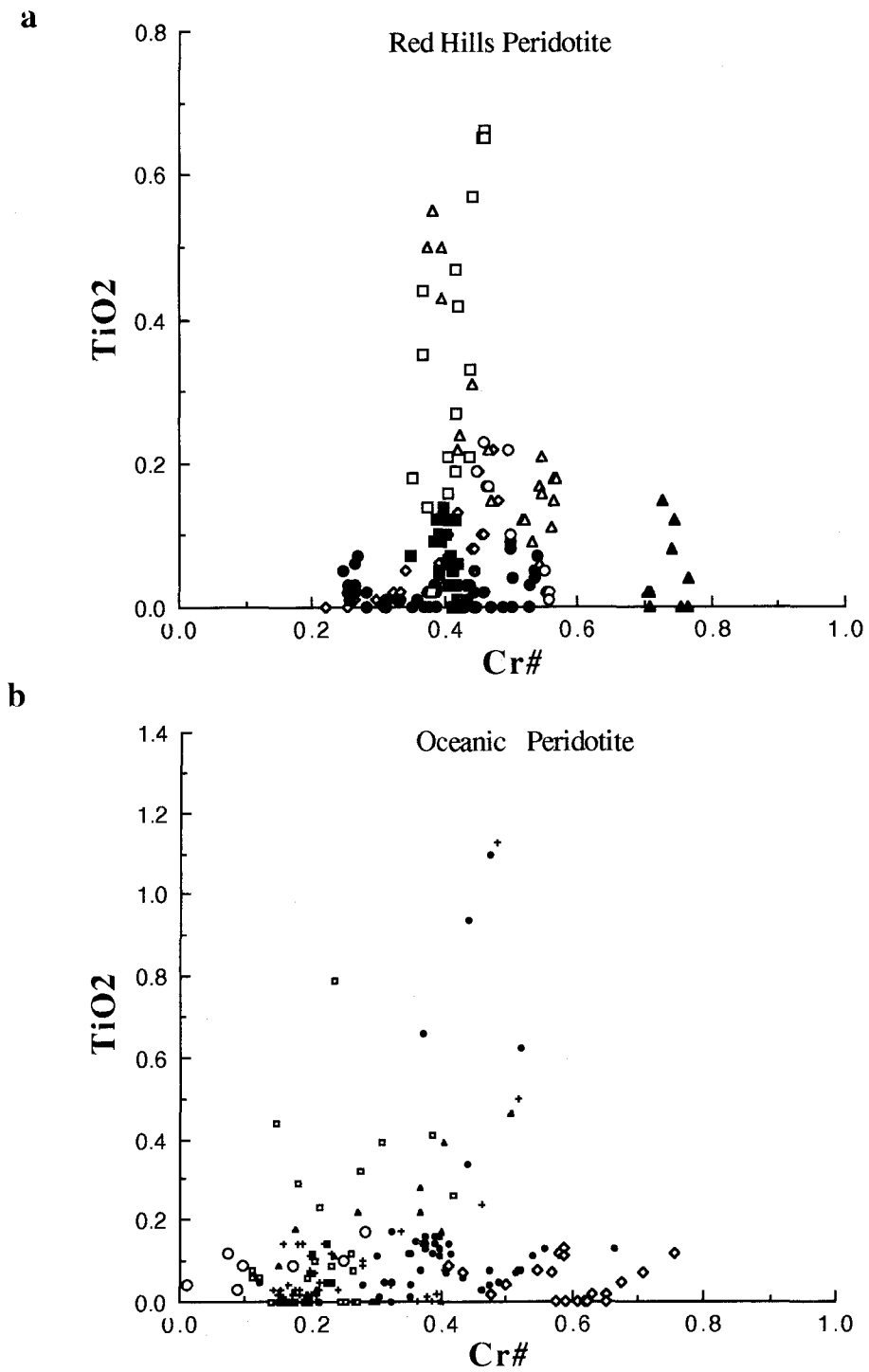

Fig.19. TiO_2 versus Cr# in peridotite spinels. **a**: Spinels from the Red Hills peridotite. Symbols are the same as in **Fig.17.** Spinels in the upper zone, especially plagioclase bearing dunite and common dunite, are obviously characterized by high TiO_2 content on Cr#=0.4. **b**: Spinels from oceanic peridotites. Data sources are the same as in **Fig.17.**

Table 4. Representative election microprobe analyses of orthopyroxenes in the Red Hills peridotite

Sample	Point	SiO_2	Al_2O_3	TiO_2	FeO	MnO	MgO	CaO	Na_2O	Cr_2O_3	Total	Si	Al	Ti	Fe	Mn	Mg	Ca	Na	Cr	Total Cation	Mg#
Upper dunite predominated zone																						
RH−03	P−27C	56.37	1.99	0.17	7.38	0.02	33.30	0.91	0.00	0.12	100.26	1.950	0.081	0.004	0.213	0.001	1.717	0.034	0.000	0.003	4.004	0.889
RH−04	P−10C	56.37	2.87	0.00	7.49	0.02	32.95	0.93	0.00	0.11	100.74	1.940	0.116	0.000	0.216	0.001	1.690	0.034	0.000	0.003	4.000	0.887
RH−06	P−18R	56.95	1.99	0.09	6.52	0.09	34.01	0.71	0.00	0.37	100.73	1.953	0.080	0.002	0.187	0.003	1.738	0.026	0.000	0.010	4.000	0.903
RH−10p	P−8R	55.52	2.46	0.12	6.71	0.01	33.20	1.27	0.00	0.53	99.82	1.929	0.101	0.003	0.195	0.000	1.720	0.047	0.000	0.015	4.010	0.898
RH−11	P−13C	55.55	2.50	0.03	8.48	0.08	32.47	0.76	0.01	0.49	100.37	1.932	0.102	0.001	0.247	0.002	1.683	0.028	0.001	0.013	4.010	0.872
RH−13	P−1C	56.21	2.20	0.06	6.68	0.01	33.42	1.43	0.00	0.55	100.56	1.938	0.089	0.002	0.193	0.000	1.718	0.053	0.000	0.015	4.008	0.899
RH−18	P−17C	54.72	3.22	0.01	7.19	0.04	32.49	1.27	0.00	0.61	99.55	1.912	0.133	0.000	0.210	0.001	1.692	0.048	0.000	0.017	4.013	0.890
RH−19	P−18R	56.15	2.50	0.02	7.31	0.18	33.08	0.82	0.00	0.49	100.55	1.939	0.102	0.001	0.211	0.005	1.702	0.030	0.000	0.013	4.003	0.890
RH−23	P−17C	55.55	3.04	0.00	7.41	0.16	32.38	1.73	0.01	0.65	100.93	1.919	0.124	0.000	0.214	0.005	1.667	0.064	0.001	0.018	4.011	0.886
RH−25	P−7C	55.48	2.28	0.02	7.02	0.10	33.71	1.15	0.00	0.44	100.20	1.924	0.093	0.001	0.204	0.003	1.743	0.043	0.000	0.012	4.022	0.895
RH−27	P−1C	55.60	2.27	0.05	6.39	0.17	34.60	1.01	0.00	0.50	100.59	1.917	0.092	0.001	0.184	0.005	1.778	0.037	0.000	0.014	4.029	0.906
RH−29	P−24C	56.77	2.01	0.04	7.74	0.04	33.10	0.86	0.00	0.33	100.89	1.954	0.082	0.001	0.223	0.001	1.698	0.032	0.000	0.009	4.000	0.884
RH−31	P−17C	56.09	3.03	0.00	7.02	0.06	33.15	0.95	0.01	0.33	100.64	1.931	0.123	0.000	0.202	0.002	1.701	0.035	0.001	0.009	4.004	0.894
RH−33	P−6C	56.40	1.71	0.03	6.05	0.01	34.37	1.12	0.00	0.17	99.86	1.950	0.070	0.001	0.175	0.000	1.771	0.041	0.000	0.005	4.012	0.910
RH−35	P−1C	55.14	3.36	0.07	6.73	0.06	32.89	0.93	0.04	0.24	99.46	1.920	0.138	0.002	0.196	0.002	1.707	0.035	0.003	0.007	4.008	0.897
Lower harzburgite zone																						
RH−37	P−4C	56.26	2.25	0.07	5.89	0.02	33.61	0.68	0.00	0.64	99.42	1.950	0.092	0.002	0.171	0.001	1.736	0.025	0.000	0.018	3.994	0.910
RH−39	P−17R	56.05	2.21	0.00	6.12	0.11	35.29	0.60	0.01	0.32	100.71	1.923	0.089	0.000	0.176	0.003	1.805	0.022	0.001	0.009	4.028	0.911
RH−40	P−26C	55.74	2.71	0.01	6.10	0.11	33.87	0.64	0.00	0.65	99.83	1.928	0.111	0.000	0.176	0.003	1.747	0.024	0.000	0.018	4.007	0.908
RH−42	P−4C	54.62	4.19	0.00	5.43	0.07	34.27	0.82	0.01	0.58	99.99	1.884	0.170	0.000	0.157	0.002	1.762	0.030	0.001	0.016	4.023	0.918
RH−43	P−26S	57.24	0.61	0.01	4.87	0.08	35.96	0.79	0.00	0.18	99.74	1.969	0.025	0.000	0.140	0.002	1.844	0.029	0.000	0.005	4.015	0.929
RH−44	P−23R	57.12	1.58	0.00	5.85	0.07	34.56	0.59	0.00	0.25	100.02	1.965	0.064	0.000	0.168	0.002	1.772	0.022	0.000	0.007	4.000	0.913
RH−45	P−27C	55.95	2.18	0.00	6.13	0.06	34.73	0.65	0.00	0.51	100.21	1.929	0.089	0.000	0.177	0.002	1.785	0.024	0.000	0.014	4.019	0.910
RH−46	P−28R	56.03	2.76	0.03	6.04	0.07	34.09	0.84	0.00	0.36	100.22	1.929	0.112	0.001	0.174	0.002	1.750	0.031	0.000	0.010	4.009	0.910
RH−47	P−12C	56.22	2.71	0.03	5.64	0.12	33.84	0.89	0.00	0.60	100.05	0.936	0.110	0.001	0.162	0.004	1.737	0.033	0.000	0.016	4.000	0.914
RH−48	P−14C	55.33	4.24	0.02	5.86	0.07	33.64	0.69	0.00	0.65	100.50	1.899	0.172	0.001	0.168	0.002	1.721	0.025	0.000	0.018	4.006	0.911
RH−49	P−22L	54.97	3.22	0.08	6.36	0.03	32.98	0.98	0.00	0.89	99.51	1.913	0.132	0.002	0.185	0.001	1.711	0.037	0.000	0.024	4.006	0.902
RH−50	P−12C	54.93	3.28	0.03	6.10	0.05	33.69	1.10	0.01	0.70	99.89	1.904	0.134	0.001	0.177	0.001	1.741	0.041	0.001	0.016	4.019	0.908

Table 4. (continued)

Sample	Point	SiO_2	Al_2O_3	TiO_2	FeO	MnO	MgO	CaO	Na_2O	Cr_2O_3	Total	Si	Al	Ti	Fe	Mn	Mg	Ca	Na	Cr	Total Cation	Mg#
Lower harzburgite zone																						
RH−51	P−16C	55.11	4.15	0.03	5.91	0.09	33.56	0.64	0.00	0.70	100.19	1.899	0.169	0.001	0.170	0.003	1.723	0.024	0.000	0.019	4.007	0.910
RH−52	P−11C	55.97	2.34	0.08	6.20	0.11	33.86	0.54	0.01	0.65	99.76	1.938	0.095	0.002	0.180	0.003	1.747	0.020	0.001	0.018	4.004	0.907
RH−53	P−19R	56.71	2.38	0.00	6.32	0.04	34.25	0.59	0.02	0.65	100.96	1.940	0.096	0.000	0.181	0.001	1.746	0.022	0.001	0.018	4.004	0.906
RH−54	P−23C	55.72	2.78	0.07	6.21	0.11	33.89	0.87	0.04	0.45	100.14	1.924	0.113	0.002	0.179	0.003	1.744	0.032	0.003	0.012	4.013	0.907
RH−55	P−7R	55.67	2.98	0.01	5.75	0.04	34.09	0.65	0.00	0.64	99.83	1.923	0.121	0.000	0.166	0.001	1.755	0.024	0.000	0.017	4.008	0.914
RH−59	POR C	56.75	0.98	0.02	5.35	0.08	35.93	0.51	0.00	0.35	99.97	1.953	0.040	0.001	0.154	0.002	1.843	0.019	0.000	0.010	4.022	0.923
RH−63	P−4C	56.16	2.72	0.01	5.56	0.02	34.18	0.64	0.00	0.58	99.87	1.935	0.110	0.000	0.160	0.001	1.756	0.024	0.000	0.016	4.002	0.916
RH−66	P−17C	56.16	2.88	0.06	5.58	0.00	34.09	0.50	0.04	0.70	100.01	1.932	0.117	0.002	0.161	0.000	1.748	0.018	0.003	0.019	4.000	0.916
RH−65	P−4C	55.59	2.38	0.00	5.56	0.00	33.49	1.40	0.00	0.59	99.01	1.937	0.098	0.000	0.162	0.000	1.740	0.052	0.000	0.016	4.006	0.915
RH−68	P−24C	56.42	3.22	0.00	5.50	0.04	34.43	0.73	0.00	0.75	101.09	1.922	0.129	0.000	0.157	0.001	1.748	0.027	0.000	0.020	4.004	0.918
RH−69	P−25	58.12	0.78	0.01	5.16	0.00	35.33	1.08	0.00	0.42	100.90	1.978	0.031	0.000	0.147	0.000	1.793	0.039	0.000	0.011	4.000	0.924

Ferric and ferrous irons of spinel are calculated to satisfy the stoichiometry. The compositional range of Cr# (Cr/(Cr+Al) ratio) and Mg# (Mg/(Mg+Fe^{2+}) ratio) in spinels in the Red Hills are overlapped with the ranges of ocean floor peridotites (Dick & Bullen, 1984) excepting the most refractory dunite in the lower zone (**Fig. 17**). The ferric iron content also is the same as that in oceanic one except for common dunite in the upper zone (**Fig. 18**). The TiO_2 content of spinel in the harzburgites in the upper zone show higher than that in the lower zone (**Fig. 16 b** and **19**). Spinel in plagioclase bearing harzburgite in the lower zone is enriched by TiO_2 than plagioclase free harzburgite in same zone. Furthermore, spinel in plagioclase bearing dunite in the upper zone is characterized by high TiO_2 content (~0.7wt%). The most refractory dunite (e.g., RH-43) in the lower zone is enriched by TiO_2 as compared with the neighboring harzburgite (RH-44).

Orthopyroxene (Table 4)

Orthopyroxene has concordant Mg# (Mg/(Mg+Fe) ratio) with that of olivine (**Fig. 16 a**). Harzburgite in the lower zone has Mg#=0.91, and the dunite shows higher value (Mg#=0.93). On the contraty, the Mg# of olivine clinopyroxenite in the upper zone shows the lowest value (Mg#=0.87~0.89). Orthopyroxene shows zoning on Al_2O_3 content. The Al_2O_3 content in harzburgites in both upper and lower zones decrease from core to rim. Orthopyroxenes in olivine clinopyroxenite and clinopyroxene bearing dunite in the upper zone, however, do not show the obvious zoning. The Al_2O_3 contents in orthopyrox-

ene in these rocks are almost constant. Relationships between modal compositions of olivones and Al_2O_3 contents in orthopyroxenes in harzburgite and dunite in the lower zone are recognized (**Fig. 20**). Namely, there is negative correlation between the modal olivine and Al_2O_3 contents of the co-existing orthopyroxene. This agrees with the relationship from present oceanic peridotites, that means residual harzburgite trend (Dick et al., 1984).

Clinopyroxene (Table 5)

The Mg# (Mg/(Mg+Fe) ratio) of clinopyroxene is generally magnesian as compared with that of olivine and orthopyroxene (**Fig. 16 a**). The Mg# of clinopyroxene in the harzburgite in the lower zone is 0.93~0.94, while the dunite and the most refractory harzburgite has Mg#=0.96. On the other hand, dunite and plagioclase bearing dunite in the upper zone shows Mg#=0.93~0.94, and the olivine clinopyroxenite and the clinopyroxene bearing dunite has Mg#=0.90~0.93. Trend of the Mg# on the whole upper zone displays that the ratio is gradually decreased to the upwards (**Fig. 16 a**). The Al_2O_3 contents of clinopyroxene in the whole body show zoning that the content decreases from core to rim. Plagioclase bearing harzburgite in the lower zone shows higher Na_2O and TiO_2 contents, and the most refractory dunite (RH-43) in the lower zone is characterized by the highest Na_2O content (**Fig. 16 b**). Common dunite and plagioclase bearing dunite in the upper

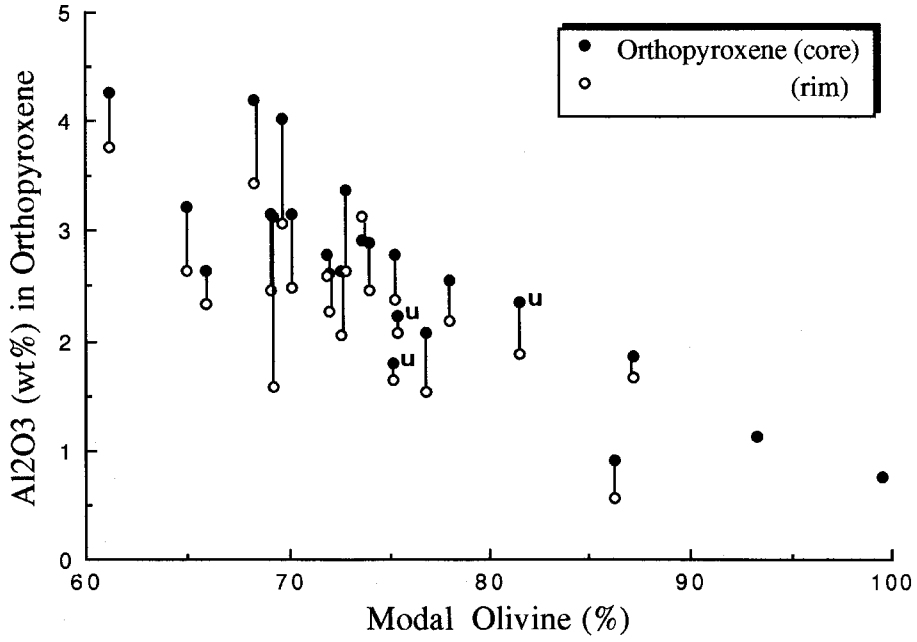

Fig.20. Modal olivine in harzburgite samples plotted versus Al_2O_3 in orthopyroxenes. Individual data points composing the averages in each sample are plotted. Data points with **u** represent those from blocky harzburgites in the upper zone of the Red Hills peridotite.

Table 5. Representative election microprobe analyses of clinopyroxenes in the Red Hills peridotite

Sample	Point	SiO_2	Al_2O_3	TiO_2	FeO	MnO	MgO	CaO	Na_2O	Cr_2O_3	Total	Si	Al	Ti	Fe	Mn	Mg	Ca	Na	Cr	Total Cation	Mg#
Upper dunite predominated zone																						
RH−03	P−26R	53.37	2.97	0.38	2.73	0.02	17.07	23.63	0.32	0.29	100.78	1.926	0.126	0.010	0.082	0.001	0.918	0.914	0.022	0.008	4.008	0.918
RH−04	P−7C	53.24	3.47	0.01	3.01	0.02	16.83	23.23	0.27	0.69	100.77	1.922	0.148	0.000	0.091	0.001	0.906	0.898	0.019	0.020	4.004	0.909
RH−06	P−16C	53.09	2.79	0.21	2.49	0.00	17.28	23.36	0.38	0.94	100.54	1.921	0.119	0.006	0.075	0.000	0.932	0.906	0.027	0.027	4.013	0.925
RH−10p	P−4R	52.42	3.43	0.19	2.76	0.01	16.73	24.12	0.18	0.88	100.72	1.900	0.147	0.005	0.084	0.000	0.904	0.937	0.013	0.025	4.015	0.915
RH−11	P−16C	53.14	3.39	0.12	3.88	0.01	16.85	22.83	0.21	0.65	101.08	1.918	0.144	0.003	0.117	0.000	0.906	0.883	0.015	0.019	4.005	0.886
RH−13	P−4C	52.89	2.90	0.12	2.65	0.00	17.10	23.02	0.23	0.93	99.84	1.926	0.124	0.003	0.081	0.000	0.928	0.898	0.016	0.027	4.003	0.920
RH−15	P−18C	52.36	3.21	0.37	3.12	0.05	17.13	22.89	0.34	0.96	100.43	1.902	0.137	0.010	0.095	0.002	0.928	0.891	0.024	0.028	4.017	0.907
RH−17	P−4C	51.89	3.70	0.35	2.51	0.09	16.33	23.29	0.46	1.06	99.68	1.898	0.160	0.010	0.077	0.003	0.890	0.913	0.033	0.031	4.013	0.921
RH−18	P−14C	51.69	3.83	0.09	2.88	0.00	16.75	23.09	0.16	0.87	99.36	1.896	0.166	0.002	0.088	0.000	0.916	0.907	0.011	0.025	4.012	0.912
RH−19	P−19R	52.55	2.92	0.04	2.73	0.02	17.08	23.47	0.15	0.79	99.75	1.919	0.126	0.001	0.083	0.001	0.930	0.918	0.011	0.023	4.011	0.918
RH−20	P−21S	53.62	1.97	0.09	1.84	0.04	16.56	24.68	0.37	0.99	100.16	1.949	0.084	0.002	0.056	0.001	0.897	0.961	0.026	0.028	4.005	0.941
RH−21	P−1IN	53.26	2.90	0.10	2.25	0.00	15.98	24.98	0.29	0.48	100.24	1.935	0.124	0.003	0.068	0.000	0.866	0.973	0.020	0.014	4.003	0.927
RH−22	P−2IN	53.49	2.40	0.10	1.95	0.02	16.59	24.55	0.29	0.95	100.34	1.940	0.103	0.003	0.059	0.001	0.897	0.954	0.020	0.027	4.003	0.938
RH−23	P−21C	52.28	3.51	0.08	2.98	0.13	16.49	22.94	0.25	0.75	99.41	1.915	0.152	0.002	0.091	0.004	0.901	0.900	0.018	0.022	4.005	0.908
RH−24	P−3	52.23	3.08	0.10	2.43	0.04	16.84	23.39	0.25	0.80	99.16	1.917	0.133	0.003	0.075	0.001	0.921	0.920	0.018	0.023	4.011	0.925
RH−25	P−4C	51.93	3.07	0.03	3.02	0.06	17.58	22.23	0.08	0.94	98.94	1.910	0.133	0.001	0.093	0.002	0.964	0.876	0.006	0.027	4.012	0.912
RH−27	P−3C	53.02	3.23	0.08	2.44	0.12	17.25	23.23	0.21	1.08	100.66	1.915	0.138	0.002	0.074	0.004	0.929	0.899	0.015	0.031	4.006	0.926
RH−28	P−3C	52.14	3.95	0.58	2.04	0.00	15.16	24.34	0.41	0.95	99.57	1.907	0.170	0.016	0.062	0.000	0.827	0.954	0.029	0.027	3.993	0.930
RH−29	P−20C	53.64	2.74	0.09	2.88	0.11	16.94	23.48	0.09	0.30	100.27	1.943	0.117	0.002	0.087	0.003	0.915	0.911	0.006	0.009	3.995	0.913
RH−31	P−15R	52.95	3.15	0.00	2.39	0.05	16.87	23.86	0.16	0.44	99.87	1.927	0.135	0.000	0.073	0.002	0.915	0.930	0.011	0.013	4.005	0.926
RH−32	P−3S	52.54	1.97	0.05	1.60	0.00	17.16	24.87	0.36	0.87	99.42	1.927	0.085	0.001	0.049	0.000	0.938	0.977	0.026	0.025	4.029	0.950
RH−33	P−3C	54.13	2.25	0.00	2.07	0.02	17.60	23.39	0.15	0.49	100.10	1.956	0.096	0.000	0.063	0.001	0.948	0.906	0.011	0.014	3.994	0.938
RH−34	P−20C	52.90	3.54	0.07	2.68	0.01	16.77	23.28	0.27	0.37	99.89	1.923	0.152	0.002	0.081	0.000	0.909	0.907	0.019	0.011	4.003	0.918
RH−35	P−2C	52.05	4.05	0.06	2.42	0.06	16.69	23.38	0.17	0.42	99.30	1.904	0.175	0.002	0.074	0.002	0.910	0.916	0.012	0.012	4.007	0.925
RH−36	P−1C	54.39	1.20	0.09	1.88	0.00	17.84	24.49	0.02	0.18	100.09	1.970	0.051	0.002	0.057	0.000	0.963	0.950	0.001	0.005	4.000	0.944

Table 5. (continued)

Sample	Point	SiO_2	Al_2O_3	TiO_2	FeO	MnO	MgO	CaO	Na_2O	Cr_2O_3	Total	Si	Al	Ti	Fe	Mn	Mg	Ca	Na	Cr	Total Cation	Mg#
								Lower harzburgite zone														
RH−37	P−5C	51.52	4.27	0.08	2.20	0.01	16.30	23.42	0.20	1.20	99.20	1.890	0.185	0.002	0.067	0.000	0.891	0.921	0.014	0.035	4.005	0.930
RH−38	P−33L	53.59	2.90	0.03	2.13	0.00	17.04	23.50	0.26	1.07	100.52	1.934	0.123	0.001	0.064	0.000	0.917	0.909	0.018	0.031	3.997	0.934
RH−39	P−18R	53.07	2.57	0.06	2.05	0.03	16.59	24.25	0.25	0.78	99.65	1.937	0.111	0.002	0.063	0.001	0.903	0.948	0.018	0.023	4.004	0.935
RH−40	P−28R	52.87	3.02	0.06	2.63	0.11	17.66	23.16	0.18	1.13	100.82	1.910	0.129	0.002	0.079	0.003	0.951	0.896	0.013	0.032	4.015	0.923
RH−42	P−15R	51.48	4.34	0.08	2.16	0.07	17.19	23.60	0.09	0.87	99.88	1.876	0.186	0.002	0.066	0.002	0.934	0.921	0.006	0.025	4.019	0.934
RH−43	P−24S	53.96	0.82	0.00	1.45	0.01	17.76	24.36	0.40	0.42	99.18	1.974	0.035	0.000	0.044	0.000	0.968	0.955	0.028	0.012	4.017	0.956
RH−44	P−27C	53.52	1.72	0.06	1.68	0.10	17.43	24.40	0.03	0.62	99.56	1.951	0.074	0.002	0.051	0.003	0.947	0.953	0.002	0.018	4.002	0.949
RH−45	P−19R	54.29	1.58	0.02	1.81	0.06	18.01	24.36	0.02	0.49	100.64	1.956	0.067	0.001	0.055	0.002	0.967	0.941	0.001	0.014	4.003	0.947
RH−46	P−25R	52.89	2.61	0.07	1.85	0.05	16.89	24.41	0.03	0.45	99.25	1.935	0.113	0.002	0.057	0.002	0.921	0.957	0.002	0.013	4.001	0.942
RH−47	P−30R	52.12	2.87	0.02	1.96	0.02	17.14	24.29	0.12	0.54	99.08	1.915	0.124	0.001	0.060	0.001	0.939	0.956	0.009	0.016	4.019	0.940
RH−48	P−32C	51.92	4.37	0.16	2.12	0.05	15.93	24.45	0.07	0.98	100.05	1.890	0.188	0.004	0.065	0.002	0.865	0.954	0.005	0.028	4.000	0.931
RH−49	P−23C	52.52	3.11	0.14	2.09	0.00	17.25	23.44	0.10	0.77	99.42	1.918	0.134	0.004	0.064	0.000	0.939	0.917	0.007	0.022	4.004	0.936
RH−50	P−21C	52.02	3.50	0.14	2.41	0.02	17.89	22.63	0.06	1.14	99.81	1.894	0.150	0.004	0.073	0.001	0.971	0.883	0.004	0.033	4.013	0.930
RH−51	P−19R	51.43	4.55	0.13	2.16	0.05	16.45	23.80	0.13	0.99	99.69	1.878	0.196	0.004	0.066	0.002	0.896	0.931	0.009	0.029	4.010	0.931
RH−52	P−12L	51.87	3.08	0.16	1.87	0.03	17.04	24.01	0.16	1.06	99.28	1.903	0.133	0.004	0.057	0.001	0.932	0.944	0.011	0.031	4.016	0.942
RH−53	P−21C	52.51	3.71	0.13	2.01	0.03	16.96	23.53	0.20	1.09	100.17	1.904	0.159	0.004	0.061	0.001	0.917	0.914	0.014	0.031	4.004	0.938
RH−54	P−20C	51.43	4.77	0.11	2.05	0.03	16.70	23.21	0.24	1.12	99.66	1.876	0.205	0.003	0.063	0.001	0.908	0.907	0.017	0.032	4.011	0.936
RH−55	P−2R	52.64	3.22	0.03	2.10	0.06	16.99	23.97	0.04	0.80	99.85	1.916	0.138	0.001	0.064	0.002	0.922	0.935	0.003	0.023	4.004	0.935
RH−59	P−11L	54.39	0.93	0.06	1.57	0.04	18.30	24.43	0.06	0.54	100.32	1.966	0.040	0.002	0.047	0.001	0.986	0.946	0.004	0.015	4.007	0.954
RH−63	P−5C	52.36	3.03	0.01	1.82	0.00	16.89	23.96	0.03	1.00	99.10	1.919	0.131	0.000	0.056	0.000	0.923	0.941	0.002	0.029	4.001	0.943
RH−66	P−21C	52.90	3.50	0.02	2.02	0.01	17.20	23.25	0.09	0.99	99.98	1.917	0.150	0.001	0.061	0.000	0.929	0.903	0.006	0.028	3.996	0.938
RH−65	P−11R	53.38	2.30	0.00	1.91	0.00	17.63	23.65	0.03	0.92	99.82	1.939	0.098	0.000	0.058	0.000	0.955	0.921	0.002	0.026	3.999	0.943
RH−68	P−22R	52.84	3.21	0.06	2.06	0.01	17.82	23.39	0.03	0.84	100.26	1.912	0.137	0.002	0.062	0.000	0.961	0.907	0.002	0.024	4.007	0.939

Table 6. Representative electron microprobe analyses of plagioclases in the Red Hills peridotite

Sample	Point	SiO_2	Al_2O_3	CaO	Na_2O	K_2O	Total	Si	Al	Ca	Na	K	Total Cation	An
					Upper dunite predominated zone									
RH−03	5	47.75	33.37	17.17	1.97	0.00	100.26	2.185	1.800	0.842	0.175	0.000	5.002	82.81
RH−12	3	47.52	33.30	16.57	2.12	0.01	99.52	2.188	1.807	0.818	0.189	0.001	5.003	81.20
RH−15	3	46.62	33.06	17.30	1.87	0.01	98.86	2.168	1.812	0.862	0.169	0.001	5.011	83.64
RH−17	1	48.83	33.73	17.12	2.08	0.00	101.76	2.199	1.790	0.826	0.182	0.000	4.997	81.98
RH−24	1	45.80	35.11	18.75	0.96	0.00	100.62	2.097	1.895	0.920	0.085	0.000	4.998	91.52
RH−28	4	46.04	34.50	18.17	1.31	0.00	100.02	2.119	1.872	0.896	0.117	0.000	5.004	88.46
RH−34	1	44.54	34.26	18.37	0.93	0.01	98.11	2.093	1.898	0.925	0.085	0.001	5.001	91.61
RH−36	4	44.80	35.40	19.54	0.54	0.00	100.28	2.064	1.922	0.965	0.048	0.000	4.999	95.24
					Lower harzburgite zone									
RH−37	4	44.54	35.62	18.87	0.62	0.00	99.65	2.061	1.943	0.936	0.056	0.000	4.995	94.39
RH−40	2	44.49	35.91	19.16	0.56	0.00	100.12	2.051	1.951	0.946	0.050	0.000	4.999	94.98
RH−49	1	43.79	36.02	19.67	0.31	0.00	99.79	2.029	1.967	0.977	0.028	0.000	5.001	97.23
RH−50	4	43.66	35.68	20.03	0.15	0.01	99.53	2.030	1.956	0.998	0.014	0.001	4.999	98.66
RH−52	1	43.93	35.78	19.31	0.31	0.00	99.33	2.042	1.960	0.962	0.028	0.000	4.992	97.18
RH−53	4	44.35	35.95	19.62	0.41	0.00	100.33	2.043	1.952	0.968	0.037	0.000	5.000	96.36
RH−54	3	44.81	35.84	19.99	0.25	0.00	100.89	2.053	1.935	0.981	0.022	0.000	4.991	97.79

Table 7. Representative electron microprobe analyses of amphiboles in the Red Hills peridotite

Sample	Point	SiO_2	Al_2O_3	TiO_2	FeO*	MnO	MgO	CaO	Na_2O	K_2O	Cr_2O_3	NiO	Total	Si	Al	Ti	Fe	Mn	Mg	Ca	Na	K	Cr	Ni	Total Cation	Mg#
Upper dunite predominated zone																										
RH−03	3	44.30	12.90	1.71	4.43	0.00	16.55	11.93	2.66	0.00	1.99	0.00	96.47	6.365	2.185	0.185	0.532	0.000	3.545	1.837	0.741	0.000	0.226	0.000	15.615	86.94
RH−12	2	45.00	12.92	1.33	3.51	0.02	18.49	12.46	3.06	0.00	0.85	0.00	97.64	6.362	2.153	0.141	0.415	0.002	3.897	1.888	0.839	0.000	0.095	0.000	15.792	90.37
RH−15	4	44.75	12.44	1.23	4.16	0.00	18.23	12.38	2.55	0.00	1.36	0.00	97.10	6.379	2.090	0.132	0.496	0.000	3.874	1.891	0.705	0.000	0.153	0.000	15.720	88.65
RH−17	2	43.78	16.15	1.33	3.41	0.00	18.17	11.57	3.04	0.02	1.89	0.07	96.43	6.278	2.223	0.143	0.409	0.000	3.884	1.778	0.845	0.004	0.214	0.008	15.785	90.47
RH−24	4	44.71	13.57	0.41	3.74	0.01	18.24	12.66	2.90	0.13	1.08	0.02	97.47	6.343	2.269	0.044	0.444	0.001	3.858	1.925	0.798	0.024	0.121	0.002	15.828	89.68
RH−28	3	42.44	13.82	1.78	3.77	0.00	17.44	12.93	3.46	0.00	1.73	0.00	97.37	6.085	2.336	0.192	0.452	0.000	3.728	1.987	0.962	0.000	0.196	0.000	15.938	89.18
RH−36	4	47.23	12.14	0.03	3.67	0.06	19.02	12.82	1.92	0.02	0.16	0.03	97.10	6.653	2.016	0.003	0.432	0.007	3.994	1.935	0.524	0.004	0.018	0.003	15.591	90.23

zone show higher Na_2O content, while olivine clinopyroxenite and clinopyroxene bearing dunite is characterized by low Na_2O and TiO_2 contents. Harzburgite in the upper zone has significantly high Na_2O and TiO_2 contents than that in the lower zone. Clinopyroxene in the plagioclase bearing dunite is particularly enriched by TiO_2 content. The variations of Na_2O and TiO_2 contents in clinopyroxenes are consistent with that of TiO_2 contents in spinels.

Plagioclase (Table 6)

Plagioclase occurs in harzburgite in upper part of the lower zone and in dunite and gabbro in the upper zone. The domain of plagioclase is characterized by the "drop" or "amoeba" shapes in the harzburgite and the dunite. The plagioclases in harzburgite in the lower zone show high An (100*Ca/(Ca+Na) ratio) contents (An=98~95), while dunite in the upper zone has plagioclases of much wider compositional variation (An=95~80). The An contents in both harzburgite and dunite correlate with Na_2O and TiO_2 contents in coexisting clinopyroxene. Calcic plagioclase (high An) is coexisting with clinopyroxene having low sodium content. The An contents increase from lower to higher as a function of the stratigraphic level of the Red Hills body (**Fig. 16 b**).

Amphibole (Table 7)

Amphiboles are found in plagioclase bearing dunite as rims of plagioclase patches. They are pargasite to pargasitic hornblende (**Fig. 21**). The compositional range of Mg# is 0.86~0.92. There is no correlation with Fo contents of olivine. The TiO_2 contents are 0.7~2.1wt% while K_2O contents are lower than 0.03wt% excepting that of one sample (RH-24). This tendency that is the high TiO_2 content with the low K_2O content agrees with the character of mid-ocean ridge basalts (Ozawa, 1988).

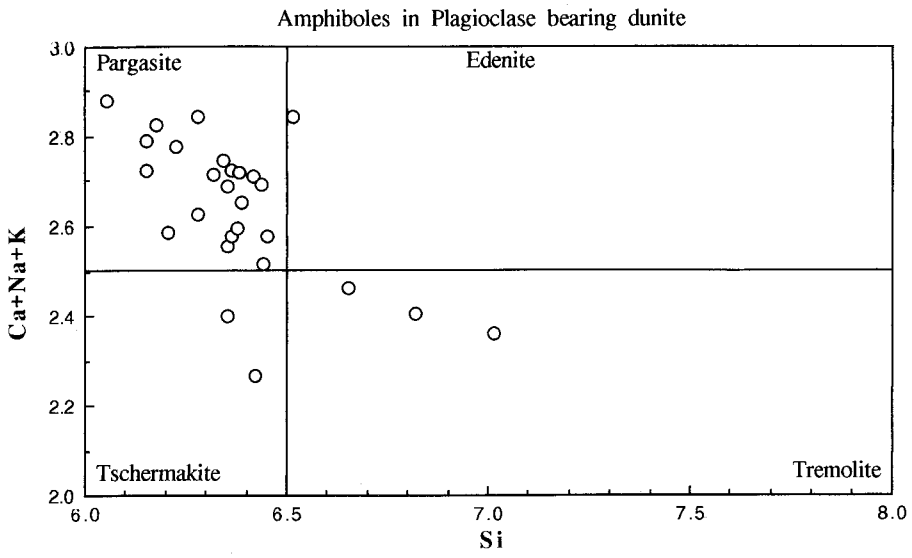

Fig.21. Compositions of amphiboles in plagioclase bearing dunite. Most compositions are ranging from pargasite to pargasitic hornblende. The classification of amphiboles is based on Leake (1978).

5. GEOCHEMISTRY OF THE RED HILLS PERIDOTITE AND THE LEE RIVER GROUP

5−1. Sample Descriptions and the Preparations

Sample descriptions

Clinopyroxenes are scattered in dunite in the upper zone of the Red Hills peridotite body for various proportions. For example, clinopyroxene rich part is suitable for the rock name of "olivine clinopyroxenite" (e.g., RH−23) while the scarce part is almost "dunite" (e.g., RH−13). The modes of clinopyroxenes often show gradual change in order of a few centimeter. There is occurrence of olivine clinopyroxenite dike (e.g., RH−29) in dunite. In this case, the boundary between olivine-clinopyroxenite and dunite is sharp. Furthermore, gabbroic dike (RH−03) scarcely occurs in the uppermost part of the upper zone. Plagioclase bearing dunite (e.g., RH−17) does almost not accompany clinopyroxene. There is no relationship between both occurrences of minerals. Gashes of plagioclases rarely cut clinopyroxene bearing dunite (e.g., RH−34) where the both minerals are recognized at same domain. In this case, the plagioclase is formed at later stage than clinopyroxene in the dunite.

It is recognized that clinopyroxene in dunite of the upper zone sometimes displays magmatic twin. The shape of clinopyroxene is xenomorphic to hypidiomorphic, and the grain size is larger than surrounding olivine. Clinopyroxene in the harzburgite of the lower zone is shown as porphyroclasts. Plagioclases in both dunite in the upper zone and harzburgite in the lower zone occurs as domains of oval or drop shapes, and develop twins.

Samples used for mineral separation are selected less altered one. Clinopyroxene grains are developed by crevages of orthopyroxene, but are not included any altered products such as serpentines.

Basalts and diabases from the Lee River Group used for Sr and Nd isotope analyses are also selected less altered one. The basalts show intergranular texture composed of plagioclase laths and granular clinopyroxenes. The diabases display medium to coarse grained subophitic texture. The latter includes greenish amphibole replacing clinopyroxene. The amphibole is probably formed by ocean floor metamorphism. The basalts and diabases make dike swarm at the Roding River area. Samples from the Lee River Group in the Roding River area are selected along the stratigraphic height. According to sample numbers of ROR from 01 to 15, the samples represent shallower to deeper level of the swarm.

Sample preparations

Rock samples are cut by using rock trimmer to 2～3cm size, and are selected unweathered and un-altered pieces. After washing the rock pieces by distilled water they are

crushed by tungsten-carbide mill as samples for analysis of major and trace element. Samples for analysis of whole rock major elements dried up overnight at 105℃ and make fused disc with JMC flux 105. Samples for analysis of trace elements are applied pressed powder pellet by means of Mowiol binder.

Clinopyroxene and plagioclase are separated by using isodynamic magnetic separator. Purity of the separates is over 95% for both minerals. Plagioclase separates, however, include some saussuritized one. Samples are totally saved from any alterations and metamorphisms. As the original mineral assemblage is olivine+orthopyroxene+clinopyroxene+spinel, clinopyroxene is the mineral concentrating incompatible elements in that mineral assemblage. Then, the purity of the separates must be enough to measure of abundances of REEs and Sr isotope ratios. Separated minerals are leacheed as following procedures that correspond to Reisburg and Zindler (1986). Clinopyroxene leached for 1 hour in hot 2.5N-HCl, and ultrasonically agitated for 10 minutes in distilled water. After that, the separates are re-leached for 20 minutes in cold 5% HF and are washed in distilled water for several times under ultrasonic bath. Moreover, that is re-leached for 15 minutes in hot 6N-HCl, and rinsed repeatedly with distilled water by means of ultrasonic bath. Finally the leached mineral rinsed with pure water that is distilled re-ionized water under sub-boiling condition. HF leaching step is skipped for plagioclase.

Analytical procedures

Concentrations of major and trace elements of whole rocks were determined by X-ray fluorescence spectrometer in Geology Department, University of Otago, New Zealand. Sr isotope ratios and Sr, Sm and Nd concentrations of minerals were analyzed by two mass spectrometers, MAT260m (modified from MAT260; Kagami et al., 1982) and MAT261 with single collectors in Institute for Study of the Earth's Interior, Okayama University. The Nd isotope ratios were measured using multi collector of MAT260 enhanced (upgraded from MAT260m). Separation procedure of each element followed to Kagami et al. (1982, 1987). Total blanks of Sr, Sm and Nd during whole procedures are: <750pg, <50pg and <200pg, respectively. The $^{87}Sr/^{86}Sr$ ratios were normalized to $^{86}Sr/^{88}Sr=0.1194$. The

Table 8. Analytical results of standard samples

Sample	Rb	Sr	$^{87}Sr/^{86}Sr$	2sigma	Sm	Nd	$^{143}Nd/^{144}Nd$	2sigma
BCR-1 (1)			0.705078	16				
BCR-1 (2)	47.13	328.21	0.705014	23	6.47	28.70		
JB-1a (1)							0.512766	6
JB-1a (2)							0.512769	26
JB-1a (3)							0.512765	9
NBS987 (1)			0.710243	32				
NBS987 (2)			0.710254	13				

Concentrations are in ppm.

$^{87}Sr/^{86}Sr$ ratios of NBS 987 during this research were 0.71024 to 0.71025. The Nd isotope ratios were normalized to $^{146}Nd/^{144}Nd = 0.7219$. The standard results are shown in **Table 8**. Concentrations of REEs (especially, Eu, Yb and Lu) in clinopyroxenes are determined by instrumental neutron activation analysis (INAA). The neutron source used was the Musashi Institute of Technology Research Reactor (TRIGA MarkII). The γ-ray measurement of each sample was carried a Ge(Li) semiconductor radiation detector and a 4096 channel pulse-height analyzer. Each counting time was 1000 seconds and 2000 seconds for the short and the long lived nuclides measurements, respectively. The standard counting errors are as follows; 20% for Eu, 15% for Yb and 10% for Lu.

5-2. Red Hills Peridotite

5-2-1. Whole Rock Chemistry

Major elements

Whole rock major element concentrations are shown in **Table 9**. All harzburgites in the lower zone of the Red Hills peridotite body show high MgO contents, and low Al_2O_3 and CaO contents. Compositions of major elements of the harzburgites are quite homogeneous. Plagioclase bearing harzburgite has the less refractory composition. That is characterized by lower MgO contents, and higher SiO_2, Al_2O_3 and CaO contents than the plagioclase free harzburgite. The compositional ranges are similar to that of harzburgites from worldwide ophiolites.

Rocks in the upper zone show wide compositionl range. Chemical compositions of clinopyroxene bearing dunite depend upon abundances of clinopyroxenes, and show higher CaO and Al_2O_3 contents than that of harzburgites from the lower zone of the body. Chemical variation of plagioclase bearing dunites is controlled by abundance of plagioclase, and the rocks show high Al_2O_3 contents. Chemical compositions of harzburgite that occurs as blocks and is infiltrated by dunite in the upper zone, differ from harzburgites in the lower zone of the body. Harzburgites in the upper zone are characterized by lower Al_2O_3 and CaO contents on same MgO contents than harzburgites in the lower zone. As shown in **Figure 22**, chemical variations of the harzburgites in the upper zone make different trend from that of harzburgites in the lower zone of the body.

Trace elements

Results are shown in **Table 9**. Harzburgites in the lower zone of the body have homogeneous compositions on Ni, Sc, Cu, Zn, Cr and V. On the other hand, rocks in the upper zone have wide compositional range on those elements (**Fig. 23**). Chemial variation of harzburgites in the upper zone make different trend on vanadium from that of harzburgite in the lower zone of the body as well as Al_2O_3 and CaO contents.

Table 9. Major* and trace** element abundances in samples of the Red Hills peridotite

SP. NO.	Code	SiO_2	TiO_2	Al_2O_3	Fe_2O_3	MnO	MgO	CaO	Na_2O	K_2O	P_2O_5	LOI	Total	Mg#	V	Sc	Cr	Ni	Cu	Zn
Upper dunite predominated zone																				
RH−03	GAB	44.40	0.13	13.39	4.96	0.08	18.71	13.12	2.15	0.03	0.02	2.71	99.70	0.882	102	24	1909	885	142	22
RH−04	CPX	49.64	0.03	3.01	5.41	0.11	22.20	17.65	0.10	0.01	0.02	1.28	99.46	0.891	159	41	3723	874	142	21
RH−06	UZH	41.72	0.06	0.80	9.37	0.15	4208	0.84	0.00	0.00	0.00	4.61	99.63	0.899	44	9	2400	2214	5	44
RH−08	UZH	42.05	0.04	0.49	9.51	0.14	46.56	0.50	0.00	0.00	0.00	1.68	100.97	0.907		7		2517	4	41
RH−11	CPX	48.95	0.11	2.51	6.55	0.13	23.85	16.15	0.00	0.00	0.01	2.10	100.36	0.878	185	45	3760	796	246	27
RH−12	PLD	39.85	0.05	4.39	10.52	0.15	42.01	2.12	0.07	0.00	0.00	1.40	100.56	0.888		6		2096	76	46
RH−13	CPD	42.61	0.06	1.21	9.41	0.15	40.27	5.28	0.00	0.00	0.00	0.14	99.13	0.895		18		2053	50	38
RH−15	PLD	40.03	0.07	3.91	11.35	0.17	41.08	2.63	0.23	0.00	0.00	0.00	99.47	0.878	58	9	4680	2323	85	51
RH−17	PLD	40.04	0.06	3.26	11.18	0.17	43.52	1.86	0.38	0.00	0.00	0.02	100.49	0.885	52	9	4910	2237	119	52
RH−18	CPD	43.88	0.03	1.43	9.48	0.15	38.04	6.91	0.03	0.00	0.00	0.01	99.96	0.888	77	21	2849	1717	76	42
RH−19	CPD	42.49	0.04	1.18	9.74	0.15	39.96	5.59	0.00	0.00	0.00	0.15	99.30	0.891	66	18	3361	1994	64	44
RH−20	UZD	39.62	0.04	0.45	9.72	0.15	49.13	0.15	0.00	0.00	0.00	0.00	99.26	0.909	24	4	4704	3383	5	42
RH−21	UZD	39.69	0.04	0.40	10.97	0.16	48.45	0.16	0.00	0.00	0.00	0.00	99.87	0.898	21	4	2712	2417	70	47
RH−22	UZD	39.57	0.05	0.52	9.70	0.15	49.02	0.14	0.00	0.00	0.00	0.44	99.59	0.909	25	6	4723	3084	4	41
RH−23	CPX	49.40	0.07	3.00	5.87	0.13	24.04	16.33	0.30	0.04	0.02	0.15	99.35	0.890	182	43	5367	963	136	24
RH−24	PLD	39.48	0.03	5.07	9.73	0.14	40.53	2.72	0.00	0.02	0.00	1.50	99.22	0.892	27	6	2362	2029	20	42
RH−25	CPD	43.93	0.06	1.31	9.61	0.15	37.26	7.40	0.00	0.01	0.00	0.00	99.73	0.885	98	23	3572	1760	141	39
RH−26	UZD	38.30	0.06	0.78	12.67	0.18	45.25	0.20	0.00	0.00	0.00	2.13	99.57	0.876	37	6	3416	2192	49	51
RH−27	UZH	43.16	0.05	0.73	10.94	0.15	43.71	1.11	0.00	0.00	0.00	0.15	100.00	0.888	48	10	2597	2284	15	46
RH−28	PLD	40.30	0.05	1.80	11.44	0.17	46.62	1.15	0.00	0.00	0.00	0.00	101.53	0.890		10		2640	43	49
RH−29	CPX	49.49	0.07	2.23	6.03	0.13	24.15	17.01	0.00	0.00	0.02	0.38	99.51	0.888	213	48	5864	973	320	22
RH−30	UZH	42.05	0.04	0.61	9.14	0.13	43.01	0.72	0.00	0.00	0.00	4.31	100.01	0.903	42	10	2363	2460	6	45
RH−32	UZD	40.21	0.04	0.19	9.75	0.14	49.26	0.20	0.00	0.01	0.00	0.16	99.96	0.909	15	5	1554	3189	9	43
RH−33	UZH	43.47	0.04	0.61	10.29	0.14	44.21	0.67	0.00	0.00	0.00	0.44	99.87	0.895	40	9	2462	2385	3	44
RH−34	CPD	45.99	0.06	2.94	7.53	0.13	31.86	10.93	0.00	0.00	0.00	0.00	99.44	0.893	95	34	4141	1384	62	33
RH−35	CPD	46.80	0.05	2.32	7.04	0.12	31.01	12.27	0.06	0.03	0.01	0.09	99.80	0.897	99	30	3718	1285	209	26
RH−36	PLD	40.43	0.05	3.19	11.38	0.17	41.37	3.36	0.00	0.00	0.00	1.05	101.00	0.878		10		2136	201	42

Table 9. (continued)

SP. NO.	Code	SiO_2	TiO_2	Al_2O_3	Fe_2O_3	MnO	MgO	CaO	Na_2O	K_2O	P_2O_5	LOI	Total	Mg#	V	Sc	Cr	Ni	Cu	Zn
					Lower harzburgite zone															
RH−37	PLH	45.31	0.04	1.84	8.68	0.13	42.46	2.05	0.00	0.00	0.00	0.05	100.56	0.907		11		2320	15	40
RH−40	PLH	44.43	0.04	1.94	8.94	0.13	42.07	2.22	0.49	0.04	0.00	0.03	100.33	0.903	69	11	2683	2316	19	42
RH−43	LZD	40.55	0.03	0.16	8.58	0.12	49.95	0.12	0.00	0.00	0.00	0.24	99.75	0.920	17	4	2813	2942	4	41
RH−44	LZH	43.22	0.04	0.58	8.98	0.14	45.81	1.21	0.00	0.01	0.00	0.06	100.05	0.910	44	10	2535	2562	6	40
RH−45	LZH	43.94	0.04	0.73	8.95	0.14	45.48	1.11	0.00	0.00	0.00	0.00	100.39	0.910	56	10	2722	2507	7	42
RH−46	LZH	44.47	0.05	1.34	8.70	0.13	44.30	1.60	0.00	0.00	0.00	0.00	100.59	0.910	62	12	2805	2404	16	41
RH−47	LZH	44.22	0.04	0.90	8.87	0.14	44.73	1.23	0.00	0.00	0.00	0.00	100.13	0.909	54	9	2645	2511	19	42
RH−48	LZH	44.83	0.04	1.81	8.70	0.14	42.55	2.12	0.00	0.00	0.00	0.00	100.19	0.907	73	11	2916	2330	21	43
RH−49	PLH	44.12	0.05	1.78	8.84	0.13	42.97	2.02	0.00	0.00	0.00	0.00	99.91	0.906	68	11	2530	2347	21	43
RH−50	PLH	44.57	0.06	1.96	8.82	0.14	42.77	2.13	0.00	0.00	0.00	0.00	100.45	0.906	71	12	2631	2326	22	43
RH−51	LZH	44.05	0.05	1.68	8.80	0.14	43.38	1.88	0.00	0.00	0.00	0.10	100.08	0.907	69	12	2813	2416	22	43
RH−52	PLH	44.98	0.06	1.89	8.93	0.13	42.29	2.07	0.00	0.00	0.00	0.00	100.35	0.904	71	12	2597	2317	23	42
RH−53	PLH	44.25	0.05	1.96	8.88	0.14	41.63	2.42	0.00	0.00	0.00	0.57	99.90	0.903	71	11	2652	2304	21	41
RH−54	PLH	44.40	0.04	1.64	9.00	0.14	42.87	1.83	0.00	0.00	0.00	0.00	99.92	0.904	66	11	2734	2339	17	42
RH−55	LZH	44.42	0.04	1.13	8.79	0.13	44.76	1.27	0.00	0.00	0.00	0.00	100.54	0.910	54	9	2658	2501	8	41
RH−59	LZD	42.99	0.03	0.29	9.31	0.14	47.11	0.35	0.00	0.00	0.00	0.00	100.22	0.909	30	5	2551	2741	4	41
RH−63	LZH	44.18	0.04	0.91	9.01	0.13	45.25	1.18	0.00	0.00	0.00	0.00	100.70	0.909	50	11	2452	2533	10	40
RH−65	LZH	43.64	0.03	0.77	9.00	0.13	45.12	1.00	0.00	0.00	0.00	0.00	99.69	0.909	51	10	2788	2528	9	40
RH−66	LZH	43.25	0.05	1.06	9.24	0.14	45.13	1.19	0.00	0.00	0.00	0.00	100.03	0.906	50	9	2833	2581	8	44
RH−68	LZH	44.73	0.04	1.28	8.80	0.13	44.03	1.40	0.00	0.00	0.00	0.00	100.41	0.908	59	11	2901	2397	8	42
RH−69	LZH	42.77	0.04	0.25	8.92	0.13	47.45	0.28	0.00	0.00	0.00	0.00	99.84	0.913	29	6	2594	2718	5	39

* : Values in wt%

** : Values in ppm.

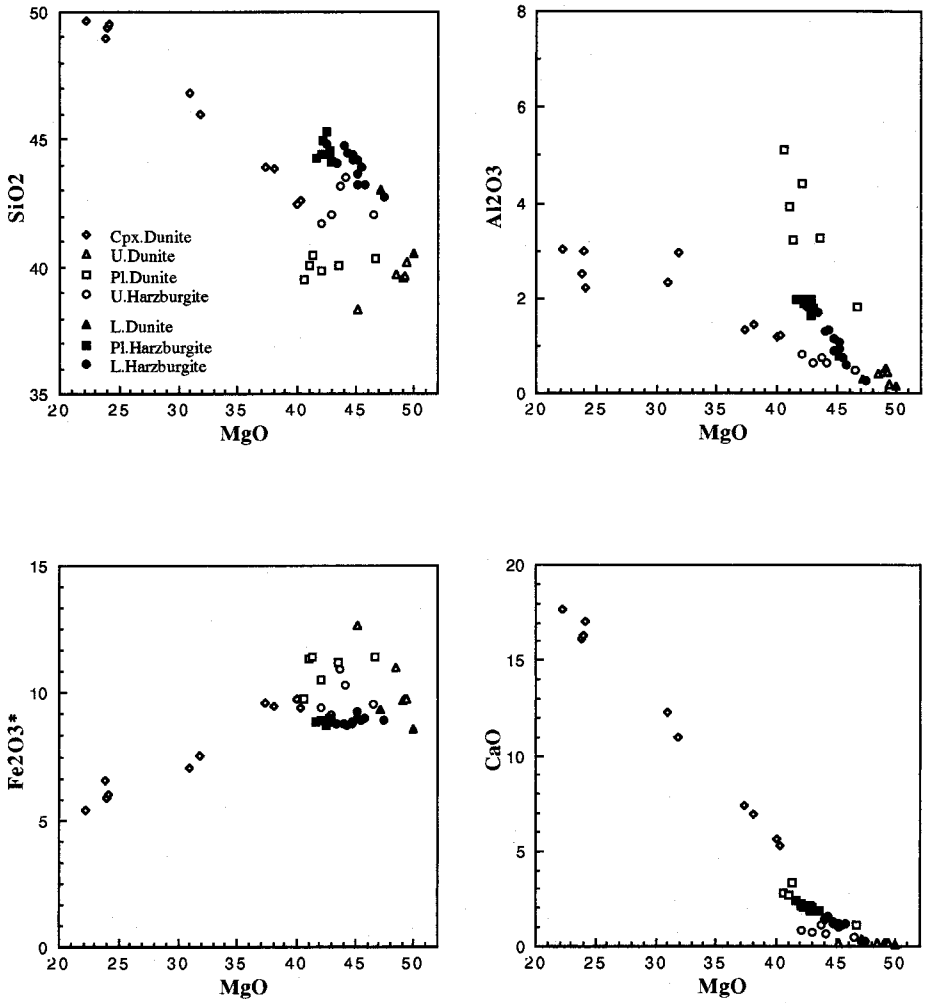

Fig.22. Oxide weight percents plotted against MgO weight percent. Fe_2O_3* means total iron as Fe_2O_3. *Open* symbols indicate samples of the upper zone. *Solid* ones indicate samples of the lower zone.

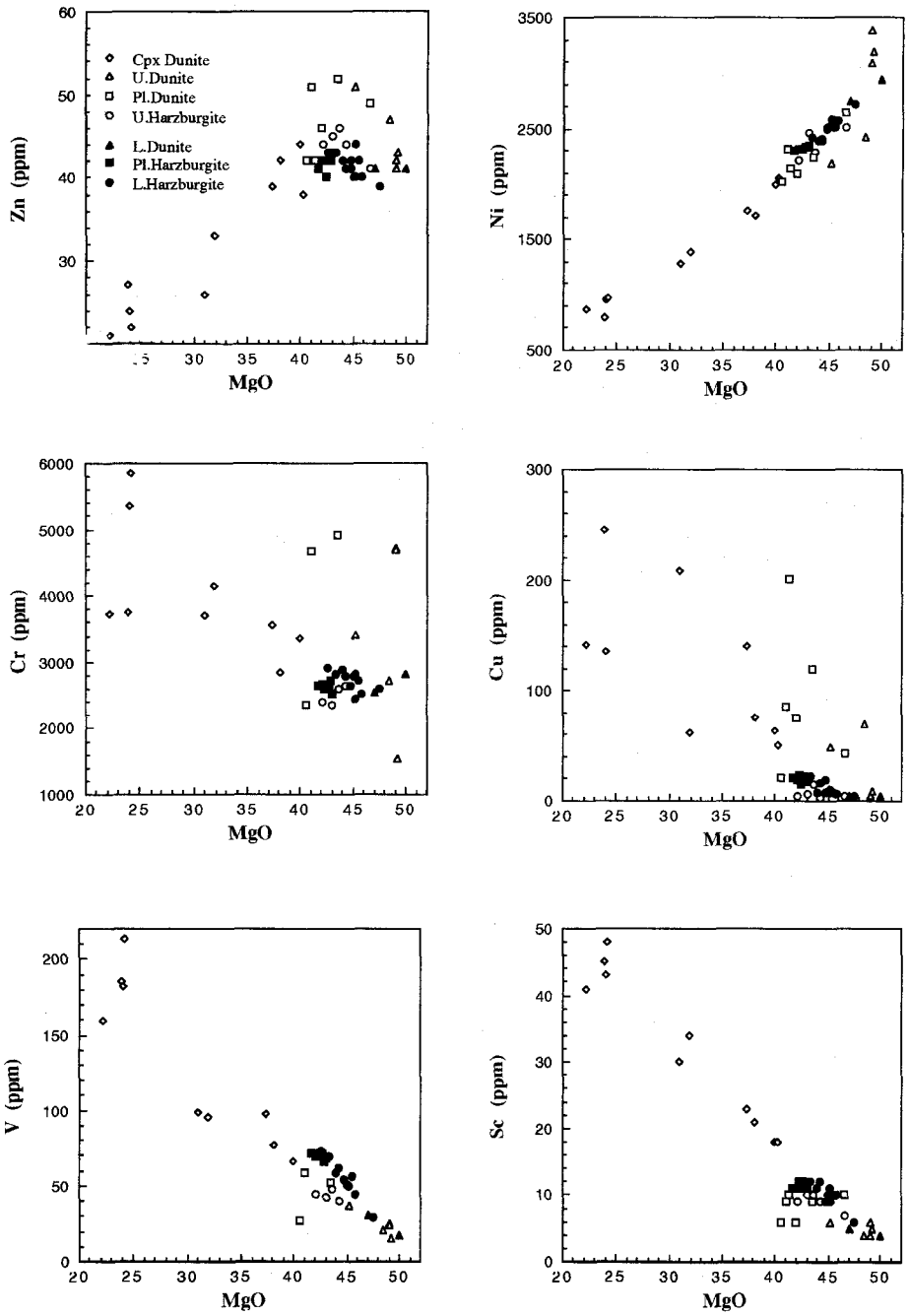

Fig.23. Elements in ppm. plotted against MgO weight percent.

5−2−2. Rare Earth Elements of Clinopyroxene

Concentrations of REEs of clinopyroxenes in harzburgites of the lower zone are depleted on LREE as compared with that in the upper zone (**Table 10**). Chondrite normalized concentrations of REEs of clinopyroxenes in rocks in the upper zone are almost same as that of clinopyroxenes in harzburgites in the lower zone at the HREE side, while at LREE side they are evidently different from the concentrations in the harzburgites in the lower zone. The former shows (Nd)n = 0.13 ~ 2.2 and the latter shows (Nd)n = 0.01 ~ 0.14 (**Fig. 24**). On the REE patterns in the upper zone the shapes of the pattern are almost parallel with each other, while the each concentration is different. Same things are also recognized in harzburgite in the lower zone of the body.

5−2−3. Sr Isotopic Compositions of Clinopyroxene and Plagioclase

Results of Sr isotope ratios of separated clinopyroxene and plagioclase in peridotites are shown in **Table 11**. The range of $^{87}Sr/^{86}Sr$ ratios is totally 0.7019 ~ 0.7027.

The ratios of clinopyroxenes in the upper zone are from 0.7019 to 0.7027, and those of plagioclases are 0.7021 and 0.7025. The $^{87}Sr/^{86}Sr$ ratios of minerals in RH-03 show the lowest value in the whole body. The $^{87}Sr/^{86}Sr$ ratio of plagioclase filling gash in clinopyroxene bearing dunite (RH-34) is 0.7025 that is in range of the other samples.

Analysis of the $^{87}Sr/^{86}Sr$ ratio of minerals in harzburgites in the lower zone excepting

Table 10. REE concentrations of clinopyroxenes in the Red Hills peridotite

Sample	Nd	Sm	Eu	Yb	Lu
	Upper dunite predominated zone				
RH−03 CPX	1.378	0.809	0.504	1.457	0.250
RH−13 CPX	0.269	0.170		0.590	0.086
RH−17 CPX	0.645	0.518	0.389	1.206	0.123
RH−19 CPX	0.083	0.075		0.373	0.063
RH−23 CPX	0.275	0.179		0.330	0.048
RH−29 CPX	0.182	0.161		0.750	0.099
RH−35 CPX	0.250	0.148		0.637	0.093
	Lower harzbutgite zone				
RH−40 CPX	0.083	0.107		0.939	0.123
RH−45 CPX	0.040	0.029		0.357	0.078
RH−47 CPX	0.047	0.042		0.925	0.113
RH−48 CPX	0.074	0.115		1.224	0.141
RH−50 CPX	0.088	0.194	0.134	1.047	0.116
RH−52 CPX	0.065	0.197		1.426	0.143
RH−54 CPX	0.045	0.125	0.084	1.174	0.119
RH−55 CPX	0.007	0.018		0.393	0.038
RH−63 CPX	0.011	0.016		0.312	0.042

Concentrations are in ppm.

one plagioclase sample was not succeeded, because the concentrations are extremely low (**Table 11**). Though the obtained result of the ratio of plagioclase in harzburgite in the lower zone is only one, the ratio is 0.7026 that agrees with the variation range of minerals in the upper zone.

The range of the Sr isotope ratios overlaps with that of recent mid-ocean ridge basalts. This is the most depleted values of rocks in oceanic region, and is clearly different from the ranges of rocks from island arc such as arc-tholeiite, calc-alkaline basalt and boninites. Detailed discussion for the analogues will be in Section 6−5−2.

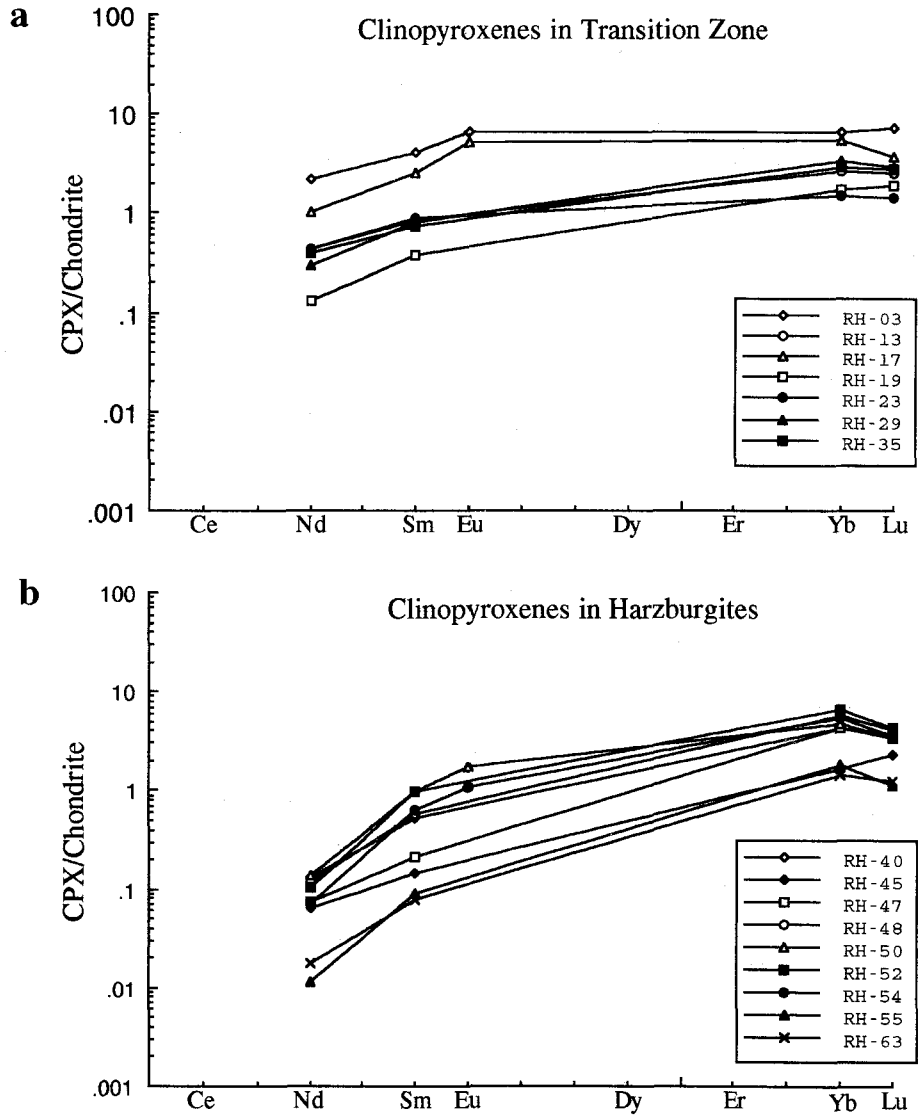

Fig.24. Chondrite-normalized REE concentrations in diopsides from the Red Hills peridotite. **a**: Seven samples from the upper zone. **b**: Nine samples from the lower zone. Note that LREE depletions in **b** are remarkable relative to those in **a**.

Table 11. Sr isotope results of minerals in the Red Hills peridotite

Sample	Sr (ppm.)	$^{87}Sr/^{86}Sr$	2sigma
	Upper dunite predominated zone		
RH−03 CPX	6.615	0.70193	6
PL		0.70209	4
RH−13 CPX	4.844	0.70252	16
RH−17 CPX	5.473	0.70235	5
PL		0.70225	2
RH−19 CPX	3.299		
RH−23 CPX	6.252	0.70270	4
RH−29 CPX	3.405	0.70272	8
RH−34 PL		0.70248	3
RH−35 CPX	7.854		
	Lower harzbutgite zone		
RH−40 CPX	0.360		
PL		0.70259	7
RH−45 CPX	0.438		
RH−47 CPX	0.543		
RH−48 CPX	0.086		
RH−50 CPX	0.500		
RH−52 CPX	0.033		
RH−54 CPX	0.176		
RH−55 CPX	0.055		
RH−63 CPX	0.025		

5−3. Lee River Group

5−3−1. Previous Works

The Lee River Group was dealt with a member of the Dun Mountain ophiolite belt by Coombs et al. (1973) for the first time. That is subdivided into the Tinline Formation mainly composed of gabbros and the Glennie Formation of basalts and diabases. Davis et al. (1980) reported that initial Sr isotope ratios at 240Ma (from *atomodesmatinid* fossil age) for the mafic volcanic and plutonic rocks are from 0.7019 to 0.7025. They concluded that the Dun Mountain ophiolite was originally formed at a mid-ocean ridge system and accreted to continental margin, based on the results of the Sr isotope ratios and trace elements and the geologic backgrounds.

5−3−2. Sr and Nd Isotopic Compositions of Basalts and Diabases in the Lee River Group

The initial Sr and Nd isotope ratios of basalts and diabases in the Roding River area of the Lee River Group at 260Ma are 0.7029～0.7046 and 0.51269～0.51273 (εNd

Table 12. Sr and Nd isotope results of basalts and diabases in the Lee River Group, and the related rocks

Sample	Rb	Sr	$^{87}Sr/^{86}Sr$	2sigma	Sm	Nd	$^{143}Nd/^{144}Nd$	2sigma	Remarks
			Roding River Basalts						
ROR−01	0.724	69.83	0.70467	2	2.922	8.132	0.513102	24	
ROR−04	0.711	88.52	0.70345	1	3.223	9.521	0.513065	17	
ROR−10	0.133	61.29	0.70333	2	2.267	6.512	0.513049	15	
ROR−12	2.659	211.5	0.70303	2	1.787	4.914	0.513084	18	
ROR−15	1.296	132.6	0.70307	1	1.539	4.339	0.513067	13	
			Dikes in the Red Hills peridotite						
RH−01	0.853	156.7	0.70302	4	0.306	1.764	0.512835	19	Plagiogranite dike in peridotite
RH−02	5.372	100.8	0.70418	9	1.615	8.566	0.512806	24	Plagiogranite dike in peridotite
RH−07			0.70307	1			0.513054	24	diabase dike in peridotite
			Datas from Davis et al. (1980)						
26.4,78.7	5.8	114.3	0.7019						Tinline Creek, gabbro
27.4,78.18	2.9	44.4	0.7023						Champion Creek, gabbro
14.2,78.5	3.76	165.3	0.7023						Dun Track, diabase
27.4,78.13	1.88	188	0.7025						United Creek, diabase
27.4,78.15	1.3	81.6	0.7025						United Creed, basalt
13.3,78.17	2.28	139.4	0.7021						Red Hills, basalt
13.3,78.1	12.6	149.1	0.7020						Red Hills, gabbro in perodotite

$= +7.5 \sim +8.3$), respectively (**Table 12**). Age of 260Ma is older than that of Davis et al. (1980). Though their age was obtained from fossils in sediments, the age of 260Ma is determined by U-Pb method using zircon in the related plagiogranites and the clastic rocks (Kimbrough et al., in prep.). Then, age of 260Ma is adopted on this study. The Roding River area correspond to upper part of the Lee River Group. The Sr isotope ratios of this study are characterized by higher than that of Davis et al. (1980). Their results are ranging from 0.7019 to 0.7025. There is a tendency of variation of the Sr isotopic composition as a function of stratigraphic level of basaltic sequence of the Roding River area. Basalt of the uppermost level shows the highest Sr isotope ratio (0.7046) while basalt of the lower level are characterized by the lower ratios (~ 0.7030). Samples reported by Davis et al. (1980) were correspond to stratigraphically deeper portion. Then, the variation of Sr isotope ratios of samples from the Roding River area probably suggests that the rocks suffer interactions between seawater and rock. The interaction is supported from field observation that sample of ROR-01 showing the highest Sr isotope ratio is directly covered by the Maitai Group sediments. This means that the rock is exposed in seawater.

Nd isotope ratios of basalts and diabases of the Roding River area are +7.5 to +8.3 on epsilon Nd unit. This compositional range agrees with that of mid-ocean ridge basalts. However, the Sr isotopic compositions of minerals of the Red Hills peridotite and of basalts and diabases reported from Davis et al. (1980) show the most depleted natures. This is not concordant with the Nd results, because the obtained isotope rarios are too low than expected values from results of the Sr isotope ratios of $0.7019 \sim 0.7027$. Moreover, the Nd isotope ratios of plagiogranite and diabase dikes intruding into dunite in the upper zone of the Red Hills peridotite body are also low (**Table 12**). It can be interpreted that dikes intrude into the peridotite body at later stage than the event characterized by the extremely low Sr isotopic composition of the host peridotite body. This is also supported from field observations that the contacts of dunite with the diabase dikes suffers severe thermal alteration.

6. DISCUSSIONS

As mentioned in **Sections 3** and **4**, the Red Hills peridotite body can divided into two zones, the dunite predominating upper zone, and the lower zone of harzburgites. The upper zone of the body corresponds to the mantle-crust transition zone in many ophiolites. Thus, the term of "transition zone" will use for the upper zone of the body from now.

6−1. Tectonic Environment

6−1−1. Previous Works

Coombs et al. (1973) and Blake & Landis (1973) reported that the peridotites and volcanic rocks in the Lee River Group are collectively ophiolite member consisting upper mantle and oceanic crust in Permian age. Furthermore, Davis et al. (1980) concluded that both harzburgite and dunite in the Red Hills peridotite body are residual mantle situated the floor of magma chamber of basalt and gabbro in the Lee River Group.

Calc alkaline volcanic rocks in the ophiolite member from the Otago area (Coombs et al., 1976) and high Cr# (0.8) spinels in dunite and chromitite from the Red Mountain peridotite (Sinton, 1977) has been reported. They obviously indicate an island arc signatures. From field evidence and chemical characteristics of volcanic rocks, Coombs et al. (1976) suggested for a possible model for evolution of the Dun Mountain ophiolite. The ophiolite is originated as ocean floor near an active plate margin during pre-Upper Permian time. Furthermore, they imagined the tectonic setting as a modern analogue that is the Juan de Fuca Ridge of the northeast Pacific, sited close to the volcanic belt of the Cascade Mountains.

6−1−2. Estimated Original Tectonic Setting by Mineral Compositions

Dick & Bullen (1984) pointed out that the spinel composition is good indicator for estimating the original tectonic environment of ophiolites. They divided alpine type peridotites into three groups based on the Cr# of spinel. The group such as Ronda, Beni Bouchera, Alps, Trinity and White Hills, which has low Cr# (<0.60) does not have island arc signature, while the group such as Troodos, Papua and Twin Sisters is characterized by spinel of high Cr# (>0.60) suggesting island arc signature. Other many ophiolites (e.g., Bay of Islands, Josephine, New Caledonia and Samail) show the intermediate character. Though spinel of high Cr# ($0.7\sim0.8$) also occurs in small dunite pockets in harzburgite in the lower zone of the Red Hills peridotite (**Fig. 17**), the extent of the dunite in field is quite small (a few meter scale) and that frequency at the outcrop is also rare. Spinels in chromitite in the dunite of the transition zone of the Red Hills show Cr#$=0.5$. On **Figure 17**, compositions of almost all spinels excepting that in the dunite of the lower zone are plotted on same area with that of oceanic peridotites.

Plagioclases are often found in the Red Hills peridotites. Plagioclases in harzburgites in the lower zone have high An contents (An=95~98) while the compositions in dunite in the transition zone are from 80 to 95 (**Fig. 16 a**). Arai & Takahashi (1988) reported that the range of An contents in oceanic peridotites is from 58 to 80, and concluded that plagioclase bearing peridotites including high An plagioclases are characterized by the peridotites occurring in the Circum-Izu terrane (e.g., peridotites in the Setogawa and the Mineoka Formations). Furthermore, they pointed out that the peridotites represent uppermost mantle of inter-arc basin (e.g., Shikoku basin) or backarc basin. It, however, is unsuitable that the low An values (58~80) are characterized in oceanic plagioclase peridotites reported on them, because their data is from the St. Paul's Rock in the Mid Atlantic that includes many hydrous minerals and alkaline features (Roden et al., 1984). Thus, that is not represent common oceanic peridotites. It has been reported that plagioclase phenocrysts or microphenocrysts in some MORBs show high An contents (An=90~93, Ayuso et al., 1976). The higher An contents of plagioclases in the Red Hills peridotites consistent with that in rocks from mid-ocean ridge environment.

Pargasite~pargasitic hornblendes are rarely found as border of domains of plagioclases (**Fig. 15 b**). The pargasites occur as only reaction rim with plagioclase and clinopyroxene. This suggests that the melt forming plagioclase includes somewhat vapor. The pargasites show high TiO_2 contents (0.5~2.0wt%) relative to K_2O contents (>0.15wt%). Ozawa (1988) inferred the original tectonic environments of peridotites from K_2O and TiO_2 contents of amphiboles in various volcanic rocks. Based on amphibole compositions, the amphiboles found in plagioclase bearing dunite in the Red Hills do not support island arc signature but support affinities to the mid-ocean ridge system.

6-1-3. Tectinic Setting inferred from Sr Isotope Ratios

Strontium isotope ratios of clinopyroxenes and plagioclases of the Red Hills peridotites are ranging from 0.7019 to 0.7027. They are characterized by quite low values that have never found in any recent island arcs, back arc basins and oceanic islands, as mentioned in **Section 6-5-2**. The obviously low Sr isotope ratios correspond to the most depleted evolution line that is represented by tie line between the most depleted MORBs and the lowest Sr isotope ratios of each ophiolite (**Fig. 25**). This strongly suggests that the Red Hills peridotite body is the dunite-harzburgite complex related to the most depleted magmatism at a mid-ocean ridge system.

6-1-4. Summary

There is no evidence of calc alkaline volcanism at the Red Hills area, while the ophiolite from the Otago area has feature of calc alkaline volcanism. It is supposed that the tectonic environment of the ophiolite in the Red Hills area is different from that in the Otago area. The basalts of the Lee River Group in the Nelson district is unconformably overlain by tuffaceous siltstone of the Maitai Group at the Roding river area. The rocks of the Maitai

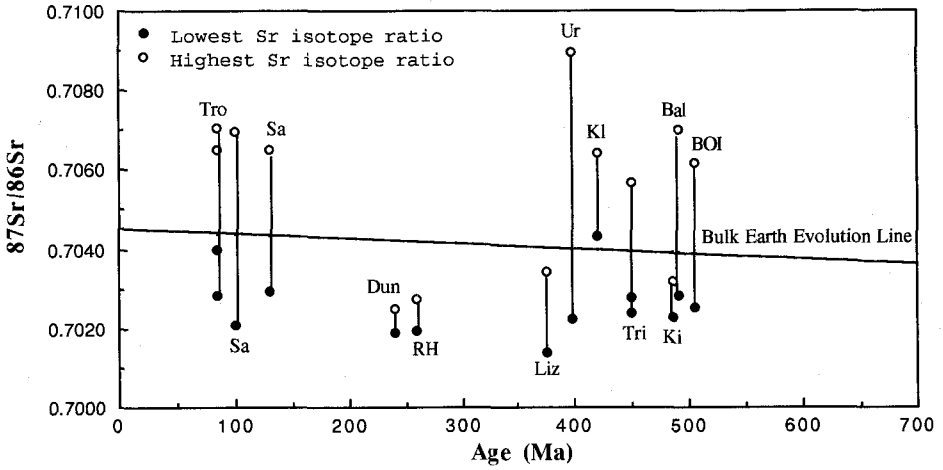

Fig.25. Relation between initial $^{87}Sr/^{86}Sr$ ratios and ages for ophiolites. Data sources are Jacobsen & Wasserburg (1979), McCulloch et al.(1980), Davis et al.(1980), Lanphere et al.(1981), McCulloch & Cameron (1983), Davies (1984), Thirlwall & Bluck (1984), Menzies (1984), Edwards & Wasserburg (1985), Shaw et al.(1987), Brouxel & Lapierre (1988) and Brouxel et al.(1988). Tro: Troodos, Sa: Samail, Dun: Dun Mountain, Liz: Lizard, Ur: Urals, Kl: Klamath, Tri: Trinity, Ki: Kings River, Bal: Ballantrae, BOI: Bay of Islands, RH: This work for the Red Hills peridotite. As Sr isotope ratios are easily modified by alterations to higher values, the lowest values can be regarded as the most reasonable values. The lowest value of each ophiolite (e.g., Samail at 100Ma, Dun Mountain, Urals, Kings River, Bay of Islands and Red Hills) is close to 0.7020 that is the lowest one of recent MORBs.

Group are characterized by shallow water facies such as limestone, acidic tuffaceous sand~siltstone and shale (Coombs et al., 1976). On the other hand, basalts in the Lee River Group have MORB signatures based on study of the chemical and isotopic characters (Davis et al., 1980). The geologic time span between the Maitai Group and the Lee River Group is small because of evidence of the fossil and zircon U-Pb age determinations. Therefore, it is inferred that the original tectonic environment of the Dun Mountain ophiolite in the Red Hills area is oceanic crust and the uppermost mantle formed near arc volcanic province. This is consistent with conclusions of Coombs et al. (1976).

6−2. Origin of Harzburgite

6−2−1. Previous Works

Previous works (Walcott, 1969; Davis et al., 1980; Johnston, 1983) have roughly been clarified that the Red Hills body is divided into lower harzburgite zone and upper dunite zone, and have described that the dunite zone is composed of mainly dunite, clinopyroxenite and harzburgite. For genesis of the Red Hills peridotite, Challis (1965) concluded that the whole peridotites are cumulates resulting from gravitational differentiation from a tholeiitic magma. Walcott (1969) also supposed cumulate origin that the ultramafic rocks are contem-

poraneous with the volcanic rocks. Sinton (1977) obscurely proposed the Red Mountain peridotite body in the Dun Mountain ophiolite in Otago area is composed of residual and transition peridotites that formed by reequilibration between residual crystal and a basaltic melt.

6−2−2. Modal Compositions of Peridotites from Various Tectonic Settings

Modal compositions of the Red Hills, oceanic and other peridotites are shown in **Figure 26**. The harzburgites in the Red Hills are always composed of four phases, olivine, orthopyroxene, clinopyroxene and spinel. Modal variation of harzburgites in the Red Hills

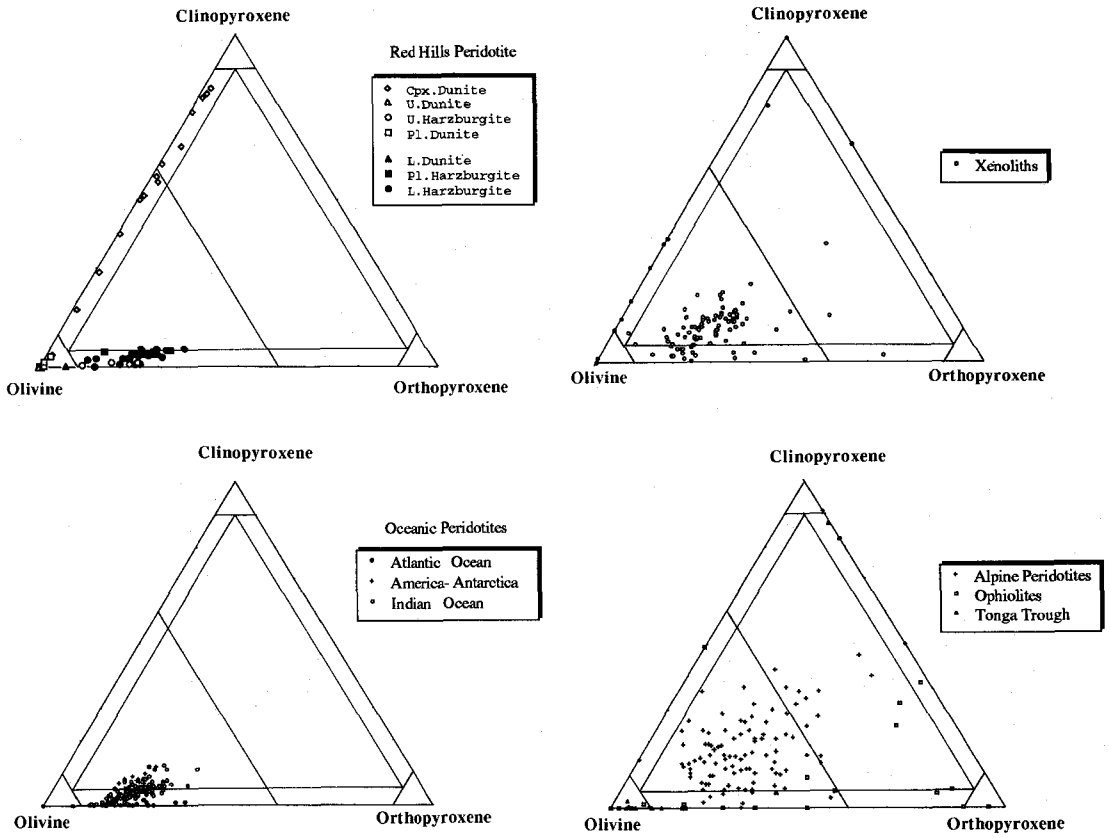

Fig.26. Modal compositions of peridotites from various tectonic settings. **a**: Red Hills peridotite. **b**: oceanic peridotites from recent spreading centers. **c**: Xenoliths in volcanic rocks. **d**: Alps and other ophiolitic peridotites. Note that modal variation of the Red Hills peridotite evidently correspond with that of oceanic one. Data sources are: England & Davies (1973), Ernst (1978), Ernst & Piccardo (1979), Hamlyn & Bonatti (1980), Takahashi (1980), Kurat et al.(1980), Dick et al.(1984), Michael & Bonatti (1985), Ishiwatari (1985), Press et al.(1986), Francis (1987), Downes & Dupuy (1987), Reay & Sipiera (1987), Bloomer & Fisher (1987), Song & Fray (1989), Edgar et al.(1989), Embey-Isztin et al.(1989), Fabries et al.(1989), Dick (1989) and Barsdell & Smith (1989).

peridotites is similar to that of oceanic peridotites. Mode of clinopyroxene in the harzburgite of the Red Hills is about 0 to 5%, especially is crowded on 3 to 5% range. There is a trend that is from pyroxene rich peridotites to pyroxene poor one (**Fig. 26 a**). This could be understood as differences of degrees of partial melting. The modal compositions of oceanic peridotite and the peridotites in the Red Hills are homogeneous than other peridotites. Xenoliths and alpine peridotites (e.g., Ronda, Lanzo, Western Alps etc.), however, show much higher modal clinopyroxene (**Fig. 26 c** and **d**). Their modal compositions are scattered on much wider area on the figure than oceanic one.

6−2−3. Mineral Compositions of Harzburgites

Chemical composition of olivine in harzburgites in the lower zone are very homogeneous (Fo=91.4) as compared with those in rocks in the transition zone. The homogeneous compositions of olivines in the harzburgites are shown in case of four phase (olivine, orthopyroxene, clinopyroxene and spinel) remaining, while clinopyroxene free harzburgites (olivine, orthopyroxene, spinel and ±clinopyroxene) and dunites (olivine, spinel,

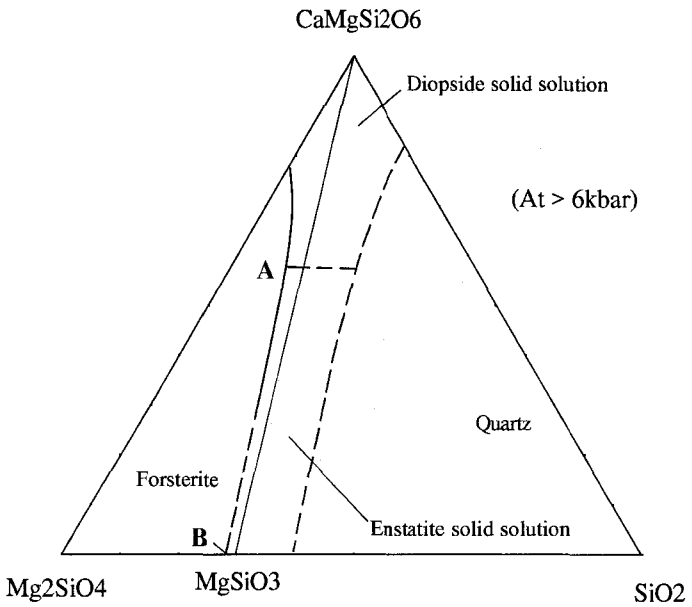

Fig.27. Mg_2SiO_4 - $CaMgSi_2O_6$ - SiO_2 diagram (Kushiro, 1969). At higher pressure condition (>6kbar), eutectic point is shown as **a** on a Iherzolitic mantle system (ol+opx+cpx). On fractional melting system, produced melt composition must be constant (**a**) until clinopyroxene is disappeared. That is, olivine composition coexisting with such melt must also be constant. When clinopyroxene is disappeared from the system, melt composition **a** will abruptly change to **b**.

±orthopyroxene and ±clinopyroxene) in the lower zone include olivines of higher Fo content (Fo=92~93). On **Figure 27**, initial melt composition is represented by eutectic point (**A**) that is co-existing with olivine, orthopyroxene and clinopyroxene. System of a fractional melting based on REE results of clinopyroxenes in harzburgites in the lower zone of the Red Hills (see **Section 6-2-5**) is assumed here. When clinopyroxene is disappeared with increasing degrees of partial melting, the melt composition (**A**) abruptly changes to **B** on this melting system. Thus, the composition of olivine co-existing with melt (**A**) must be changed to much Fo rich olivine co-existing with melt (**B**), according to disappearance of clinopyroxene (**Fig. 27**). This is consistent with the case of the lower zone of the Red Hills.

Range of the Cr# in harzburgites in the lower zone is 0.25~0.58 excepting that of the most refractory peridotites (RH-43, 59, 69). This range agrees with that of oceanic peridotites (Dick & Bullen, 1984). Arai (1987) proposed that mantle peridotites make an array on Cr# of spinels as a function of Fo of olivines ("olivine spinel mantle array"; OSMA). The chemical compositions of minerals in peridotites in the lower zone of the Red Hills are overlain on the array (**Fig. 28**).

Dick et al. (1984) has suggested that modal compositions of oceanic harzburgites and

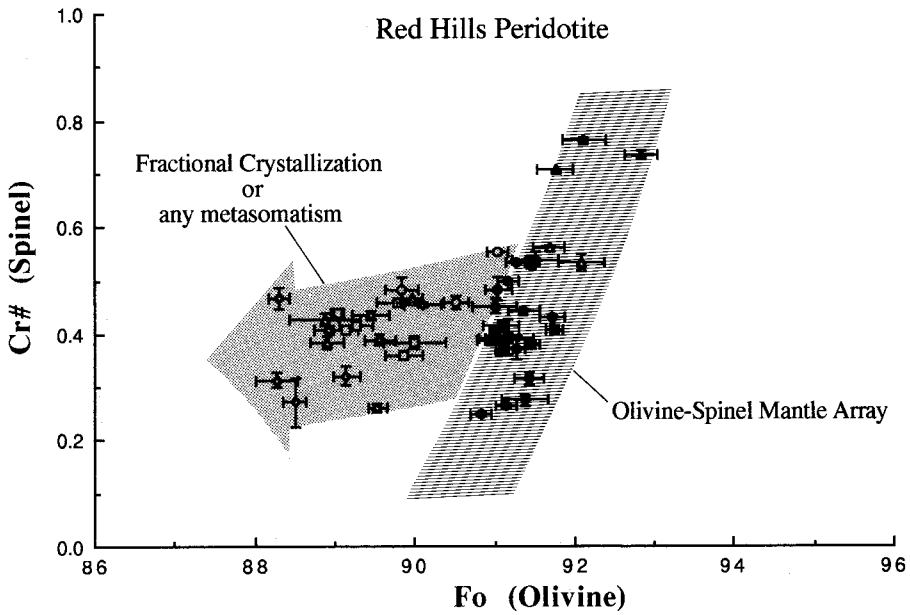

Fig.28. Relation between Fo in olivine and Cr# in spinel. Symbols are the same as in **Fig.10.** Individual data points composing the averages in each sample are plotted. Shaded area is an olivine-spinel mantle array (OSMA; Arai, 1987). Though most harzburgites are in the area, the rocks of the transition zone (*open* symbols) are shifted to low Fo side of the array.

lherzolites correlate with the chemical compositions of minerals. They have also pointed out that they are the probable residues of variable degrees of melting. There is good correlation between modal olivines and Al_2O_3 contents in orthopyroxenes in the Red Hills harzburgites (**Fig. 20**). On **Figure 20** the most refractory peridotite shows Al_2O_3 poor orthoproxene, on the contrary, the most fertile one co-exists with Al_2O_3 rich pyroxene. It can be interpreted that the correlation is explained by differences of degrees of partial melting.

The frequencies of occurrences of dunites that makes small pockets surrounded by harzburgite in the lower zone are low, and the neighboring harzburgite is the much depleted than the other one (**Fig. 12 m** and **o**). These field observations are consistent with observations from the Trinity ophiolite reported by Quick (1981a, b). He pointed out that the harzburgite close to the dunite has the most refractory features, and concluded that origin of the dunite bordered on such refractory harzburgite is a residual material. The small dunite pockets surrounded by harzburgites in the lower zone of the Red Hills are characterized by high Cr# (0.70～0.78) in spinel, high Fo (92～93) in olivine and porphyroclastic texture with suture grain boundaries. It is suggested that the dunite is the most depleted residual mantle material.

6－2－4. Whole rock chemical compositions

Chemical variations of harzburgites in the lower zone of the Red Hills peridotite (**Fig. 22**) agree with those in oceanic, ophiolitic and alpine peridotites in world (e.g., Ernst, 1978; Quick, 1981a; Prinz et al., 1976; Kornprobst, 1969; Dick, 1989; Moores, 1970; Loney & Himmelberg, 1989). It has been generally accepted that they are originated from residual mantle material processed any partial melting events. The variations of MgO contents range from 37 to 50wt%. That variation of harzburgite in the lower zone in the Red Hills peridotite body is from 42 to 50wt%. The MgO contents of a primitive mantle composition are regarded as about 37～38wt% (Jaques & Green, 1980; Sun, 1982; Ringwood, 1975). Then, the harzburgites in the Red Hills peridotite body must be residual mantle material suffered partial melting from a primary mantle, like worldwide lherzolite and harzburgite massifs. Higher MgO (>42wt%) contents of harzburgites in the body than that of other residual peridotites probably means that the harzburgite in the Red Hills peridotite is residual material suffered much higher degrees of partial melting.

6－2－5. REE Patterns of Clinopyroxenes and the Suitable Melting Model

REE patterns of clinopyroxenes in harzburgites in the lower zone of the Red Hills peridotite are characterized by remarkable depletion of light REE. The REE concentrations of hypothetical melts in equilibrium with the clinopyroxenes in the peridotites, calculated by using the distribution coefficients on **Table 13**, are inconsistent with the concentration of normal basaltic melt on terrestrial earth. The concentrations of REEs of the calculated melt are too low (**Table 14 a**). The estimated melt compositions are obviously different from

Table 13. Distribution coefficients between mineral and melt (Johnson et al., 1990)

	olivine	orthopyroxene	clinopyroxene	spinel
Ce	0.001	0.005	0.10	0.0005
Nd	0.002	0.01	0.19	0.0008
Sm	0.003	0.02	0.30	0.0009
Eu	0.003	0.03	0.42	0.0009
Dy	0.012	0.045	0.50	0.0015
Er	0.025	0.06	0.51	0.003
Yb	0.059	0.075	0.50	0.0045

Table 14a. Hypothetical melt compositions in equilibrium with the harzburgite clinopyroxenes in the Red Hills

	RH−40	RH−45	RH−47	RR−48	RH−50	RH−52	RH−54	RH−55	RH−63
Nd	0.437	0.211	0.247	0.389	0.463	0.342	0.237	0.037	0.058
Sm	0.357	0.097	0.140	0.383	0.647	0.657	0.417	0.060	0.053
Eu					0.319		0.200		
Yb	1.878	0.714	1.850	2.448	2.094	2.852	2.348	0.786	0.624

Concentrations are in ppm.

Table 14b. Compositional Ranges of N−MORBs (Viereck et al., 1989)

	N−MORBs
Ce (ppm)	4.8 −11.2
Nd	5.0 − 9.9
Sm	1.9 − 3.4
Eu	0.79− 1.31
Yb	2.20− 3.74

usual MORBs (**Table 14 b**).

The difference between MORB and the hypothetical melt should be too large to be attributed to the original chemical difference in the source mantle or the effect of differentiation by extraction of olivine (<15%) which could have changed composition of MORB from that of the primary magma. Alternatively the difference mentioned above could be explained by changing composition of the melt formed at each stage of advancing partial melting, which were successively removed from the source: the melt equilibrated with harzburgite should be the melt formed at the final stage and its composition could be different from bulk composition of primary melts formed during whole partial melting process.

Johnson et al. (1990) have reported for REE concentrations of clinopyroxenes in lherzolites and harzburgites dredged from the American-Antarctica Ridge (AAR) and Southwest Indian Ridge (SWIR). The REE patterns of clinopyroxenes in residual peridotites indicate advancing LREE depletion with increasing degrees of partial melting (**Fig. 29**). Johnson et al. (1990) pointed out that these LREE depleted patterns of clinopyroxenes are not resulted from batch equilibrium melting process but from fractional melting process: concentrations of incompatible elements in clinopyroxenes in peridotites are well modelled by repeated melting and segregation in $\leq$ 0.1% increments to a total of

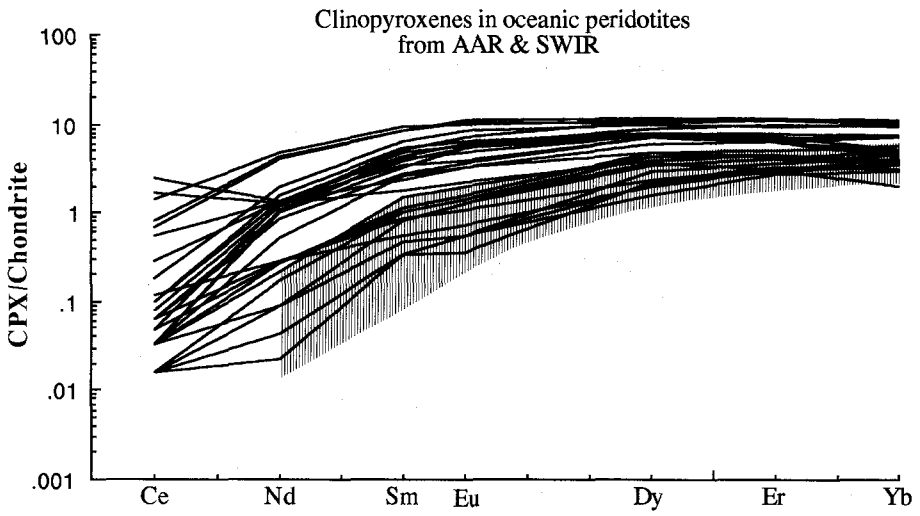

Fig.29. Chondrite-normalized REE concentrations in diopsides from peridotites of the Southwest Indian and America-Antarctica Ridges. Data are from Johnson et al.(1990). Shaded area represents REE patterns of clinopyroxenes in harzburgites of the lower zone of the Red Hills. Note that both clinopyroxenes in recent oceanic peridotites and in the Red Hills harzburgites show remarkable LREE depletion.

5~25% melting. REE patterns of clinopyroxenes in harzburgites in the Red Hills body are well similar to those of clinopyroxenes in peridotites of AAR and SWIR and the fractional melting should be also responsible for the origin of harzburgite in the Red Hills peridotite.

This may suggest the more advancing partial melting of harzburgite or the more depleted nature of the original source in Red Hills peridotite than in AAR and SWIR. In general, it has been reported that the MORBs in the Indian Ocean (especially Southwest Indian Ridge) are undepleted in incompatible trace elements than those in the Pacific and Atlantic Oceans. Sr and Nd isotope ratios also indicated nature of the source peridotite of the MORBs in the Indian Ocean (Dupre & Allegre, 1983; LeRoex et al., 1983; Hamelin & Allegre, 1985; Michard et al., 1986; Price et al., 1986; Mahoney et al., 1989). Therefore, it is expected that the residual mantle extracted such basaltic melts is also less-depleted. In fact, peridotites dredged from the Indian Ocean have high modal clinopyroxenes as compared with other oceanic peridotites and ophiolitic residual peridotites (**Fig. 26**). Moreover, this is supported by spinel compositions (**Fig. 17**). The lower REE concentrations in clinopyroxenes in the harzburgites of the Red Hills mentioned above may more or less reflect the more depleted nature of the original mantle peridotite in the Red Hills than in SWIR.

Harzburgites in the lower zone of the Red Hills peridotite is a residue of N-type MORB source which is depleted in incompatible elements by extraction of incipient partial melts from primordial mantle (Loubet et al., 1975; Wood et al., 1979, 1981). Degrees of partial melting and the suitable melting model for making the harzburgite residue from the MORB

Table 15a. REE concentrations of source mantle and chondrite

	Starting MORB-type source mantle composition*	Chondrite normalization values (Anders & Grevesse, 1989)
Ce	0.790	0.603
Nd	0.745	0.452
Sm	0.293	0.147
Eu	0.116	0.056
Dy	0.537	0.243
Er	0.381	0.159
Yb	0.387	0.163
Lu		0.024

Values in ppm.
* Sources of data : Loubet et al. (1975), Wood et al. (1979)

Table 15b. Phase proportions in the models (Johnson et al., 1990)

Phase	Starting mode (vol%)	Melt mode (vol%)
olivine	0.55	0.10
orthopyroxene	0.25	0.20
clinopyroxene	0.18	0.68
spinel	0.02	0.02

souce mantle is estimated by using the REE patterns. Based on Nd isotopic composition of MORB, starting mantle composition for model calculation is a LREE depleted lherzolite (Wood et al., 1979; Johnson et al., 1990). Used mantle composition of MORB-type source, phase proportions and chondrite normalization values are shown in **Table 15**. Distribution coefficients used in the models are shown in **Table 13**. The model calculations are followed by Gast (1968) and Shaw (1970). Based on the model calculations, obvious LREE depleted patterns of clinopyroxenes in harzburgite residues of the Red Hills body can not be explained by batch melting model (**Fig. 30 a**). The fractional melting model is much reasonable rather than the previous one (**Fig. 30 b**). This model can well explain the LREE depletions of the clinopyroxenes. It is concluded that the harzburgites in the lower zone of the Red Hills peridotites are residual materials suffered fractional melting of 12~20%.

6-2-6. Primary Melt Composition Inferred from Residual Peridotite

The primary melt composition equilibrated with the harzburgite residue in the Red Hills is inferred from olivine composition. The olivine compositions in the harzburgites are remarkably homogeneous (Fo=91.4±0.5). The finally equilibrated melts with the olivines

can be estimated from the olivine composition. The calculated Mg# of the melt is about 0.74 (**Fig. 31**), if the Fe-Mg partition coefficient (K_D) between melt and olivine is assumed to 0.28. Furthermore, Sr isotopic compositions of minerals in the Red Hills peridotites strongly suggest mid-ocean ridge signature (see **Section 5-2-3**). On **Figure 31**, chemical compositions of recent MORB glasses are also plotted. Because the most MgO rich glasses are co-existing with only olivine crystal, the trend of the MgO rich glasses is controlled by behavior of olivine (**Fig. 31 a**). Therefore, the chemical composition of primary melt equilibrated with the harzburgite is represented by the intersection (**A**) between constant Mg / (Mg+Fe) line (**B**) and olivine control line (**C**) on **Figure 31 a**. Consequently, the estimated primary melt is picritic composition having 12.5~15.0wt% MgO and 7.8~9.4wt% FeO. As apparently shown in this figure, the most high magnesian MORB glasses can not co-exist with olivine of Fo_{91}, but rather co-exist with olivine of Fo_{87}. Although olivine compositions in peridotites dredged from the Southwest Indian Ridge are $Fo_{88\sim89}$, olivine compositions in peridotites sampled from many Mid Atlantic Ridges are almost $Fo_{90\sim91}$. These olivine compositions give a condition of limitation for considering the origin of primary melt of MORBs. In other words, what is the primary melt of MORBs, picritic composition or the most magnesian olivine tholeiitic (10wt% MgO) composition? The results of harzburgite residues in the Red Hills are strongly support the picritic origin as primary melt of MORBs.

Since the primary melt inferred from harzburgites in the Red Hills is picritic composition having 12.5~15wt% MgO and 7.8~9.4wt% FeO, it is supposed that the most magnesian glasses of MORBs suffer some degrees of fractionation of olivine from the picritic melt. The most magnesian glasses must be needed fractional crystallization of olivine of 10~15% from the picritic melt (**Fig. 31 b**). The compositional variation of fractionated olivine is expected for $Fo_{87\sim91}$. The range of olivine composition surprisingly agrees with the range of olivine in rocks of the transition zone of the Red Hills. Accordingly, the olivine in rocks of the transition zone of the Red Hills. Accordimgly, the olivine in rocks of the transition zone can *compositionally* be formed from fractional crystallization of olivine of 10~15% from the primary picritic melt, though the volumetric problem is remaining.

6-2-7. Summary

Harzburgites in the lower zone of the Red Hills must represent residual mantle material from following reasons; 1) the modal compositions are agreed with the trend of those in oceanic residual peridotites (**Fig. 26**), 2) the harzburgites show porphyroclastic texture that is recognized in tectonite in many ophiolites and oceanic peridotites, 3) correlation between the modal compositions of olivines and Al_2O_3 contents in the orthopyroxenes (**Fig. 20**), 4) the olivine and spinel compositions fit to the area of the olivine-spinel mantle array on **Figure 28**, 5) the most depleted harzburgites and dunites (RH-43, 59, 69) in the lower zone have the most magnesian olivines ($Fo_{92\sim93}$, **Fig. 16 a**), and 6) REE patterns of clinopyroxenes in the harzburgites are characterized by obvious LREE depletion (**Fig. 24 b**).

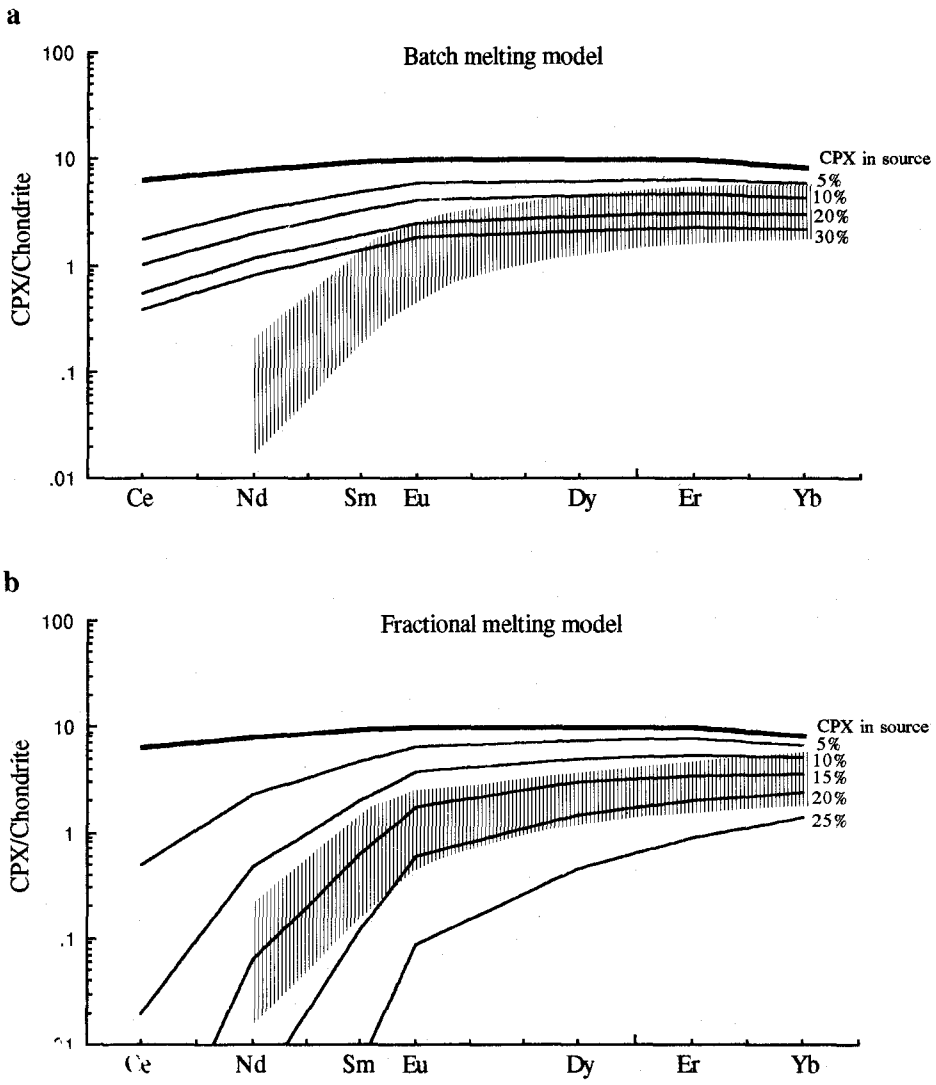

Fig.30. *Results of calculations of melting model based on REE concentrations in* clinopyroxenes in harzburgites. Each REE pattern represents the concentration in clinopyroxenes equilibrating with melt that produced by each melting mechanism from MORB-type source mantle. Used distribution coefficients are shown in **Table 14.** Source mantle composition and estimated melting proportions are displayed on **Table 16**, according to Johnson et al.(1990). **a**: Batch melting model, **b**: Fractional melting model. Shaded area is the concentration range of clinopyroxenes in the Red Hills harzburgites. The range corresponds to the results of fractional melting model. Harzburgites in the Red Hills must be suffered degrees of the melting of 12～20% from a LREE-depleted, MORB-type source mantle.

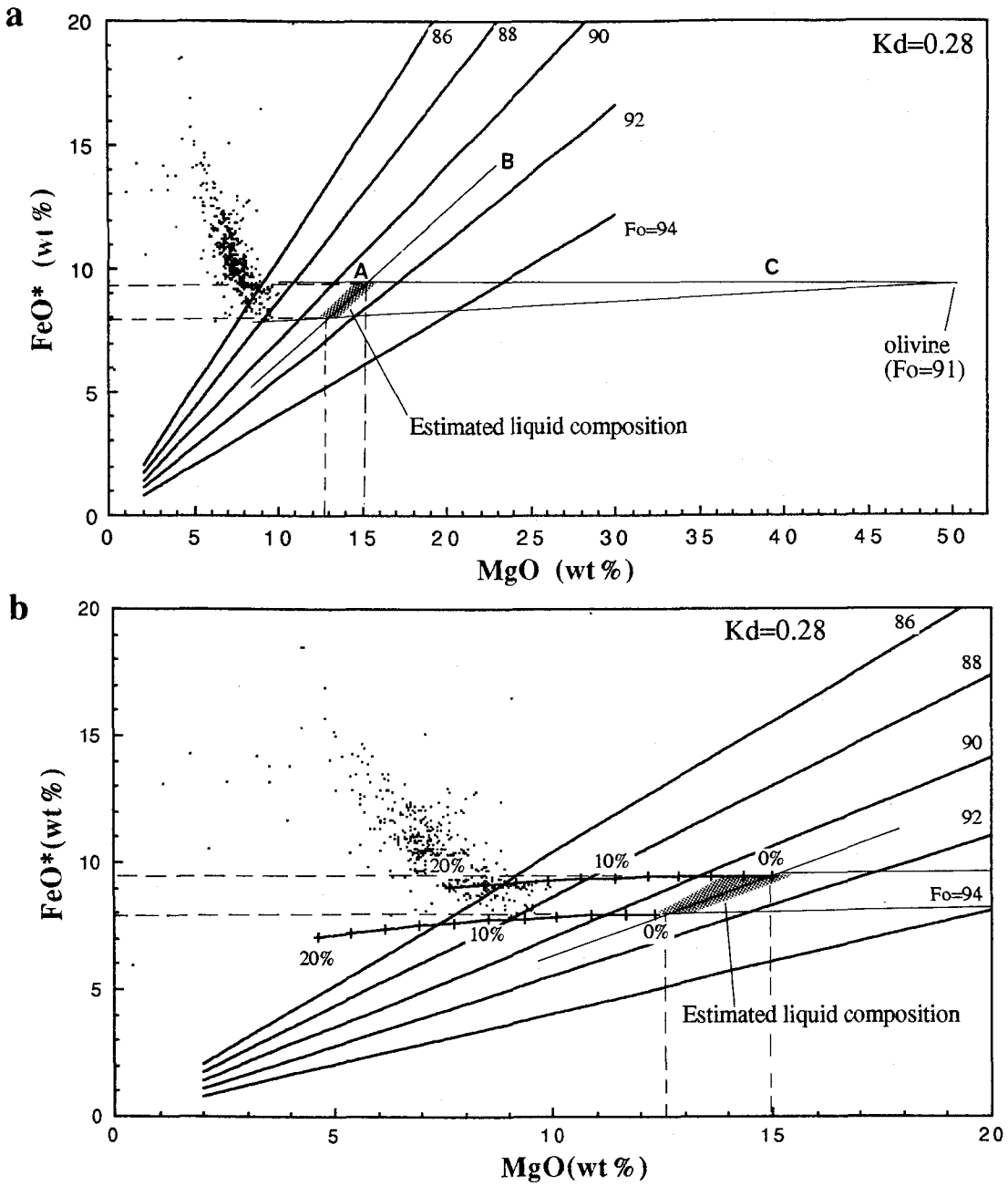

Fig.31. FeO* versus MgO relation of MORB glasses. **a**: Estimation of primary melt composition is applied the method of Sato & Tohara (1985). Constant FeO*/MgO lines are estimated from equilibrating olivine composition by using Kd=0.28 where Kd is Fe-Mg partition coefficient for melt and olivine. Obtained primary melt compositions are 12.5~15.0 wt% MgO and 7.0~9.4wt% FeO, that is picritic composition. **b**: Estimation of degrees of crystal fractionation of olivine from such primary magmas. Calculated degrees of the fractionation are about 10~15%. After the fractionation, the fractionated melts are equivalent to magnesian olivine tholeiitic compositions (the most magnesian MORBs). MORB glass data are from: Melson et al.(1976), Melson & O'Hearn (1979), Dmitriev et al.(1984), Dixson et al.(1986), Eissen et al.(1989), Hekinian et al.(1989), Michael et al.(1989), Natland (1989).

From REE patterns of clinopyroxenes in the harzburgites, it is supposed that the harzburgites are residual mantle suffered fractional melting of 12～20% from a MORB-type source mantle. The consequent melt must be picritic composition having 12.5～15.0wt% MgO and 7.8～9.4wt% FeO. Furthermore, the picritic melt must be suffered fractional crystallization of olivine of 10～15%, to equilibrate with the most magnesian MORB glasses.

6－3. Origin of Dunite

6－3－1. Previous Works

Thickness of the dunite in transition zone in the worldwide ophiolites has been reported. There are large varieties of the thickness in each ophiolite. For example, the thickness of dunite in transition zone in the Bay of Islands ophiolite is 40 to 3000m (Girardeau & Nicolas, 1981; Elthon et al., 1982; Nicolas & Prinzhofer, 1983), 0 to 1200m in the Oman ophiolite (Pallister & Hopson, 1981; Nicolas & Prinzhofer, 1983; Benn et al., 1988), and the New Caledonia ophiolite has the dunite of 300 to 600m (Prinzhofer et al., 1980). The Red Hills peridotite has a maximum thickness (about 3000m), though the thickness of the dunite in the Red Mountain peridotite in the Dun Mountain ophiolite is about 500m (Sinton, 1980). The thickness of the dunite must be important to consider the origin of the transition zone.

There are four main interpretations for origin of the large dunite body as follows; 1) cumulate origin (Jackson et al., 1975; George, 1978; Pallister & Hopson, 1981; Elthon et al., 1982), 2) residual mantle origin (Church & Stevens, 1971; Girardeau & Nicolas, 1981; Dick, 1977), 3) products of mantle residue with impregnating basaltic magma or magmatic fluid (Lorand, 1987; Bodinier, 1988), 4) complex with residue and cumulate (Quick, 1981a, b).

Jackson et al. (1975) reported for the transition zone in the Vourinos ophiolite that makes cyclic layering of olivine, olivine＋clinopyroxene, olivine＋clinopyroxene＋plagioclase and clinopyroxene＋plagioclase. Cumulate or metacumulate origin for transition zone is discussed from chromite-olivine adcumulate texture for the Oman (Pallister & Hopson, 1981) and the Troodos (George, 1978) ophiolites. Furthermore, for the Bay of Islands ophiolite Elthon et al. (1982) argued for the cumulate origin of the transition zone that is composed of interlayered ultramafic cumulates such as dunite, wehrlite, clinopyroxenite, websterite, lherzolite and harzburgite with minor chromitite.

On the other hand, Church & Stevens (1971) suggested that the presence of high pressure mineral assemblages and the occurrences of the complex deformation structure represent upper mantle rather than in situ gravity cumulate. From field evidence that are 1) progressive transition between harzburgite and dunite, 2) presence of dunite patches inside the highly depleted harzburgite, 3) thickness (3000m, Blow-Me-Down Mountain) and 4) homogeneity of the massive dunite, Girardeau & Nicolas (1981) introduced residual origin for the transition zone in the Bay of Islands ophiolite. Dick (1977) pointed out some

evidence of restricted mineral composition, lithology and granulite texture for residual origin of the dunite in the transition zone in the Josephine ophiolite.

Evidence of the third category that is products of mantle residue with impregnating basaltic magma or magmatic fluid have reported from the New Caledonia (Nicolas & Dupuy, 1984), the Oman (Benn et al., 1988) and the Red Mountain (Sinton, 1977), based on textural and geochemical informations.

Quick (1981a, b) discussed for the forth category that the large dunite body in the Trinity peridotite is formed by mixture with residue and cumulate. He concluded that at least near the harzburgite wall the dunite caused by partial assimilation between picritic magma and plagioclase-lherzolite, but at the center of the body they are originated from crystal fractionation of olivine from ascending picritic magma through in plagioclase lherzolite wall. He proposed for them "zone refining" of the mantle wall rock by the migrating melt.

6-3-2. Possibility of Crystal Fractionation of Olivine

Possibility of crystal fractionation of olivine for dunite body in the transition zone is considered, based upon a point of view of mass balances between a olivine and melt. On **Figure 32**, at first if thick dunite (3km thickness) is formed by crystal fractionation of olivine of 10~15% from primary picritic melt, thickness of the fractionated melt, namely crust, must be 17~27km (**Fig. 32, case 1**). There is no evidence for the thick crust in the Dun Mountain ophiolite. If the crust is very thick (17~27km), higher metamorphic grade like amphibolite to granulite facies is expected at the deepest position of the crustal parts. Secondary, if oceanic crust that has about 6km thickness represents product suffered crystal fractionation of olivine of 10~15% from picritic melt, the fractionating olivine only makes dunite of 670~1100m thick (**Fig. 32, case 2**). Finally, if thickness of the crust is 6km and the thickness of dunite is 3km, it can not be explained that the thick dunite body is formed by crystal fractionation of olivine from a picritic melt. Though a part of the dunite can be explained by the fractionation, other origin must be applied to be explained for the whole dunite (**Fig. 32, case 3**).

6-3-3. Field Occurrences of Harzburgite and Dunite in the Transition zone

Harzburgites are also recognized in the transition zone of the Red Hills peridotite. Field relationships between harzburgites and dunite in the transition zone display that the dunite *intrudes* into the harzburgite (**Fig. 11 a~d**). There are various steps on the dunite *intrusion* as follows; 1) the dunite infiltrates into harzburgite at random direction (**Fig. 11 a**), 2) the dunite cuts harzburgite in parallel (**Fig. 11 b**), 3) the harzburgite occurs as lenticular blocks in dunite matrix (**Fig. 11 c**), and 4) the harzburgite is scattered as small flakes in dunite matrix (**Fig. 11 d**).

From above field observations it is confirmed that the dunite *intrudes* into harzburgite. However, it is physically impossible that the dunite (olivine) melt intrudes into harzburgitic

solid. Because the melting point of dunite (Fo=90) is about 1800℃ at 1 atm (Yoder, 1976), it is unlikely at the uppermost mantle condition. What is this dunite *dyke*?

The Most important things are flaky occurrences of the harzburgite in dunite matrix (**Fig. 11 d**). If the flakes are only formed by mechanical decomposition of originally large harzburgite body, the harzburgite flakes must be dispersed in all over the dunite of the transition zone. However, the phenomenon is not recognized in the whole transition zone, and the flakes occur in restricted small area of the transition zone. As shown in **Figures 7** and **8**, the blocky harzburgites occur in the restricted upper part of the dunite zone. From field relationships between the harzburgites and dunite in the transition zone, it can be estimated that the dunite is formed by a reaction between harzburgite and any melt. For example, the reaction may be incongruent dissolution of pyroxenes to olivine plus melt.

On the other hand, there are four types of occurrences of spinels in transition zone dunite; 1) spinel grains arrange in center of olivine matrix between harzburgite walls (**Fig.**

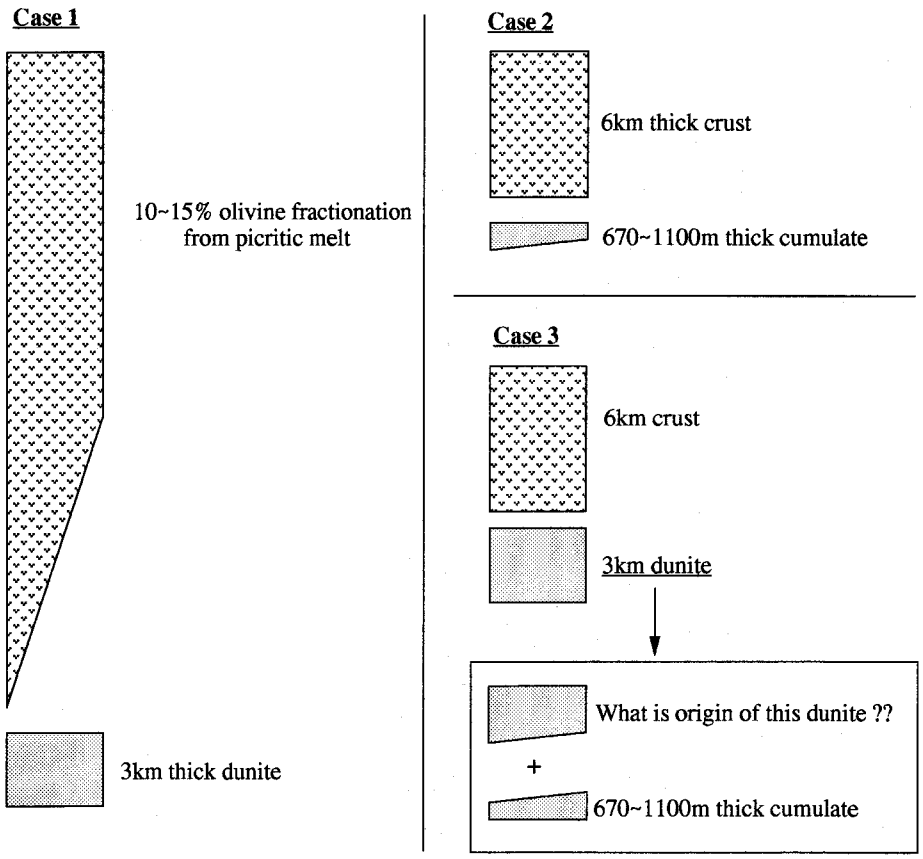

Fig.32. Relation of thicknesses between crust and the possible complemental cumulate. In case of the Red Hills peridotite, thick dunite (3km) can not be explained by simple fractionation of olivine (olivine cumulate). Detail discussions, see text.

12 f), 2) spinel grains are grading into olivine matrix, 3) monomineralic spinel aggregations show irregular shape (like amoeba-shape) in the dunite matrix, and 4) spinel occurs as seam in dunite matrix. From above field occurrences, it is inferred the various situations of spinel setting. Especially, in the first case, it is supposed that the spinels crystallized at earliest time arrange in center of "conduit" walled by harzburgite, like flowage differentiation mechanism (Bhattacharji & Smith, 1964). First and second cases suggest that the spinels are formed by the crystallization from a magma. Namely, the dunites including such spinels are cumulates. This is also supported from the shapes of spinels such as euhedral and rectangular in dunite in the transition zone, because the shapes of spinel crystals are formed under igneous processes.

These spinel habits mentioned above indicate that the dunite essentially came from crystal cumulates. However, many *in situ* harzburgites exists in dunite matrix in the upper part of the transition zone (occurrence such as in **Fig. 11 a**). The field relationships in the transition zone, such as in **Figure 11 a**, can not be explained by crystal accumulation for dunite. Thus, from field observations it is concluded that the thick dunite body in the transition zone must have derived from much complex origin like mixture of cumulus olivine and products by reaction between harzburgite wall and a melt.

6-3-4. Whole Rock Chemical Compositions

Rocks in the transition zone show wide chemical variation. They are divided roughly into three groups, clinopyroxene bearing dunite, plagioclase bearing dunite and harzburgite. There are good correlations on MgO against Al_2O_3 and MgO against CaO on clinopyroxene bearing and plagioclase bearing dunites (**Fig. 22**). These correlations are depending upon modal abundances of clinopyroxene or plagioclase as compared with olivine. Both trends on **Figure 22** are, namely, shown as tie lines of end members of clinopyroxene or plagioclase and olivine, Blocky harzburgites in dunite matrix in the transition zone also show good correlations on the diagrams (**Fig. 33**). The trends of the blocky harzburgites differ from that of harzburgites in lower zone of the body. On same MgO contents, both Al_2O_3 and CaO contents of the blocky harzburgites are characterized by lower contents than that of the lower zone. This probably depends upon low modal clinopyroxene in the blocky harzburgite (**Fig. 10**).

Harzburgites in the transition zone are comparatively depleted on incompatible (on peridotite compositions) major (Al_2O_3 and CaO) and trace (V, Sc and Cu) elements than those in the lower zone (**Fig. 22** and **23**). However, Na_2O contents of clinopyroxenes in blocky harzburgites in transition zone are relatively higher than that in harzburgites in the lower zone (**Fig. 16 b**), in spite of whole rock chemical compositions (especially Al_2O_3 and CaO) of former harzburgites are depleted than that of the latter.

Above dilemma can be interpreted by a kind of metasomatisms such as an interaction of harzburgite wall with any melt. By melt impregnation, the pyroxene components in the harzburgites will react with the melt, and incongruently dissolve to olivine and other melt.

Though the clinopyroxenes in the harzburgites will be dissolved, the Na_2O contents of the saved clinopyroxenes from the melting probably become to higher than that of original ones. If the reacting melt is much fractionated, the melt is enriched in incompatible elements. Thus, the interaction will dissolve clinopyroxenes in the harzburgites, in other words, the modal clinopyroxene will become to low. On the other hand, the compositions of remaining clinopyroxenes from the reaction will be changed to higher Na_2O contents than that of original clinopyroxenes.

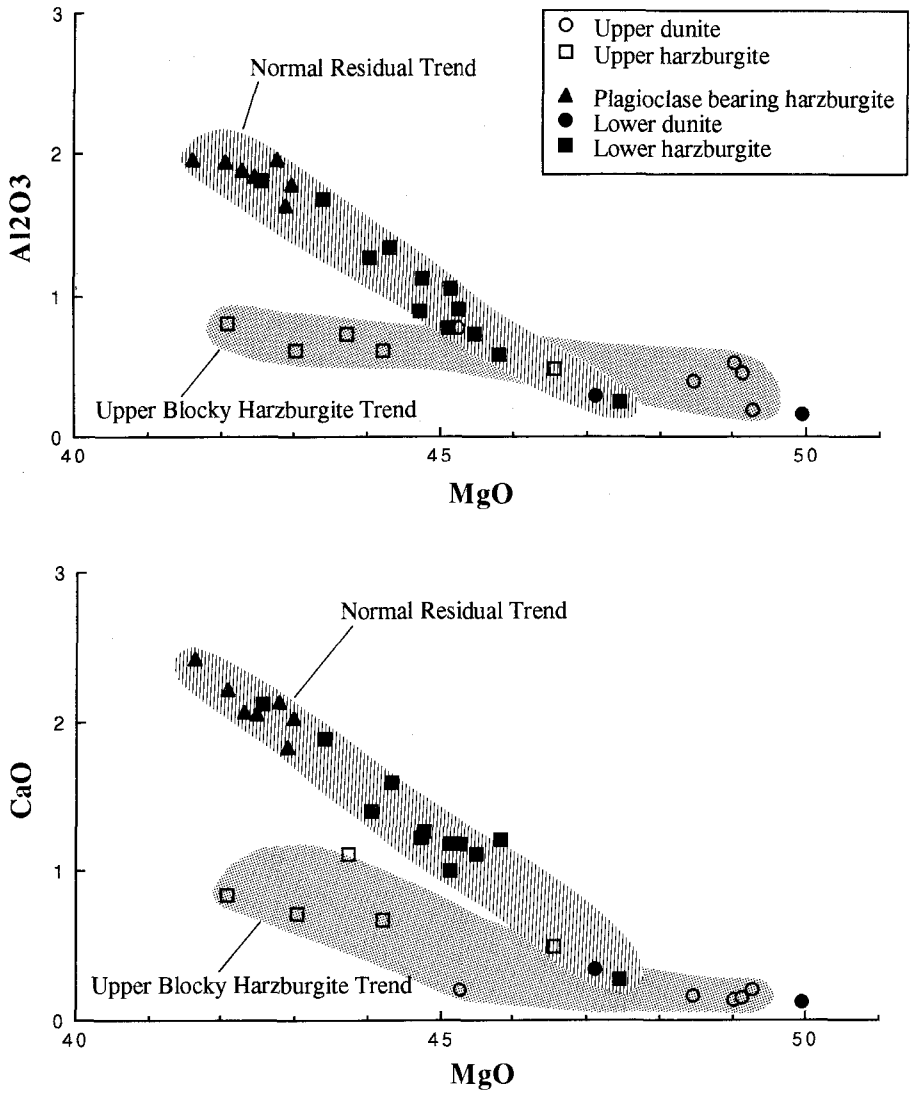

Fig.33. Al_2O_3 and CaO wt% plotted against MgO wt% for harzburgites. Open symbols: Samples of the upper zone. Solid symbols: Samples of the lower zone. Trend of harzburgites and dunites in the lower zone fits to that of usual residual peridotites. Note the trend of blocky harzburgites in the upper zone makes much gentle slope.

6−3−5. Mineral Compositions of Dunites and the Related Rocks

Spinel compositions in the transition zone are different from those in the peridotites in the lower zone. On the relationship between Cr# and Mg# in spinel composition, spinels in the transition zone excepting blocky harzburgites have lower Mg# than those in harzburgites in the lower zone, and are plotted on different areas (**Fig. 17**), spinels in both transition zone and the residual peridotites make two types of cluster each other. Harzburgites (harzburgite in the transition zone, and common harzburgite and plagioclase bearing harzburgite in the lower zone) make one group that agrees with range of spinels in oceanic mantle peridotites. On the other hand, clinopyroxene bearing and plagioclase bearing dunites, common dunite and olivine clinopyroxenite in the transition zone make a parallel cluster with former group.

Dick & Bullen (1984) pointed out that the Mg#'s of spinels in oceanic dunites are shifted to lower Mg# side than the trend formed by other spinel perridotites, and concluded that the spinels in the dunites are equilibrated with or are precipitated from iron-rich melt than the spinels in surrounding other peridotites because it is physically unlikely that only the spinels in the dunites are re-equilibrated under the condition of lower temperature than the spinel in surrounding associated peridotites. On OSMA plot, Arai et al. (1988) suggested that the peridotites plotted on lower Fo side than the mantle array are originated from some mantle metasomatisms such as addition of iron-titanium rich magma and/or any fluid into the dunite and harzburgite though almost all mantle peridotites saved from any mantle metasomatisms are included into OSMA area (**Fig. 28**). From the spinel compositions, it can be supposed that the dunites in the transition zone in the Red Hills are derived from cumulate or resulted from re-equilibration with more iron and titanium rich melt.

Blocky harzburgites in dunite in the transition zone, however, show recrystallized porphyroclastic texture (**Fig. 13 c**) characterized by aggregated spherical spinel grains (Mercier & Nicolas, 1975). Olivine and spinel compositions in the harzburgite blocks are shifted from the array to the left side (**Fig. 28**). It is likely that the blocky harzburgites in the transition zone are originated from residual mantle, because the blocky harzburgites show good correlation between modal olivine and Al_2O_3 contents in orthopyroxenes (**Fig. 20**) and also shows resemble modal compositions (**Fig. 26**) with that of residual peridotites. The spinel and olivine compositions in blocky harzburgites are presumably re-equilibrated with the iron rich melt (**Fig. 28**).

Ca zoning in olivine

The above discussion that is for possibility of reaction between harzburgite wall and a fractionated melt (e.g., iron-titanium rich melt), is also supported from Ca zoning of olivine in dunite of the transition zone in the Red Hills peridotite. As shown in **Fig. 34 c**, the Ca content of a olivine in the dunite decreases from core to rim. Olivines showing Ca zoning in **Fig. 34 c** directly contact with another olivine. There is no chemical difference on each

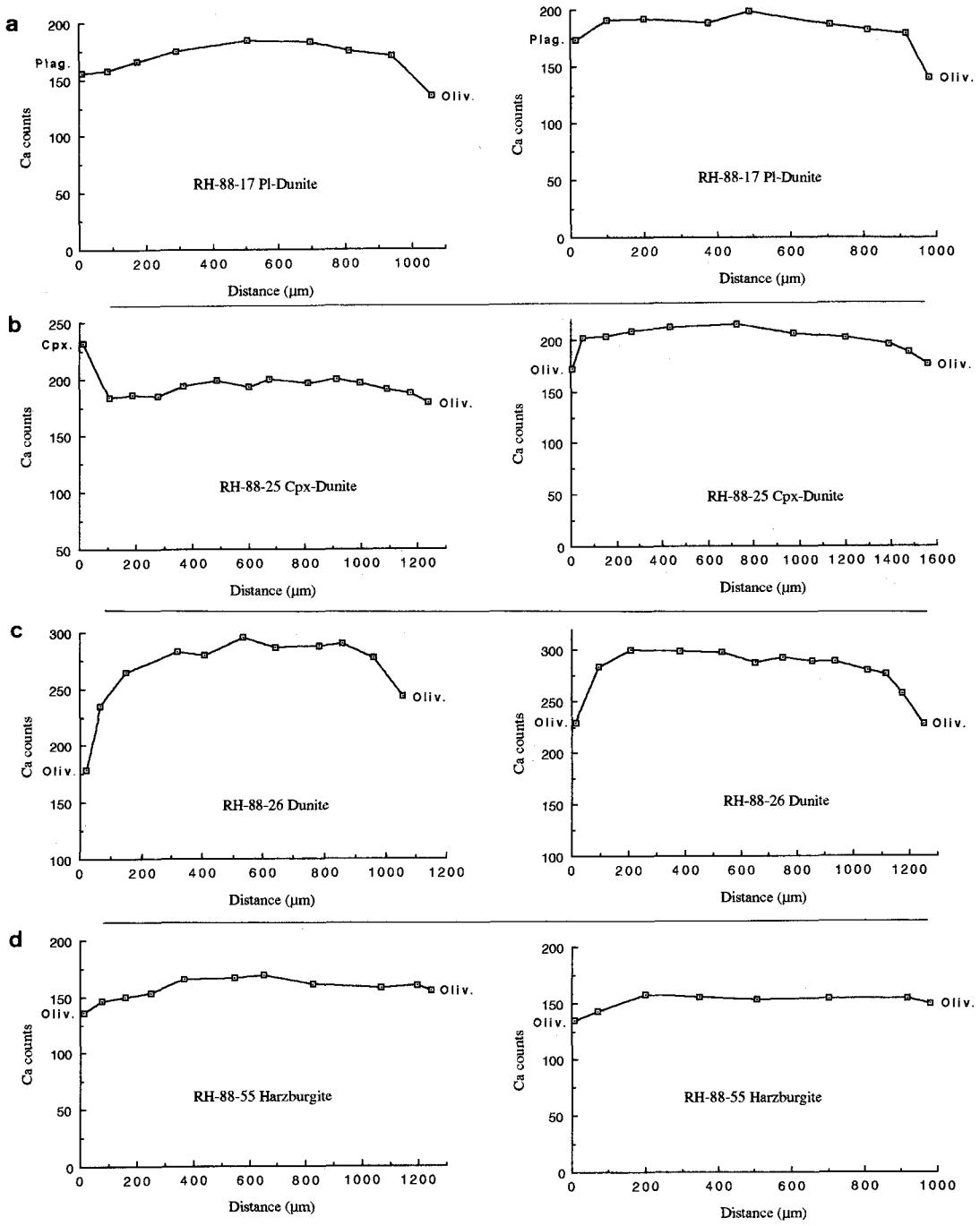

Fig.34. Patterns of Ca zoning of olivines. Ca count means counts per ten seconds. This qualitative analysis are obtained by counting times of three to five times 40 seconds. **a**: there is no clear Ca zoning besides contacts with other minerals (RH-17; plagioclase bearing dunite). **b**: Zoning can recognized at rim with clinopyroxene (RH-25; clinopyroxene bearing dunite). **c**: Obvious Ca zonings are recognized. Note the higher core Ca contents than the others (RH-26; dunite). **d**: There is no Ca zoning (RH-55; harzburgite).

other olivine core, that is, they have same Fo content at the core. There are some possibilities for Ca zoning of olivine in dunite of the transition zone as follows; 1) simple fractional crystallization, 2) metamorphic zoning, and 3) certain reaction with unequilibrated material.

If all dunites (olivines) in the transition zone dunite (olivine) were formed by fractional crystallization, there is no evidence for the mechanism making large quantities of complementary melts against thick olivine cumulate of about 2000~3000m. Furthermore, even if olivine makes zoning by simple fractional crystallization of the olivine, the zoning pattern must be normal one such as Ca content increases from core to rim because of dependence of distribution coefficient between melt and olivine ($Dc_aO=0.03$, Bender et al., 1978). The zoning of Ca decrease, therefore, can not explain by simple fractional crystallization. For second case, olivines in ophiolitic peridotites have been generally pointed out that the compositions are homogeneous except for porphyroblastic olivine formed by metamorphism. It has been reported that metamorphic olivines formed by recrystallization from serpentines have iron and manganese enriched core (Pinsent & Hirst, 1977). They pointed out that the range of manganese contents of the metamorphic olivine porphyroblasts is 0.4~1.8wt% at the core with Fo=86~93. The manganese contents of olivines are extremely higher than that of olivines in the Red Hills peridotite. Moreover, if the origin of Ca zoning in olivines in dunite of the transition zone is by recrystallization process from serpentines, the Ca content in single olivine crystal must be decreased at the edges on cracks replaced by serpentine in the grain. But such zoning can not observed along the serpentine filled cracks. Thus, the Ca zoning can not also explain by metamorphism.

The Ca zoning in olivine in dunite of the transition zone is possible to explain as following differnt two ways :

1) The zoning have resulted from processes of chemical diffusion. It is unlikely that the zoning by chemical diffusion between same minerals showing same chemical compositions, because diffusion is understood as the physicochemical processes that ions and atoms are transferred by gradients of the chemical potential. Therefore, it is expected that a further material at the grain boundaries of olivines exists. In case of olivine in the Red Hills transition zone, as the Ca content decreases to the rim, a further material must have lower Ca content or have smaller distribution coefficient for Ca than melt crystallizing the olivine.

Nabelek & Langmuir (1986) reported that the unusual zoning of olivine phenocrysts in the FAMOUS basalts comes from hybrid origin because it is impossible to explain for the unusual zoning by crystallization of simple rapid cooling. As distribution coefficients between olivine and melt for Ni and Mg are larger than 1, the result on the Rayleigh fractionation causes normal zoning. They suggested for one of possibilities of unusual zoning resulting from the incorporation of different pulse olivine basalt with plagioclase-pyroxene bearing low-Ni olivine series basalt.

For zoning of Ca decrease of olivine in the transition zone, it is expected that if the olivines in dunite of the transition zone dunite adjoin a melt having relatively low Ca con-

tent than the melt equilibrated with the dunite, the olivine will make the zoning of Ca decrease. The melt having relatively low Ca content is expected by crystallizations of clinopyroxene and plagioclase from a melt. The above inference is also supported from spinel and olivine compositions in rocks of the transition zone. That is, the Mg# of spinels in rocks of the transition zone are lower than that of general trend on Cr# vs. Mg# diagram (**Fig. 17**), and the Fo contents of olivines in rocks of the transition zone are sifted from the OSMA to the lower Mg# side (**Fig. 28**).

2) It is also possible to explain that the zoning represents recrystallization product from orthopyroxene to olivine caused by a melt impregnation. As shown in **Figure 34**, relative Ca contents of core of olivine in dunite (**c**) are evidently higher than others. Furthermore, the obvious zoning is never found in other rock types (**a, b** and **d**). In general, orthopyroxene contains higher CaO contents than olivine. If the orthopyroxene contacts with a fractionated melt, the orthopyroxene is incongruently decomposed to olivine by the melt. Such olivine maybe include higher Ca contents than the cumulus olivine.

Two possibilities has been described to explain the Ca zoning in olivine in dunite of the transition zone. Especially, importance of the zoning is that two types of olivines exist in dunites of the transition zone. One of olivine type is characterized by high Ca contents at the core and obvious Ca zoning, while the other type shows the lower Ca contents and does not show Ca zoning. It is strongly supported that a fractionated melt such as iron-titanium rich melt is needed to form the Ca zoning of olivine in dunite of the transition zone.

6-3-6. Two Pyroxene Equilibrium Temperatures

Equilibrium temperatures of Red Hills peridotite are calculated by Wells two pyroxene geothermometer (Wells, 1977). Results are shown in **Figure 35**. Average temperature in whole body is about 920℃ at the rim-rim pair, and is about 940℃ at the core-core pair. Temperatures obtained from the rims and the cores of pyroxenes of the transition zone are about 970℃ and 990℃, respectively, On the other hand, the temperatures of the residual harzburgites in the lower zone are about 890℃ and 900℃, respectively, Difference of the temperatures between transition zone and residual harzburgite is about 90℃ at the core-core pair and is about 80℃ at the rim-rim pair. These differences of the temperatures must be significant.

The obtained temperatures naturally do not record magmatic temperature when the pyroxenes are crystallized. The original magmatic temperatures are namely changed to lower. The re-equilibration of the temperature is occurred by effects of diffusion of elements during the cooling time. The chemical compositions of orthopyroxene and clinopyroxene do not show so significant variations on the Red Hills body. Furthermore, there is no tectonic gap between the transition zone and residual harzburgite in the lower zone. Based on higher equilibrium temperature (80~90℃) of the transition zone in the upper part of the body than residual harzburgite in the lower part of the body, it is inferred that the transition zone is kept in condition of high temperature till later period than

residual harzburgite. In other word, certain melt is probably stored in the transition zone till later period. This consideration that the transition zone is storage zone of melt is also supposed from differences of density between a basaltic melt ($\rho = 2.8$g / cm^3) and residual harzburgite ($\rho = 3.3$g / cm^3). As the density of a basaltic melt at the uppermost mantle is obviously smaller than that of harzburgite, the melt can be segregated in harzburgite to upward. On the other hand, at the mantle-crust boundary (seismic moho), as density of the melt is almost same as gabbroic rock constituting crust, the melt is hard to remove over the seismic moho. Therefore, it is supposed that a melt can be stored under the seismic moho,

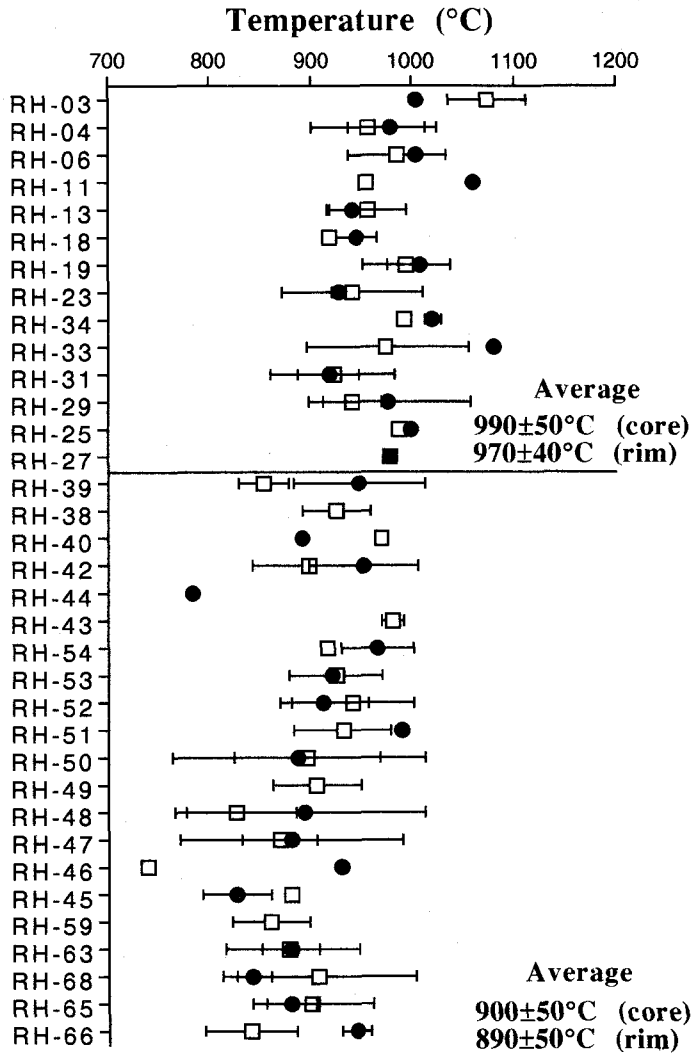

Fig.35. Two pyroxene temperatures with stratigraphic heights. Each point is average of plural results in one sample. The error means standard deviation. Note the temperatures of upper dunite predominated zone are higher than those of lower harzburgites.

namely that is the mantle-crust transition zone.

6-3-7. Magmatic Processes inferred from REE Patterns of Clinopryroxenes in the Transition Zone

Though the clinopyroxenes in the harzburgites in the lower zone of the Red Hills peridotite are residual phase judging from the textures and very low abundances of incompatible elements (e.g. Sr, Sm, Nd), the clinopyroxenes in the transition zone are magmatic products based on evidences of the textures and existence of magmatic twins. Chondrite-normalized REE abundances of clinopyroxenes in the transition zone are shown in **Figure 24**. The patterns are parallel each other. The chondrite-normalized abundances are 0.18~3.05 for Nd, and 2.03~8.94 for Yb. To explain the variation of REE abundances of clinopyroxenes in the transition zone, there are three possible processes as follows: 1) fractional crystallization process, 2) assimilation-fractional crystallization (AFC) processes, and 3) direct effect of differences of degrees of fracional melting at source region.

At first, as mentioned in **Section 6-2-5**, it is estimated that the harzburgites are residual materials suffered fractional melting of 12~20% from MORB-type source mantle based on REE concentrations of clinopyroxenes in harzburgites in the Red Hills. The REE concentrations of the melt are shown in **Table 16-A**. From chemical variation of olivine in the rocks of the transition zone, the primary picritic melt probably fractionated 10~15% olivine. The REE concentrations of melt after crystal fractionation of olivine from the primary melt are shown in **Table 16-B**. REE concentrations of co-existing clinopyroxenes with the melt (**B**) calculated by using distribution coefficients (**Table 13**) are in **Table 16-C**. The highest values of REE concentrations of clinopyroxenes in the transition zone of Red Hills peridotite (**Table 16-D**) coincide with the range of clinopyroxenes

Table 16. Calculated REE concentrations of primary melt, fractionated melt and the clinopyroxenes.

	A	B	C	D
Ce	3.95-6.58 (6.41-10.68)	4.38-7.73 (7.12-12.55)	0.44-0.77 (0.71-1.25)	
Nd	3.72-6.11 (8.15-13.36)	4.13-7.17 (9.03-15.69)	0.78-1.36 (1.71-2.98)	0.08-1.38 (0.18-3.05)
Sm	1.46-2.25 (9.79-15.11)	1.62-2.64 (10.86-17.69)	0.49-0.79 (3.26-5.31)	0.08-0.81 (0.51-5.50)
Eu	0.57-0.81 (10.17-14.48)	0.63-0.95 (11.27-16.92)	0.26-0.40 (4.73-7.10)	-0.50 (-9.00)
Dy	2.55-3.38 (10.41-13.80)	2.82-3.94 (11.50-16.10)	1.41-1.97 (5.75-8.05)	
Er	1.75-2.25 (10.96-14.06)	1.93-2.62 (12.07-16.37)	0.99-1.34 (6.16-8.35)	
Yb	1.67-2.06 (10.49-12.93)	1.84-2.39 (11.56-15.01)	0.92-1.19 (5.78-7.51)	0.33-1.46 (2.03-8.94)

A : Melt compositions inferred from fractional melting model. Degrees of melting are 12~20% (see Section 6-2-5)

B : Melt compositions inferred from fractional crystallization model. Degrees of olivine fractionation are 10~15%. Original melt composition is A.

C : Clinopyroxene compositions equilibrating with melt B.

D : Clinopyroxene compositions in trasition zone of the Red Hills peridotite.

Parenthesis means chondrite-normalized value.

(C) equilibrating with fractionated melt mentioned above. Because all minerals that are crystallized from picritic or basaltic melt have lower contents of REEs than the melt, the obviously lower concentrations of REEs in other clinopyroxenes in the transition zone can not be explained by further crystal fractionation of the melt.

Secondary, even if the fractionated melt assimilated with harzburgite that was the residual material extracting primary picritic melt, advancing LREE depletion of the melt could not be expressed by assimilation-fractional crystallization (AFC) processes as discussed below. During AFC processes on basaltic-peridotitic system, behavior of abundances of REEs in the melt mainly depends on (assimilation rate) / (crystallization rate), distribution coefficients between fractionating mineral and melt, and concentrations of the elements in assimilating material. Kelemen (1990) thermodynamically pointed out that the crystallization rate is almost equal to assimilation rate if temperature of the system is nearly constant. When both rates are equal, the concentration of an incompatible trace element in melt is controlled by the bulk distribution coefficients of assimilating material and crystallizing phases. As the assimilating material is harzburgite, the REE abundances are extremely low (e.g. Bloomer & Hawkins, 1987). However, the main crystallizing phase simultaneously is olivine. Distribution coefficients of REEs of olivine against melt are close to zero. It is inferred that the REE abundances in melt do not decrease than the abundances in original melt through the AFC processes. LREE depleted patterns of clinopyroxenes in the transition zone of the Red Hille peridotite, therefore, can not be explained by AFC processes.

Thirdly, for understanding the low abundances of REEs of clinopyroxenes in the transition zone, it must be explained that the possibility of direct influence of melt composition produced by different degrees of fractional melting at source region. REE patterns of melts estimated from clinopyroxene compositions in rocks of the transition zone are shown in **Figure 36** (shaded area). The melt compositions are calculated by using distribution coefficients in **Table 13**. The REE patterns in **Figure 36 a** are of calculated melts that are continuously removed and collected from source mantle region by fractional partial melting. The REE patterns, especially on LREE side, of melts inferred from clinopyroxene compositions in the transition zone are obviously different from the patterns of continuously removed and collected melts (**Fig. 36 a**). The melt compositions in case of fractional melting without process of collection of melt are shown in **Figure 36 b**. The REE patterns of melts estimated from clinopyroxenes in the transition zone are well agreed with the patterns calculated by fractional melting model without continuous removal and collection of melt. Namely, clinopyroxenes of the transition zone are certainly crystallized from each ascending melt blob produced at degrees of melting of each 5 to 15%. Each melt blob separates by turns from the source region without mixing each other. In other word, ascending each melt blob melted at source mantle by different degrees of fractional melting is not mixed with other blobs, when they are passing through and are crystallizing the clinopyroxenes in region of current transition zone. Though the residual harzburgite totally suffers degrees of fractional melting of 12~20%, the degrees of melting of 12~20% repre-

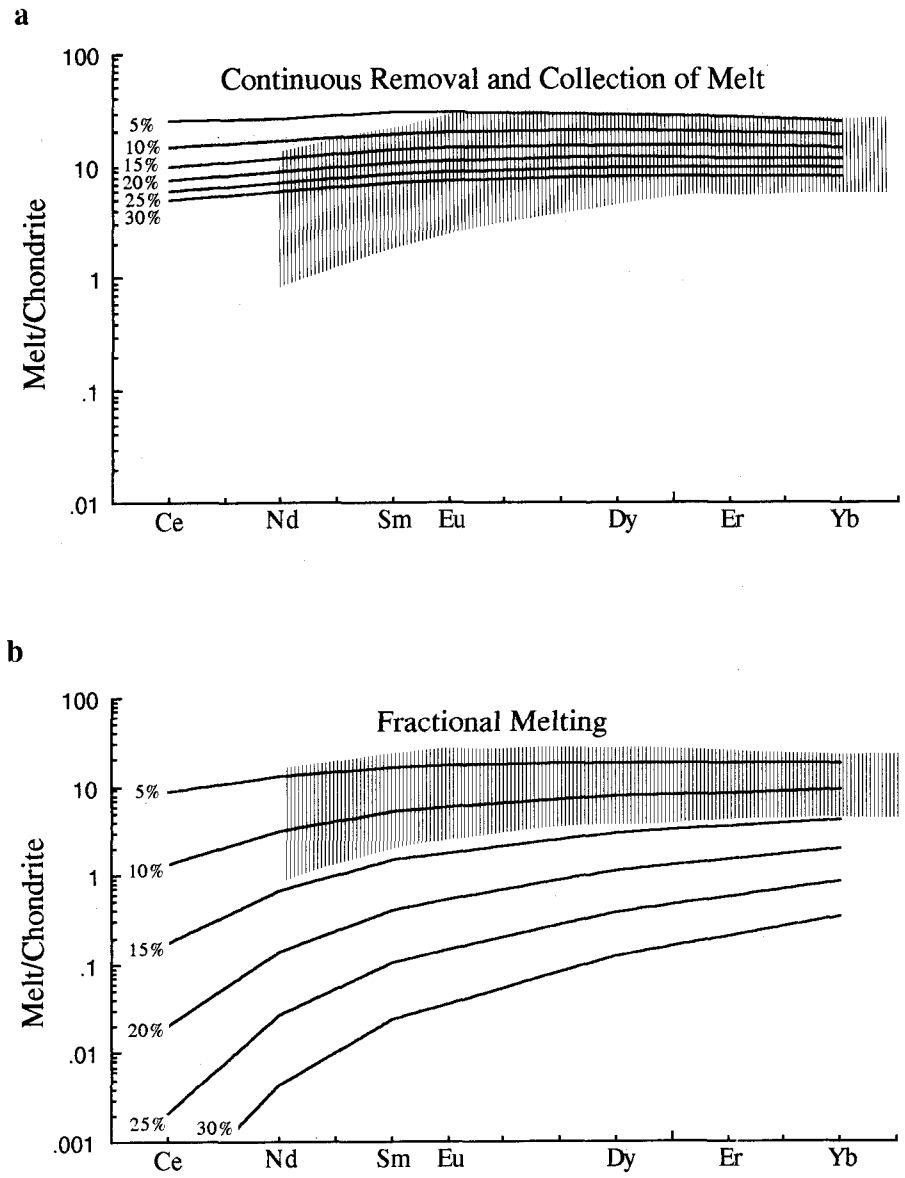

Fig.36. Suitable melting mechanism inferred from REE concentrations of clinopyroxenes in the trasition zone. As clinopyroxenes in the transition zone are magmatic products (crystallized from a magma), the shaded area indicates range of hypothetical melt composition equilibrated with the clinopyroxenes. **a**: melt composition that is intergrated one (continuous removal and collection of melt) produced by fractional melting. **b**: melt composition without collection of each melt blob produced by fractional melting.

sent integrated one and mean final results after whole melting events.

6−3−8. Summary

The dunites in the transition zone can be regarded as mixture of cumulus dunite and reaction products between harzburgite residue and a fractionated basaltic melt. Evidence of the cumulate origin are as follows; 1) grading structures of spinels are found, and 2) Fo contents of olivines (Fo=87～91) in the transition zone can be *compositionally* formed by olivine fractionation from a picritic melt. On the other hand, evidence of the reaction products are as follows; 1) decomposition structures of pyroxenes in blocky harzburgites are found in field, 2) the spinels show much iron rich compositions than that of residual harzburgites, 3) Ca zoning in common dunite, and 4) the REE patterns of clinopyroxenes can not be explained by simple fractional crystallization in magma chamber.

Furthermore, the transition zone must have been a melt storage zone, because the two pyroxene equilibrium temperature of the transition zone is higher than that of the residual harzburgites. The REE patterns of clinopyroxenes and Sr isotopic compositions of minerals suggest that the probable melting mechanism is similar to dynamic melting.

6−4. Petrogenesis of the Red Hills Peridotite

The cartoon for the petrogenesis of the Red Hills peridotite is shown in **Figure 37**. From mineral compositions in residual harzburgites of the lower zone of the body, the primary melt is picritic composition having 12.5～15.0wt% MgO and 7.8～9.4wt% FeO. The primary picritic melt must be generated by degrees of fractional melting of 12～20%. The each melt blob separates from the melting region, and segregates to upward without mixing of each other. During the upwelling, the primary picritic melt fractionates olivine. Consequently, the melt composition changes to basaltic one. The each blob is composed of mixture of basaltic melt and olivine crystal. With further fractional crystallization of olivine, the melt must be unequilibrated with the surrounding harzburgite wall. Thus, reaction between the fractionated melt and wall of harzburgite residue is certainly occurred at the shallow level of uppermost mantle. At the almost same time with the reaction (at before and after of the reaction), plagioclases and clinopyroxenes are crystallized from the fractionated melt. The each melt blob is still independent with other blobs, because this is suggested from REE patterns of clinopyroxenes in the transition zone. The melts inferred from the clinopyroxenes show still obvious LREE depletion. The fractionated melt is stored in the uppermost mantle (2～3kbar). This is supported from reversed thermal structure of the transition zone to the uppermost mantle. The melt infiltrates into the harzburgite wall and reacts with the wall. The orthopyroxenes in the harzburgites are incongruently dissolved to olivine and a melt. After the reaction, the reacted melts squeeze out from this reaction zone. Therefore, the dunite of the transition zone is composed of mixture of cumulus olivine fractionated from picritic melt and the reaction products. The each melt squeezed out from the transition zone will be mixed in magma chamber with the other melts.

6−5. Suitable Magmatic Processes beneath a Mid-Ocean Ridge inferred from the Red Hills Peridotite

6−5−1. Previous Works

Thick discordant dunite between mafic crustal rocks and the beneath residual mantle materials has been reported from many ophiolites. There are two main ideas for origin of this dunite as follows; cumulate formed by olivine crystallization from a picritic melt (e.g., Moores, 1969; Jackson, 1971; Greembaum, 1972; Jackson et al., 1975; Dick, 1977; Malpas, 1978; Elthon et al., 1982, 1984; Smewing et al., 1984), and residual mantle suffering relatively higher degrees of melting (e.g., Church & Stevens, 1971; Dick, 1977; Sinton, 1977, 1980; George, 1978; Dick & Sinton, 1979; Nicolas et al., 1980; Girardeau & Nicolas, 1981; Nicolas & Prinzhofer, 1983; Nicolas & Dupuy, 1984; Benn et al., 1988). Differences of both ideas have important key to discuss on evolution of MORBs, namely, of oceanic crusts. If the dunite in the mantle-crust transition zone is cumulate, the complementary large volume of fractionated melt must be formed. In this case, the primary melt is certainly picritic composition, because the melt forming oceanic crust is processed large degrees of fractionation of olivine (olivine cumulate). As the picritic magma is regarded as product at deeper mantle (<40km), the initial MORB source is derived from deeper mantle material. On the other hand, if the dunite is residual mantle, the primary melt can be estimated to tholeiitic composition.

There are many studies for primary magma of MORBs. They are divided into three categories. First category is that higher magnesian MORBs represent one of primary magma (Engel et al., 1965; Kushiro, 1973; Frey et al., 1974; Fujii & Kushiro, 1977; Langmuir et al., 1977; Bender et al., 1978; Bryan, 1979; Presnall et al., 1979; Walker et al., 1979; Fujii & Bougault, 1983). Especially, Fujii & Bougault (1983) experimentally clarified that a glassy magnesian olivine tholeiite from the FAMOUS area coexists with olivine, orthopyroxene, clinopyroxene, spinel and plagioclase at 10 kbar and within 10℃ of the liquidus. They explained that a melt of this magnesian tholeiite can coexist with mantle peridotite at about 10 kbar. Second category includes that, since all MORBs erupted are already fractionated, the original melt is picritic composition generated at higher pressure condition (O'Hara, 1968; Yoder, 1976; Elthon, 1979, 1986; Green et al., 1979; Duncan & Green, 1980; Stolper, 1980). Elthon (1979) pointed out that the primary melt segregated from the upper mantle beneath an oceanic ridge is shown to contain ~18% MgO based on field evidence of the Tortuga ophiolite complex, Chile. He also estimated the chemical composition of average oceanic crust, that is picritic composition. Stolper (1980) suggested the picritic composition for primary melt of MORBs. He indicated that compositions of "primitive MORB"(the most magnesian olivine tholeiite) do not lie on the *ol*+*opx* cotectic, and concluded that picritic melt equilibrates with harzburgite (or lherzolite) at 15~20 kbar, and thus, that is primary. Above ideas of the two categories are based on concept of partial

melting of homogeneous mantle. Chemical compositions of the primary melts are modified by fractional crystallization of minerals during upwelling of the melt and/or in magma chamber.

On the other hand, as third category, it has been proposed that the chemical variation of MORBs are caused by partial melting of heterogeneous source mantle materials (Schill-

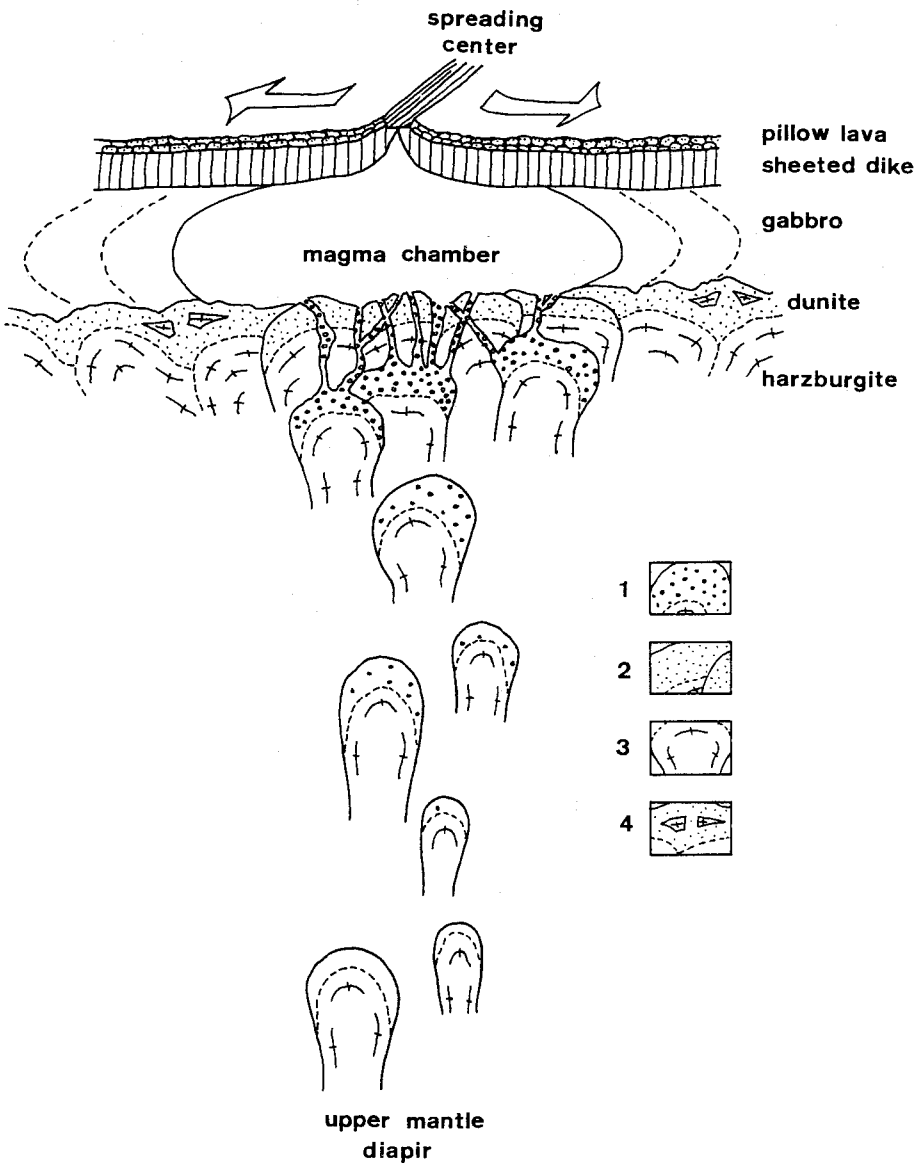

Fig.37. Cartoon for a possible petrogenetic model of the Red Hills peridotite. **1**: melt blob with crystallized olivine from a primary picritic melt. **2**: produced dunite equivalent to the transition zone. **3**: harzburgite residue. **4**: blocky harzburgite surrounded by dunite.

ing, 1973; Langmuir et al., 1977; Wilkinson, 1982; Prinzhofer et al., 1989). Langmuir et al. (1977) pointed out that the geochemical variation is explained by mixing of melts occurred by different degrees of partial melting of heterogeneous mantle (Dynamic melting), because REE patterns and the Sr isotopic compositions of MORBs drilled from same hole can not be understood by simple crystal fractionation from a homogeneous primary magma. Prinzhofer et al. (1989) proposed a melting model that the both laminated pyroxenite layer considered as recycled oceanic crust and the surrounding host depleted peridotite would be melted with different melting proportions and be mixed (Stochastic melting).

Chemical diversity of MORB magmas can be caused by near-surface crystallization, crystal fractionation within the mantle, magma mixing and the source mantle heterogeneity. Depth of crystal fractionation depends on depth of the initial partial melting. This is important problem to consider the primary melt of MORBs. For origin of chemical diversity of MORB magma excepting crystal fractionation, O'Hara (1977) suggested that magma mixing such as successive and repeated magma injection in open magma chamber can be occurred. Magma mixing is supported from petrographic, mineralogical studies (Rhodes et al., 1979; Rhodes & Dungan, 1979; Nabelek & Langmuir, 1986).

Chemical variations of MORBs must be formed through the above complex processes. Because the study for uppermost mantle beneath oceanic crust can omit to consider any processes in magma chamber, it can be much accurately discussed for the melt behaviors at the uppermost mantle excepting chemical modifications of MORB magma in magma chamber.

Scope of this section

It has been proposed the idea that the dunite is produced by reaction of wall rocks with melt removal at shallow level mantle, such as incongruent melting of orthopyroxene in residual mantle (Dick, 1977; Cassard et al., 1981; Quick, 1981a, b; Nicolas & Prinzhofer, 1983). In spite of they have pointed out the importance of the reaction on formation of large discordant dunite in ophiolites, they have not applied the concepts for magmatism at mid-ocean ridge system. Because the boninites and/or high magnesian andesites from many ophiolites have been discovered, the large discordant dunites have been regarded as products at tectonic settings of island arcs. Therefore, genesis of calc-alkaline rock, high magnesian andesite and/or boninite magmas at island arcs have been discussed to connect with formation of large discordant dunite in many ophiolites (Fisk, 1986; Kelemen, 1986, 1990; Kelemen et al., 1990). They have pointed out and experimentally confirmed for importance of reaction between a basaltic melt and depleted harzburgite to produce those magmas beneath island arcs.

On the other hand, for origin of boninites characteristically accompanied with island arc volcanisms, Cameron et al. (1983) and Cameron (1989) have suggested the mixing of LREE depleted magma derived from depleted peridotite and LREE enriched fluids related to sub-

ducting plate, based on geochemical approaches. The Sr isotope ratios of the boninites are 0.7034 to 0.7064 (Cameron et al., 1983; Cameron, 1989). Furthermore, Sr isotope ratios of many island arc volcanic rocks are ranging from 0.7028 to 0.7101, and the peak of frequencies is 0.7034～0.7036 (**Fig. 38**). If any calc-alkaline magmas are formed from reaction between depleted mantle (harzburgite) and a fractionated basaltic melt as discussed by Fisk (1986), Kelemen (1986, 1990) and Kelemen et al. (1990), it is impossible to explain for variation of Sr isotope ratios of island arc rock. Because the original basaltic melt must have higher Sr isotope ratio to make volcanic rocks of island arc showing the Sr isotope ratios ranging from 0.7028 to 0.7101.

By the way, the Red Hills peridotite also includes large discordant dunite as the mantle-crust transition zone. Though a part of the dunite shows cumulus texture such as grading of spinel, it can be understood that parts of the dunite is formed by reaction between residual harzburgite and any basaltic magma. The Sr isotope ratios of minerals in the transition zone range from 0.7019 to 0.7027. The isotope results strongly indicate that the rocks in the transition zone formed under condition of a mid-ocean ridge system (see below discussions). This is inconsistent with Sr isotope signatures of island arcs. Namely, it is

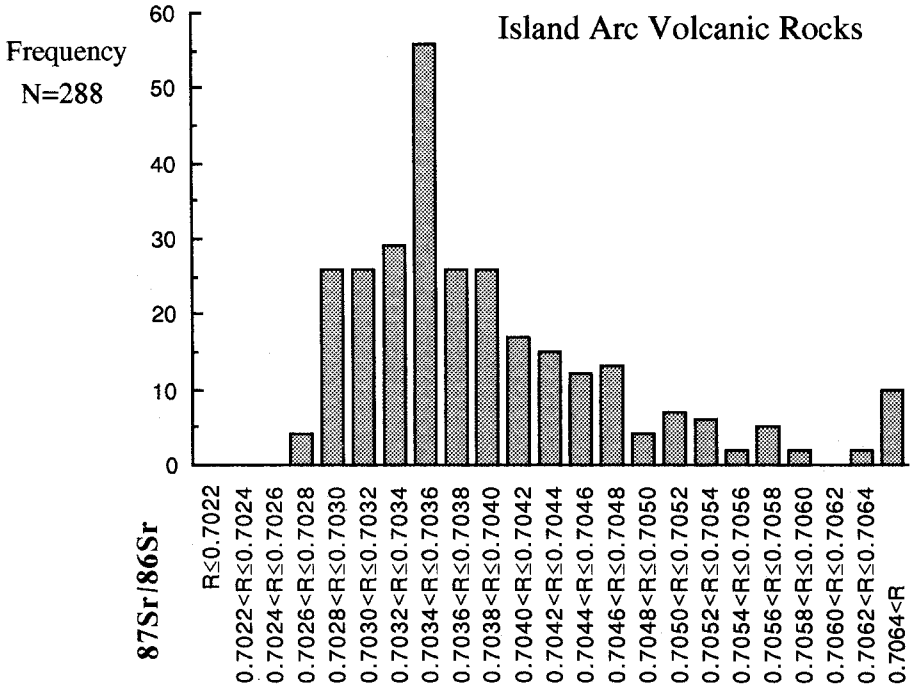

Fig.38. Histogram for Sr isotope data of basalts from various island arcs. Data sources are: Hawkesworth et al.(1977, 1979), McCulloch & Perfit (1981), Nohda & Wasserburg (1981), Whitford et al.(1981), Gill (1984), Thirlwall & Graham (1984), Davidson (1985), Kay et al.(1986), von Drach et al.(1986), White & Dupre (1986), Ewart & Hawkesworth (1987), Volpe et al.(1987), and Woodhead et al.(1987).

suggested that the above mentioned reaction can also occurs at a mid-ocean ridge system.

The large discordant dunites have been found from the Bay of Islands ophiolite and Lanzo peridotite, where are not shown any island arc signatures yet. It has been reported that the maximum thickness of dunite in the Bay of Islands is 3000m (Girardeau & Nicolas, 1981). Thus, we must look into such dunites in the transition zone that do not show island arc signatures. As mentioned above, the Red Hills peridotite regards as a good example of the mantle-crust transition zone beneath a mid-ocean ridge. In following sections, chemical properties of the Red Hills peridotite will be compared with those of oceanic peridotites, and possible factors of chemical diversities of magma at a mid-ocean ridge system will be inferred from case study of the Red Hills peridotite.

6-5-2. Comparisons between Recent Mid-Ocean Ridge Rocks and the Red Hills Peridotite

Equilibrium temperatures

Equilibrium temperatures for oceanic peridotites (harzburgite and lherzolite) are estimated by using Wells' two pyroxene geothermometer (Wells, 1977) (**Table 17**). The equilibrium temperatures of peridotites are about 980℃ at the north Atlantic Ridge (Shibata & Thompson, 1986), 1000℃ at the Central Indian Ridge (Hamlyn & Bonatti, 1980) and 1170℃ at the Southwest Indian to America-Antarctica Ridges (Dick, 1989). There is wide variation for equilibrium temperatures on each locality. On the other hand, the temperature for peridotites from the Ogasawara fore-arc (Ishii, 1985) is about 830℃. This is characterized by relatively lower temperature than that of oceanic peridotites. The average temperatures for the transition zone and the residual harzburgite of the Red Hills peridotite body are 980℃ and 900℃, respectively. The former temperature is the lowest value of range for data of current oceanic peridotites, but the latter one is fairly low. It seems that the temperature of each locality is in proportion to the spreading rate. The Southwest Indian to the America-Antarctica Ridges that represent ridges of slow spreading rate show the hihest equilibrium temperature. On the contrary, the Central Indian and the north Mid Atlantic

Table 17. Two pyroxene temperature* and spreading rate data**

Location	T (℃)	Spreading rate (mm/yr)
America-Antarctica Ridge	1208	9.0
Southwest Indian Ridge	1146	17.2
Central Indian Ridge	1007	
North Mid-Atlantic Ridge	976	10-20 (20 at FAMOUS area)
Ogasawara Fore-Arc	827	

* Estimated from Wells (1977) geothermometer
Data sources : Hamlyn & Bonatti (1980), Ishii (1985), Shibata & Thompson (1986), Dick (1989)

** Data sources : Batiza (1984), Lawver & Dick (1983)

Ridges that represent ridges of higher spreading rate than the Southwest Indian and America-Antarctica Ridges, show lower equilibrium temperature. Though there is no data from the East Pacific Rise, the temperature may be show much lower than former two cases if the peridotites would be collected from the East Pacific Rise. Thus, the Red Hills peridotite that shows lower equilibrium temperature may stands for the mantle-crust transition beneath fast spreading ridge. This view point that the Red Hills peridotites represent the mantle-crust transition beneath fast spreading ridge system such as the East Pacific Rise and the Juan de Fuca Ridge, is also concordant with results of the Sr isotope study. Namely, both Red Hills peridotites and the basalts from fast spreading ridges (e.g., East Pacific Rise) have the lowest Sr isotope ratios.

Variation of Sr isotope ratios of MORBs

Variations of Sr isotope ratios of MORBs are shown in **Table 18**. There is wide compositional variation. The MORBs in the Pacific Ocean show relatively low Sr isotope ratios though the MORBs in the Indian Ocean are characterized by higher Sr isotope ratios. The MORBs showing remarkable low Sr isotope ratios are only occurred in the Juan de Fuca and the Gorda Ridges where located on the northern parts of the Pacific Ocean. Average Sr isotope ratio of the basalts from the Juan de Fuca Ridge is 0.7024 (n=36), and the range is from 0.7021 to 0.7026. On **Figure 39**, peak of the frequency of basalts from the East Pacific Rise is also low ranging from 0.7024 to 0.7026, like ranges of the Juan de Fuca and Gorda Ridges.

These compositional variation of Sr isotope ratios obtained from the MORBs in the Pacific Ocean is well overlapped with the variation of clinopyroxenes and plagioclases from

Table 18. Average Sr isotope variations of MORBs and the related rocks

Location	n	Average	95%C.L.
Red Hills peridotite (minerals)		0.70193−0.70272	
Juan de Fuca Ridge	36	0.70244	0.00003
Gorda Ridge	8	0.70250	0.00012
Southern East Pacific Rise	48	0.70255	0.00003
Northern East Pacific Rise	35	0.70258	0.00005
Galapagos Spreading Center	40	0.70275	0.00006
Northern Mid Atlantic Ridge	78	0.70288	0.00008
Back Arc Basins	19	0.70295	0.00008
Red Sea	25	0.70295	0.00009
Southern Mid Atlantic Ridge	24	0.70298	0.00019
Central Indian Ridge	34	0.70305	0.00011
Iceland	42	0.70319	0.00005
Southwest Indian Ridge	41	0.70322	0.00023
Southeast Indian Ridge	25	0.70328	0.00027

Data sources are in Fig. 39

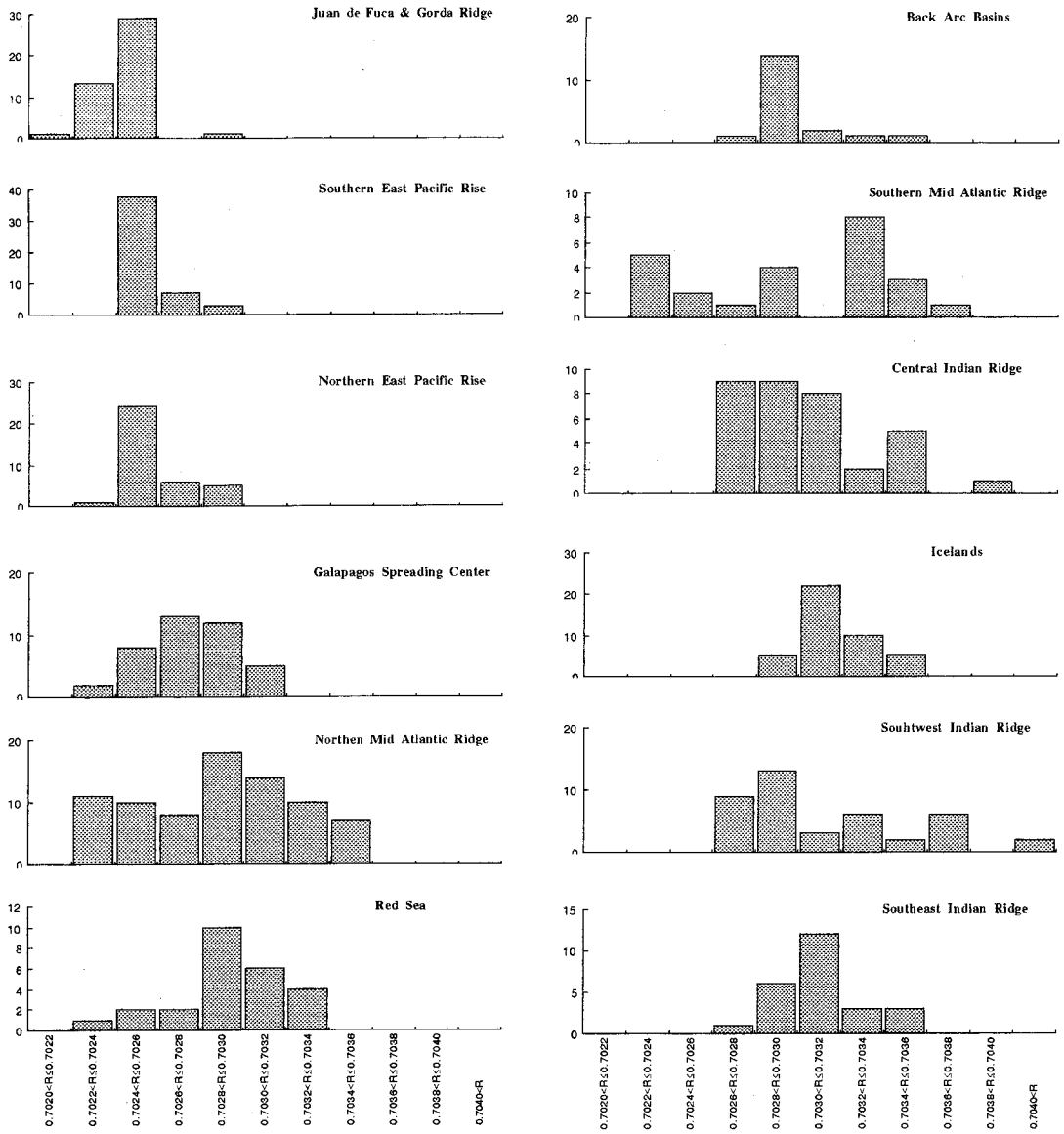

Fig.39. Histograms for Sr isotope data of basalts from MORBs and the related tectonic environments. Averages of each histogram are also shown in **Table 17.** Data sources are: O'Nions & Pankhurst (1974), Sun & Jahn (1975), O'Nions et al.(1977), Zindler et al.(1979, 1984), Cohen et al.(1980), Dupre et al.(1981), Cohen & O'Nions (1982a, b), Machado et al.(1982), White & Hofmann (1982), Dupre & Allegre (1983), LeRoex et al.(1983, 1987), Verma et al (1983), Hamelin et al (1985), Hamelin & Allegre (1985), Macdougal & Lugmair (1985, 1986), Michard et al.(1986), Price et al.(1986), Ito et al.(1987), Shirey et al.(1987), Volpe et al.(1987), White et al.(1987), Eissen et al.(1989), Hegner & Tatsumoto (1989), Mahoney et al.(1989), Natland (1989), Altherr et al.(1990), and Rhodes et al.(1990).

the Red Hills peridotites. The Sr isotope ratios of the Red Hills peridotite are obviously different from the data from the Indian and Atlantic Oceans. Furthermore, the Sr isotope ratios of the Red Hills peridotite do not support the other tectonic environments, spreading center combined with hotspot (i.e., Iceland and the MOR near the Azores), narrow speading ocean lain between continental crusts (i.e., Red Sea) and back arc basins (i.e., Scottia Sea and Philippine Sea). The average Sr isotope ratios from above three tectonic environments are 0.7032 on the Iceland and neighbor Reykjanes Ridge, 0.7030 on the Red Sea, and 0.7030 on the Scottia Sea and Philippine Sea. These ratios are also evidently higher than the ratios of minerals in the Red Hills peridotite (0.7019～0.7027). Furthermore, the Sr isotope ratios from the Sumisu rift in the Izu-Mariana arc system in the western Pacific has been preliminarily reported (Nohara et al., 1990). They concluded that the Sumisu rift represents oceanic crust in back arc side and the opening is just started. The Sr isotope ratios are from 0.7030 to 0.7033 and are also higher than those of MORBs in the Pacific Ocean and of the Red Hills peridotites.

The rocks characterized by the obviously low Sr isotope ratios ranging from 0.7020 to 0.7027 are occurring on restricted areas on the earth, the East Pacific Rise and the Juan de Fuca Ridge. It is concluded that the Red Hills peridotite body may represents an example of the mantle-crust transition zone beneath fast spreading ridge such as the East Pacific Rise or the Juan de Fuca Ridge.

6－5－3. Possibility of Modification of MORB Magma Composition by Reaction between a Fractionated Melt and Harzburgite Wall

It has been discussed that reaction between a melt and harzburgite residue can explain for generation of island arc magma (Fisk, 1986; Kelemen, 1986, 1990; Kelemen et al., 1990). In this section, it will be considered for the possibility that the reaction generates a MORB magma.

Chemical variations of MORB glasses, island arc basalts, and experimental and calculated results from Kelemen et al. (1990) are shown in **Figures 40** and **41**. Quartz normative MORB glasses are plotted on higher SiO_2 field as a function of same Mg# than olivine normative glasses. The SiO_2 contents (**Fig. 40 a**) of quartz normative glasses on Mg#＝0.50～0.60 are 51～53wt%. The quartz normative glasses have wider range on Mg# than olivine normative glasses on same figure. Though parts of the experimental and calculated results (Kelemen et al., 1990) of 1050℃ show higher SiO_2 contents than MORB glasses, the results of 1150℃ are almost overlapped with region of quartz normative MORB glasses (**Fig. 40 a**). The SiO_2 contents of island arc basalts are plotted on much wider area. Kelemen et al. (1990) concluded that their experimental results from hydrous condition and at 1050℃ show signatures of calc-alkaline magma. Their results on 1050℃ are high alumina basalts (basaltic andesite) showing 17～18wt% Al_2O_3 (**Fig. 40 b**). This agrees with island arc basalts on Kuno's discriminant diagram (Kuno, 1960). However, their results on 1150℃ excepting two analytical points are overlapped with the trend that is

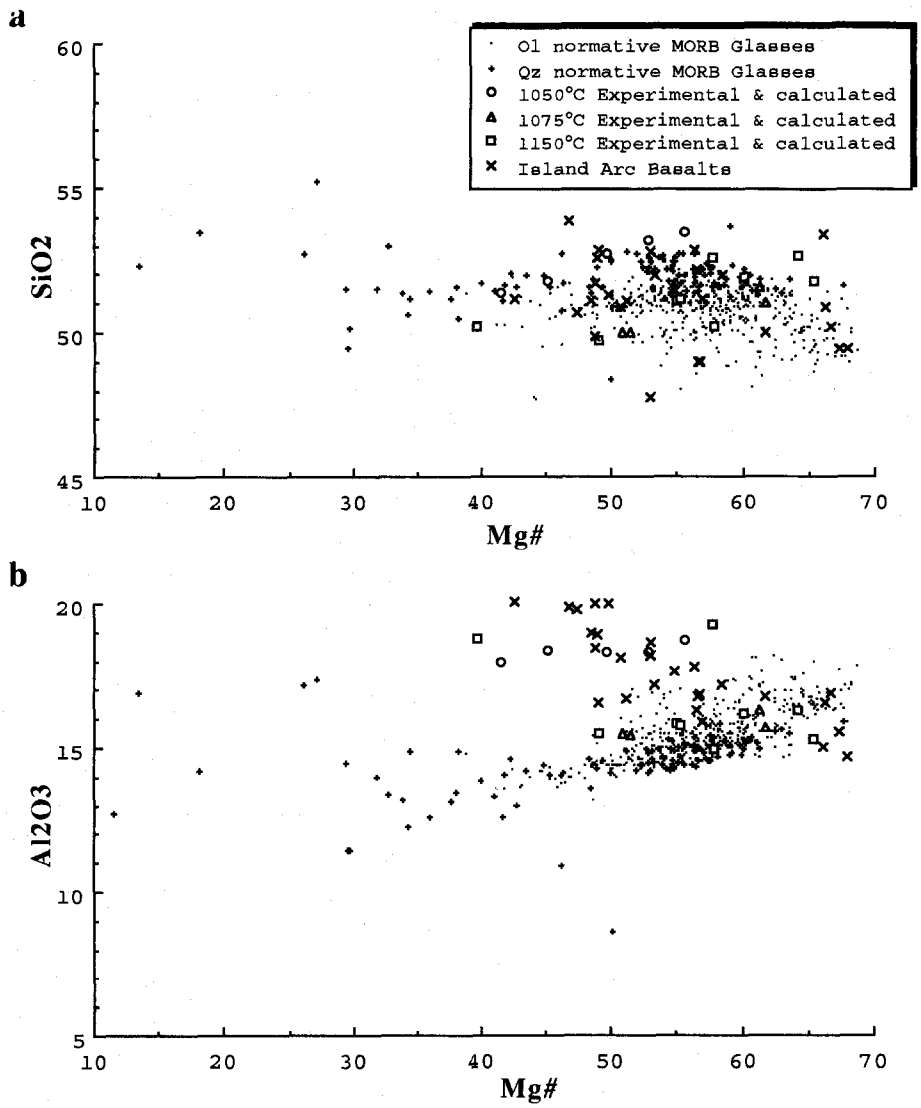

Fig.40. Chemical variations of MORB glasses, island arc basalts and experimental and calculated melt compositions by Kelemen et al.(1990). Data sources : MORB glasses are the same as in **Fig.31**, island arc basalts are from Basaltic Volcanism Study Project (1981).

made by MORB glasses rather than that of island arc basalts. Moreover, in spite of Al_2O_3 contents of results of 1050℃ is obviously high, the trend parallels with that of MORB glasses (**Fig. 40 b**). It is also clear that their experimental results agree with tholeiitic trend of MORB glasses on Miyashiro diagram (**Fig. 41**). As also pointed out on Kelemen et al. (1990), the Al_2O_3 contents in melt produced from experiments of the reaction are strongly controlled by H_2O contents in starting melt. Namely, high H_2O contents in melt

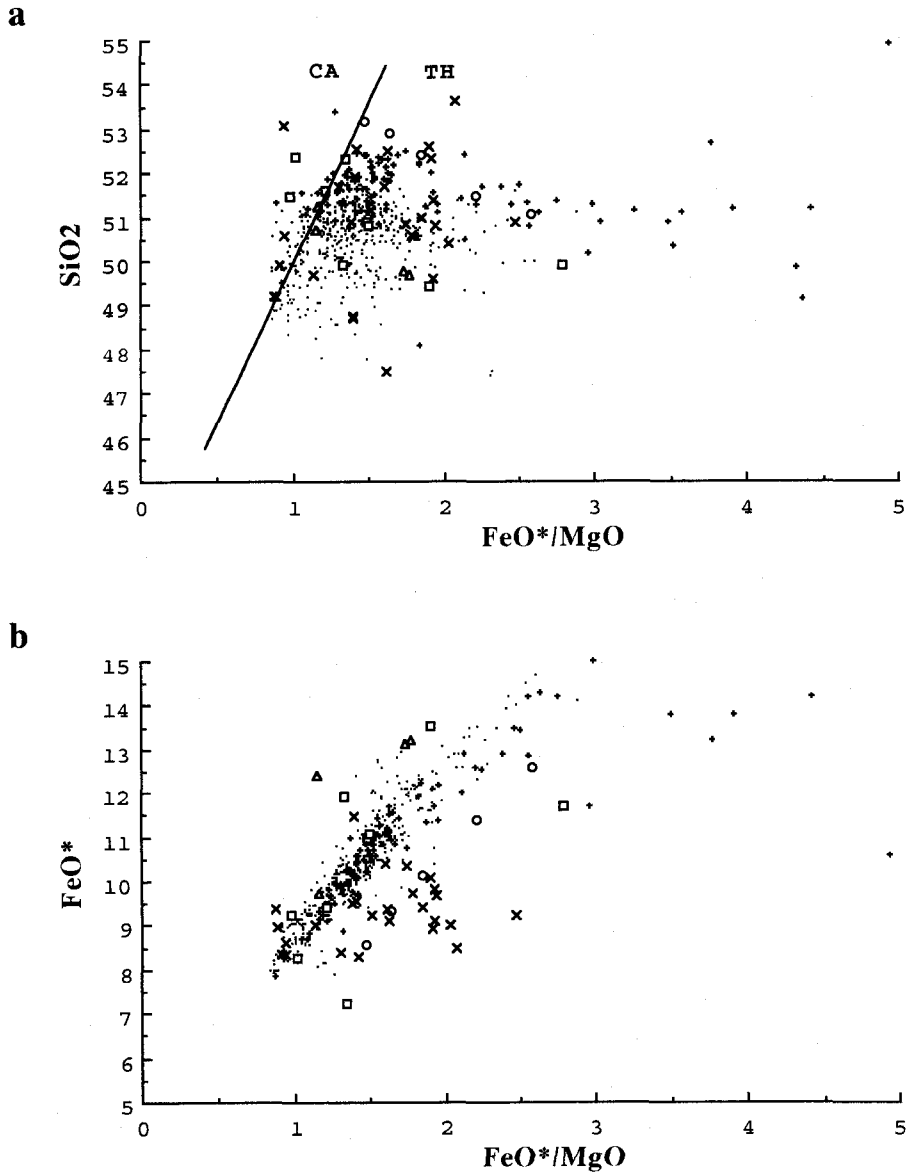

Fig.41. SiO_2 and FeO* plotted against FeO*/MgO ("Miyashiro diagram") for MORB glasses, island arc basalts and experimantal data from Kelemen et al.(1990). Data sources are the same as in **Fig.40**.

before the reaction lead high Al_2O_3 contents of melt after the reaction (**Fig. 42**). The Al_2O_3 contents of the produced melt also controlled by the reaction temperature besides the H_2O contents. In other word, low reaction temperature makes melts having high Al_2O_3. Though the composition of produced melt depends on the composition of starting melt, the composition must be also controlled by the conditions that are H_2O contents of starting melts and the reaction temperature. At the conditions of low H_2O contents of starting melts

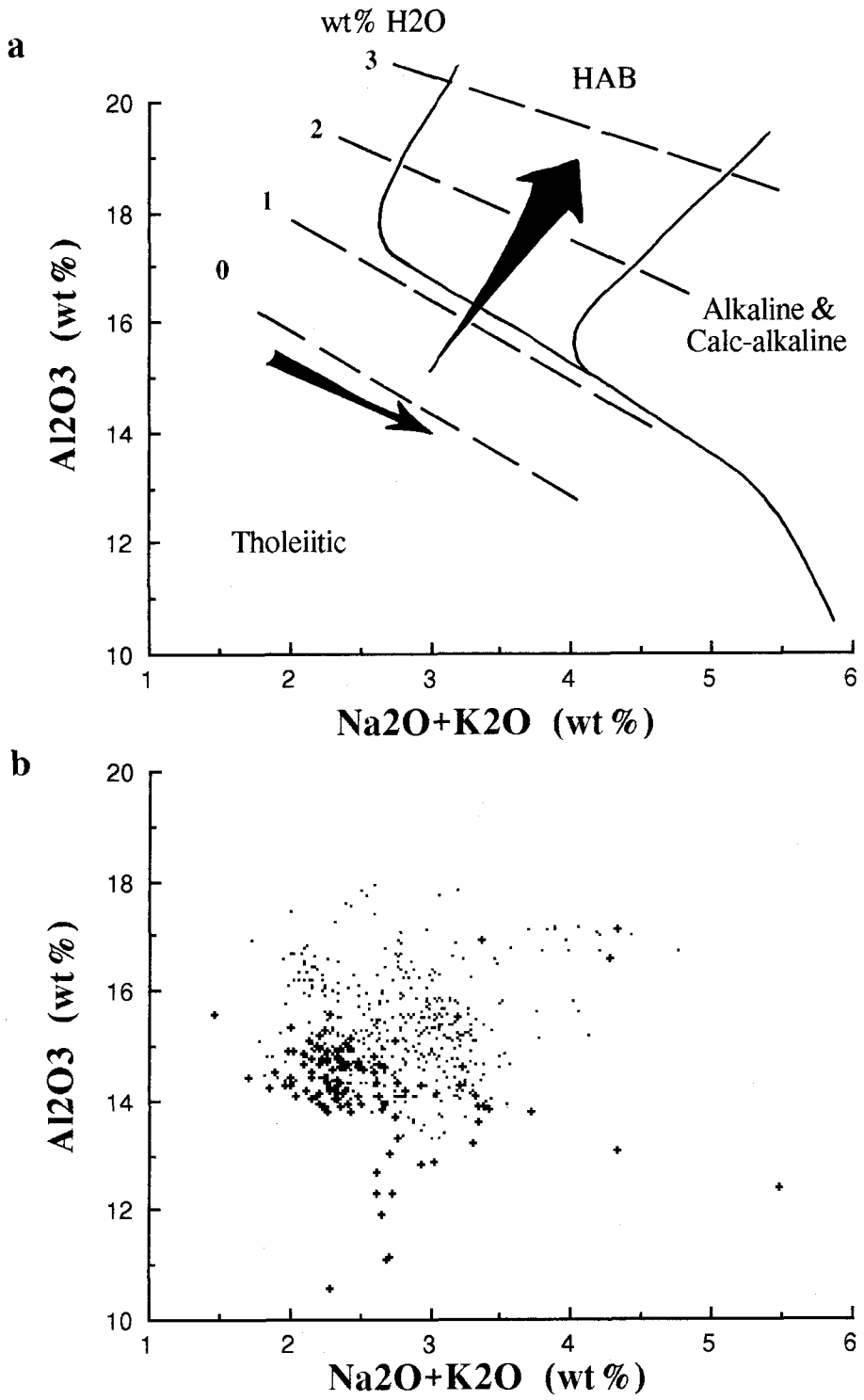

Fig.42. Discriminant diagram of Kuno (1960). **a**: The diagram used is for liquids with 50–52.5 wt% SiO_2. The dashed lines indicate isopleths of derivative liquid composition, as a function of H_2O content in the initial melt, from 0 to 3 wt% (Kelemen et al., 1990). **b**: MORB glass compositions. Symbols are the same as in **Fig.40**.

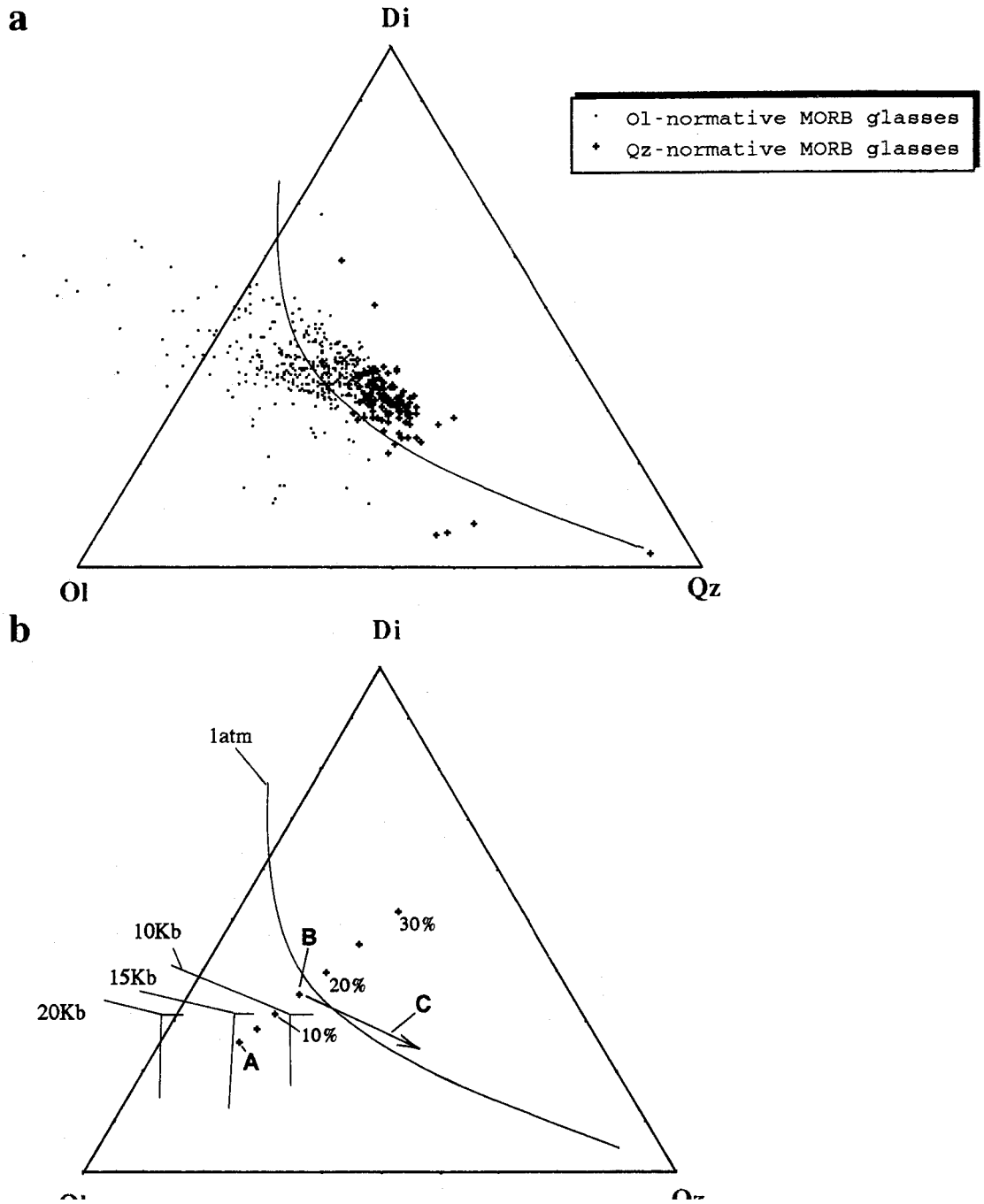

Fig.43. Diopside (**Di**) – Olivine (**Ol**) – Silica (**Qz**) diagram (Walker et al., 1979). The surface is projected from plagioclase. **a**: MORB glasses compositions. **b**: The multiple saturation points at 10, 15, 20 kbar are from Stolper (1980). Hypothetical primary melt composition (**A**) is picritic from Green et al.(1979) excepting FeO* and MgO. Namely, $SiO_2 = 48.3$, $TiO_2 = 0.6$, $Al_2O_3 = 13.7$, FeO* = 9.4, MnO = 0.12, MgO = 15.0, CaO = 10.9, $Na_2O = 1.65$ and $K_2O = 0.01$. Used FeO* and MgO is result from the Red Hills. Plus marks indicate melt compositions fractionated olivine. Numbers, 10%, 20% and 30% mean degrees of the fractionation.

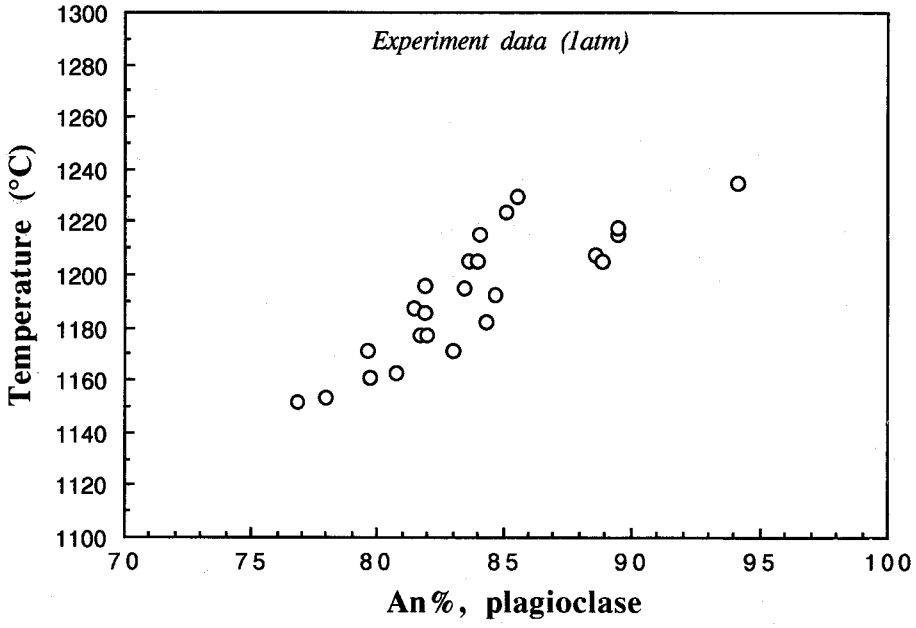

Fig.44. Experimental results of partial melting for mid-ocean ridge basaltic system at 1 atom. Data sources are Bender et al.(1978) and Tormey et al.(1987). Good correlation between temperature and An% in plagioclase is recognized. It is also recognized that plagioclases having An contents of about 95 are formed at about 1250℃. Therefore, the reaction must be occurred at that temperature.

and the higer reaction temperature, it is introduced that the products of the reaction are not compositions of island arc basalts, but rather composition of a fractionated MORB.

The reaction between a melt and harzburgite can be graphically interpreted by using olivine (Ol)−diopside (Di)−silica (Qz) diagram (**Fig. 43**). On the Red Hills peridotite, because it is estimated that initial melt is picritic composition having 12.5～15.0wt% MgO (see **Section 6−2**), the depth of melting event can be inferred as about 15kbar. The composition of the initial melt is represented by **A** on **Figure 43 a**. That is close to eutectic point among olivine, orthopyroxene and clinopyroxene at 15kbar. As the composition of the melt indicated by **A** is modified by fractionation of olivine at shallower levels in mantle, the composition changes to **B** that is on olivine−clinopyroxene cotectic line at about 2～3 kbar. Composition **B** is obtained by fractionation of olivine of 15% from initial picritic melt (**A**). As discussed on **Sections 6−2** and **6−3**, it is expected that the melt (**B**) can not be equilibrated with olivine of Fo_{91} in harzburgite residue, but can only coexist with olivine of Fo_{86-88}. So, the melt (**B**) suffered crystal fractionation of olivine is unequilibrated with surrounding harzburgite at the mantle of shallower level (about 2～3kbar). Thus, the melt on cotectic line (**B**) is presumably reacted with harzburgite. It is estimated that the reaction is incongruent melting indicated by; opx→ol+melt. The composition of the melt (**B**), therefore, must be modified to direction of cluster of quartz normative MORB glasses

shown as arrow **C** in the figure. Namely, the quartz normative MORB glasses are possible products of the reaction.

Spinels in dunite of the transition zone in the Red Hills peridotite generally shows higher TiO_2 content than those in harzburgite, and the Mg# are characterized by lower values (**Figs. 17** and **19**). Furthermore, rocks in the transition zone are plotted on low Fo side than the OSMA (**Fig. 28**). These suggest that the compositions of the melt reacting with harzburgite wall are richer in titanium and iron than the melt (picritic melt) equilibrated with harzburgites. The melt having high titanium and iron must be represented by composition **B** on Ol−Di−Qz diagram (**Fig. 43**), and modified to direction (**C**) of cluster of quartz normative MORB glasses.

Plagioclase crystallized from trapped melt in uppermost harzburgite in the lower zone of the Red Hills contains high An contents (An_{94-98}). This plagioclase must be crystallized from relatively high temperature (**Fig. 44**). There is no positive evidence for hydrous condition in the Red Hills peridotite. Based on the conditions of anhydrous and high temperature for the Red Hills peridotite, it is suggested that the MORB like melt can be formed from the reaction between a melt fractionated from picritic melt and harzburgite.

6−5−4. Summary

From geological, mineralogical and geochemical approaches it is pointed out that the Red Hills peridotite is composed of the mantle-crust transition zone of the upper part of the body and the residual mantle of the lower part. The Sr isotope ratios of minerals in rocks of the Red Hills peridotite are remarkably low (0.7019～0.7027). Such extremely low Sr isotope ratios are found in restricted rocks that are from recent mid-ocean ridges. Thus, it is concluded that the Red Hills peridotite must be related to magmatism at a mid-ocean ridge system.

In this section, the importances of mantle-crust transition zone in ophiolites are discussed from results of many previous works. Especially, it is pointed out that the equilibrium temperatures of peridotites sampled from mid-ocean ridges correlate with the spreading rates, and applied the correlation to the Red Hills peridotite. Namely, the Red Hills body that shows lower equilibrium temperature may be derived from relatively fast spreading ridge system. Strontium isotopic compositions of MORBs and the related rocks are considered in detail to compared with the results of the Red Hills. MORBs characterized by extremely low Sr isotope ratios are only from the Juan de Fuca and Gorda Ridges and the East Pacific Rise. These Sr isotope ratios well agree with those of the Red Hills. Therefore, it is estimated that the Red Hills peridotite may also derived from mid-ocean ridge system such as the Juan de Fuca and Gorda Ridges and the East Pacific Rise.

It has not been discussed that MORB magmas cna be formed from reaction between a melt and harzburgite. In this section, possibility of genesis of a MORB magma by the reaction are discussed, based on the assumption that the Red Hills peridotite is an example of mantle-crust transition at mid-ocean ridge system. As mentioned on **Section 6−2−6**,

the melt equilibrated with residual peridotite including olivine of Fo_{91}, is picritic composition having 12.5～15.0wt% MgO. This composition is plotted near 15kbar eutectic point on Ol–Di–Qz diagram (**Fig. 43**). The estimated initial melt fractionates olivine of about 15%, and then the frfactionated melt can finally coexists with olivine of Fo_{87}. This olivine composition (Fo_{87}) can coexists with relatively magnesian MORBs. Furthermore, the composition of the fractionated melt are plotted on cotectic line of about 2kbar on Ol–Di–Qz diagram. The melt obviously unequilibrates with residual peridotite extracted picritic melt. Thus, reaction between a fractionated melt and a residual peridotite wall may be expected. The reaction is similar to process of incongruent melting of pyroxenes to olivine and a melt. Above consideration is consistent with theoretical and experimental results of Kelemen et al. (1990), and chemical composition of the reacted melt is also consistent with that of MORBs.

7. CONCLUDING REMARKS

1. The Red Hills peridotite is divided into upper dunite-predominated zone and lower harzburgite zone based on detailed field observations. The upper dunite-predominated zone is equivalent to mantle-crust transition zone, and the lower harzburgite zone corresponds to residual uppermost mantle beneath the transition zone, judged from mineralogical and geochemical evidences.

2. Strontium isotope ratios of clinopyroxenes and plagioclases in the Red Hills peridotite are extremely low (0.7019～0.7027). These low Sr isotope ratios strongly suggest the depleted nature that the original environment of magmatism is mid-ocean ridge system, and the isotope ratios do not support other tectonic environments. Moreover, the Sr isotope ratios correspond to those of rocks from the Juan de Fuca and Gorda Ridges and the East Pacific Rise that represent fast spreading ridges.

3. Harzburgite in lower part of the Red Hills is considered as the residual mantle material. Based on Mg/Fe distribution coefficient between melt and olivine, composition of the initial melt inferred from the harzburgite residue is picritic melt having 12.5～15.0wt% MgO and 7.8～9.4wt% FeO. Possible melting process inferred from abundances of rare earth elements of clinopyroxenes in the harzburgites is 12～20% fractional melting of the LREE depleted, MORB-type source mantle. As composition of olivine in the transition zone is Fo=86～91, the primary picritic melt may fractionates 10～15% olivine.

4. Dunite predominated upper zone of the Red Hills corresponds to mantle-crust transition zone. The dunite can be regarded as the mixture of cumulus olivine crystallized from picritic melt and olivine produced by the reaction between fractionated basaltic melt and harzburgite residue. From REE patterns of clinopyroxenes in the transition zone, it is inferred that each segregated melt blob extracted from deeper mantle is not mixed with the other melt blob at this zone.

5. The Sr isotopic compositions indicate that the Red Hills peridotite represents an example of the section beneath the mid-ocean ridge from mantle-crust transition zone to the uppermost mantle. Based on the case study of the Red Hills peridotite, possible primary melt of MORBs is picritic melt generated at about 15kbar. The composition of primary picritic melt is modified by 10～15% crystal fractionation of olivine to magnesian basaltic one at shallower level of uppermost mantle. The fractionated melt equilibrates with olivine of Fo≦87. This melt is not in equilibrium with harzburgite residue with olivine of Fo=91. The non-equilibrium reaction that proceeded in the upper transition zone of the Red Hills peridotite could produce piles of dunite and left the harzburgite septa in dunite zone as a

result of insufficient digestion. It is expected that the reaction is similar to incongruent melting of pyroxene component in the harzburgite. Chemical composition of melt after the reaction may be quartz normative melt. Occurrences of quartz tholeite in mid-ocean ridge basalts will support this expected reactions.

Based on case study of the Red Hills peridotite in the Dun Mountaen ophiolite, it is clearly shown that one of possible primary melt of mid-ocean ridge basalts is picritic composition, and that the reaction between harzburgite and fractionated tholeiitic melt is important to consider the chemical diversity of mid-ocean ridge basalts.

Acknowledgements

The author expresses his appreciation to Professor Hiroji Honma and Dr. Hiroo Kagami of Institute for Study of the Earth's Interior, Okayama University, and Professor Koichi Tazaki of Department of Earth Science, Faculty of General Education, Ehime University, for many helpful suggestions during the course of this study.

This study was started at Department of Geology, Otago University, New Zealand. I am grateful to Dr. Teruo Watanabe of Department of Geology and Mineralogy, Faculty of Science, Hokkaido University, who afforded an opportunity for study in New Zealand as a student to me. The author wishes to thank staffs and students of Otago University. Professor Douglas Coombs supervised me in Otago University, and he gave me many precious suggestions. Mr. Andrew Constantine helped my field work. Dr. Antony Reay and Mr. Roy Johnston supported my chemical analysis of whole rocks. Dr. Yosuke Kawachi assisted my microprobe analysis. Mr. Donald Weston developed and printed many photos for me. Dr. Mike Johnston of Department of Science and Industrial Research in Nelson, gave me a lot of information of field condition of the Red Hills area. Thanks also to Dr. Yosuke Kawachi and Andrew, who looked after my general life in New Zealand. My friends, Sellery, Alister, Allibone, Bob, Allan, Damian, Steve, Hylam, Dave, Mike, Kate, Nick and Dhana, gave me great cheerful life in Otago.

The author wishes also to thank staffs of Institute for Study of the Earth's Interior, Okayama University. The latter half of this course was carried out at the institute, atter I came back from New Zealand. I am grateful to Professor Hiroji Honma and Dr. Hiroo Kagami for useful suggestions. I thank Mr. Hitoshi Asada and Miss Yumi Kawamoto for technical supports. I also thank Dr. Teruyuki Honda of Atomic Energy Research Laboratory, Musashi Institute of Technology for technical supports of instrumental neutron activation analysis. I acknowledge many beneficial discussions from Professor Koichi Tazaki, Professor Masayuke Komatsu of Department of Earth Science, Ehime University, Dr. Tsugio Shibata of Department of Earth Science, Okayama University, and Dr. Kazuhito Ozawa of Geological Institute, Faculty of Science, University of Tokyo.

I would like to express my appreciation to Professor Kazuaki Kawabuchi and Dr. Morimitsu Tanimoto of Science Education Laboratory, Faculy of Education, Ehime University, who gave me good circumstance to finish my Ph.D. work.

REFERENCES

Altherr, R., Henjes-Kunst, F. & Baumann, A., 1990. Asthenosphere versus lithosphere as possible sources for basaltic magmas erupted during formation of the Red Sea: constraints from Sr, Pb and Nd isotopes. *Earth Planet. Sci. Lett.* **96**, 269–86.

Anders, E. & Grevesse, N., 1989. Abundances of the elements: Meteoritic and solar. *Geochim. Cosmochim. Acta* **53**, 197–214.

Arai, S., 1987. An estimation of the least depleted spinel peridotite on the basis of olivine-spinel mantle array. *Neues Jb. Miner. Monat.* **8**, 347–54.

—— & Fujii, T., 1979. Petrology of ultramafic rocks from site 395. *Initial Reports DSDP* **45**, 587–94.

—— & Takahashi, N., 1988. Relic plagioclase-bearing harzburgite from the Mineoka belt, Boso Peninsula, central Japan. *J. Miner. Petrol. Econ. Geol.* **83**, 210–14.

——, Inoue, T. & Oyama, T., 1988. Igneous petrology of the Ochiai-Hobubo ultramafic complex, the Sangun zone, western Japan: a preliminary report. *J. Geol. Soc. Japan* **94**, 91–102.

Ayuso, R. A., Bence, A. E. & Taylor, S. R., 1976. Upper Jurassic tholeiitic basalts from DSDP Leg 11. *J. Geophys. Res.* **81**, 4305–25.

Barsdell, M. & Smith, E. M., 1989. Petrology of recrystallized ultramafic xenoliths from Merelava volcano, Vanuatu. *Contr. Miner. Petrol.* **102**, 230–241.

Basaltic Volcanism Study Project, 1981. *Basaltic Volcanism on the Terrestrial Planets* Pergamon Press, New York.

Batiza, R., 1984. Inverse relationship between Sr isotope diversity and rate of oceanic volcanism has implications for mantle heterogeneity. *Nature* **309**, 41–44.

Bell, J. M., 1909. Work in Dun Mountain subdivision. *New Zealand Geological Survey 3rd annual report (n. s.)* **6**.

Bender, J. F., Hodges, F. N. & Bence, A. E., 1978. Petrogenesis of basalts from the project FAMOUS area: experimental study from 0 to 15 kbars. *Earth Planet. Sci. Lett.* **41**, 277–302.

Benn, K., Nicolas, A. & Reuber, I., 1988. Mantle-crust transition zone and origin of wehrlitic magmas: evidence from the Oman ophiolite. *Tectonophysics* **151**, 75–85.

Bhattacharji, S. & Smith, C. H., 1964. Flowage differentiation. *Science* **145**, 150–53.

Blake, M. C., Jr. & Landis, C. A., 1973. The Dun Mountain ultramafic belt - Permian oceanic crust and upper mantle in New Zealand. *U. S. Geol. Survey Jour. Research* **1**, 529–34.

Bloomer, S. H. & Fisher, R. L., 1987. Petrology and geochemistry of igneous rocks from the Tonga trench - A non-accreting plate boundary. *J. Geology* **95**, 469–95.

—— & Hawkins, J. W., 1987. Petrology and geochemistry of boninite series volcanic rocks from the Mariana trench. *Contr. Miner. Petrol.* **97**, 361–77.

Bodinier, J. L., 1988. Geochemistry and petrogenesis of the Lanzo peridotite body, western Alps. *Tectonophysics* **149**, 67–88.

Bonatti, E. & Hamlyn, P. R., 1978. Mantle Uplifted Block in the Western Indian Ocean. *Science* **201**, 249–51.

——, Hamlyn, P. & Ottonello, G., 1981. Upper mantle beneath a young oceanic rift: Peridotites from the island of Zabargad (Red Sea). *Geology* **9**, 474–79.

Brouxel, M. & Lapierre, H., 1988. Geochemical study of an early Paleozoic island arc - back arc basin system. Part 1: Trinity Ophiolite (northern California). *Geol. Soc. Am. Bull.* **100**, 1111–19.

——, ——, Michard, A. & Albarede, F., 1988. Geochemical study of an early Peleozoic island arc - back arc basin system. Part 2: Eastern Klamath, early to middle Paleozoic island arc volcanic rocks (northern California). *Geol. Soc. Am. Bull.* **100**, 1120–30.

Bryan, W. B., 1979. Regional variation and petrogenesis of basalt glasses from the FAMOUS area, Mid-Atlantic Ridge. *J. Petrology* **20**, 293–325.

Cameron, W. E., 1989. Contrasting boninite-tholeiite associations from New Caledonia. In Crawford, A. J. (ed.) *Boninites* 314−38.

—— , McCulloch, M. T. & Walker, D. A., 1983. Boninite petrogenesis: chemical and Nd-Sr isotopic constraints. *Earth Planet. Sci. Lett.* **65**, 75−89.

Cassard, D., Nicolas, A., Rabinovitch, M., Moutte, M., Leblanc, M. & Prinzhofer, A., 1981. Structural classification of chromite pods in Southern New Caledonia. *Econ. Geol.* **76**, 805−31.

Challis, G. A., 1965. The origin of New Zealand ultramafic intrusions. *J. Petrology* **6**, 322−64.

Church, W. R. & Stevens, R. K., 1971. Early Paleozoic ophiolite complexes of the Newfoundland Appalachians as mantle-oceanic crust sequences. *J. Geophys. Res.* **76**, 1460−66.

Cohen, R. S., Evensen, N. M., Hamilton, P. J. & O'Nions, R. K., 1980. U-Pb, Sm-Nd and Rb-Sr systematics of mid-ocean ridge basalt glasses. *Nature* **283**, 149−53.

—— & O'Nions, R. K., 1982a. The Lead, Neodymium and Strontium Isotopic Structure of Ocean Ridge Basalts. *J. Petrology* **23**, 299−324.

—— & —— , 1982b. Identification of recycled continental material in the mantle from Sr, Nd and Pb isotope investigations. *Earth Planet. Sci. Lett.* **61**, 73−84.

Coombs, D. S., Landis, C. A., Norris, R. J., Sinton, J. M., Borns, D. J. & Nakamura, Y., 1973. The Dun Mountain ophiolite belt, New Zealand. in *Ophiolites in the Earth's Crust: USSR, Nauka Press, Acad. Sci.*

—— , —— , —— , —— , —— , —— & Craw, D., 1976. The Dun Mountain ophiolite belt, New Zealand, its tectonic setting, constitution, and origin, with special reference to the southern portion. *Am. J. Sci.* **276**, 561−603.

Davidson, J., 1985. Mechanisms of contaminaion in Lesser Antilles island arc magmas from radiogenic and oxygen isotope relationships. *Earth Planet. Sci. Lett.* **72**, 163−74.

Davies, G. R., 1984. Isotopic evolution of the Lizard Complex. *J. Geol. Soc. Lond.* **141**, 3−14.

Davis, T. E., Johnston, M. R., Rankin, P. C. & Stull, R. J., 1980. The Dun Mountain ophiolite belt in east Nelson, New Zealand. *Proc. International Ophiolite Symposium, Cyprus* 1979 480−96.

Dick, H. J. B., 1977. Partial melting in the Josephine peridotite 1, the effect on mineral composition and its consequence for geobarometry and geothermometry. *Am. J. Sci.* **277**, 801−32.

—— , 1989. Abyssal peridotites, very slow spreading ridges and ocean ridge magmatism. *Saunders, A. D. and Norry, M. J. (eds) Magmatism in the Ocean Basins, Geological Society Special Publication* **42**, 71−105.

—— & Sinton, J. M., 1979. Compositional layering in alpine peridotites: evidence for pressure solution creep in the mantle. *J. Geology* **87**, 403−16.

—— & Bullen, T., 1984. Chromian spinel as a petrogenetic indicator in abyssal and alpine-type peridotites and spatially associated lavas. *Contr. Miner. Petrol.* **86**, 54−76.

—— , Fisher, R. L. & Bryan, W. B., 1984. Mineralogic variability of the uppermost mantle along mid-ocean ridges. *Earth Planet. Sci. Lett.* **69**, 88−106.

Dixson, J. E., Clague, D. A. & Eissen, J-P., 1986. Gabbroic xenoliths and host ferrobasalt from the Southern Juan de Fuca Ridge. *J. Geophys. Res.* **91**, 3795−820.

Dmitriev, L. V., Sobolev, A. V., Uchanov, A. V., Malysheva, T. V. & Melson, W. G., 1984. Primary differences in oxygen fugacity and depth of melting in the mantle source region for oceanic basalts. *Earth Planet. Sci. Lett.* **70**, 303−10.

Downes, H. & Dupuy, C., 1987. Textural, isotopic and REE variations in spinel peridotite xenoliths, Massif Central, France. *Earth Planet. Sci. Lett.* **82**, 121−35.

Duncan, R. A. & Green, D. H., 1980. Role of multistage melting in the formation of oceanic crust. *Geology* **8**, 22−6.

Dupre, B. & Allegre, C. J., 1983. Pb-Sr isotope variation in Indian Ocean basalts and mixing phenomena. *Nature* **303**, 142−46.

—— , Lambret, B., Rousseau, D. & Allegre, C. J., 1981. Limitations on the scale of mantle heterogeneities under oceanic ridge. *Nature* **294**, 552−54.

Edgar, A. D., Lioyd, F. E., Forsyth, D. M. & Barnett, R. L., 1989. Origin of glass in upper mantle

xenoliths from the quatenary volcanics of Gees, West Eifel, Germany. *Contr. Miner. Petrol.* **103**, 277−86.

Edwards, R. L. & Wasserburg, G. J., 1985. The age and emplacement of obducted oceanic crust in the Urals from Sm-Nd and Rb-Sr systematics. *Earth Planet. Sci. Lett.* **72**, 389−404.

Eissen, J. P., Juteau, T., Joron, J. L., Dupre, B., Humler, E. & Al'mukhamedov, A., 1989. Petrology and Geochemistry of Basalts from the Red Sea Axial Rift at 18° North. *J. Petrology* **30**, 791−839.

Elthon, D., 1979. High magnesia liquids as the parental magma for ocean floor basalts. *Nature* **278**, 514−18.

——, 1986. Comments on "Composition and depth of origin of primary mid-ocean ridge basalts" by D. C. Presnall and J. D. Hoover. *Contr. Miner. Petrol.* **94**, 253−56.

——, Casey J. F. & Komor, S., 1982. Mineral chemistry of ultramafic cumulates from the North Arm Mountain Massif of the Bay of Islands ophiolite: evidence for high pressure crystal fractionation of oceanic basalts. *J. Geophys. Res.* **87**, 8717−34.

——, —— & ——, 1984. Cryptic mineral chemistry variations in a detailed traverse through the cumulate ultramafic rocks of the North Arm Mountain massif of the Bay of Islands ophiolite, Newfoundland. *Ophiolites and Oceanic Lithosphere* 83−100.

Embey-Isztin, A., Scharbert, H. G., Dietrich, H. & Poultidis, H., 1989. Petrology and Geochemistry of Peridotite Xenoliths in Alkali Basalts from the Transdanubian Volcanic Region, West Hungary. *J. Petrology* **30**, 79−105.

Engel, A. E. J., Engel, C. G. & Havens, R. G., 1965. Chemical characteristics of oceanic basalts and the upper mantle. *Geol. Soc. Am. Bull.* **76**, 719−34.

England, R. N. & Davies, H. L., 1973. Mineralogy of ultramafic cumulates and tectonites from eastern Papua. *Earth Planet. Sci. Lett.* **17**, 416−25.

Ernst, W. G., 1978. Petrochemical Study of Lherzolitic Rocks from the Western Alps. *J. Petrology* **19**, 341−92.

—— & Piccardo, G. B., 1979. Petrogenesis of some Ligurian peridotites-1. Mineral and bulk-rock chemistry. *Geochim. Cosmochim. Acta* **43**, 219−37.

Ewart, A. & Hawkesworth, C. J., 1987. The Pleistocene-Recent Tonga-Kermadec Arc Lavas: Interpretation of New Isotopic and Rare Earth Data in Terms of a Depleted Mantle Source Model. *J. Petrology* **28**, 495−530.

Fabries, J., Bodinier, J. L., Dupuy, C., Lorand, J. P. & Benkerrou, C., 1989. Evidence for Modal Metasomatism in the Orogenic Spinel Lherzolite Body from Caussou (Northeastern Pyrenees, France). *J. Petrology* **30**, 199−228.

Fisk, M. R., 1986. Basalt magma interaction with harzburgite and the formation of high-magnesium andesites. *Geophys. Res. Lett.* **13**, 467−70.

Francis, D., 1987. Mantle-Melt Interaction Recorded in Spinel Lherzolite Xenoliths from the Alligator Lake Volcanic Complex, Yucon, Canada. *J. Petrology* **28**, 569−97.

Frey, F. A., Bryan, W. B. & Thompson, G., 1974. Atlantic Ocean Floor: Gcochemistry and petrology of basalts from legs 2 and 3 of the Deep-Sea Drilling Project. *J. Geophys Res.* **79**, 5507−27.

Fujii, T. & Kushiro, I., 1977. Melting relations and viscosity of an abyssal tholeiite. *Carnegie Inst. Washington Yearb* **76**, 461−5.

—— & Bougault, H., 1983. Melting relations of a magnesian abyssal tholeiite and the origin of MORBs. *Earth Planet. Sci. Lett.* **62**, 283−95.

Gast, P. W., 1968. Trace element fractionation and the origin of tholeiitic and alkaline magma types. *Geochim. Cosmochim. Acta* **32**, 1057−86.

George, R. P., Jr., 1978. Structural petrology of the Olympus ultramafic complex in the Troodos ophiolite, Cyprus. *Geol. Soc. Am. Bull.* **89**, 845−65.

Gill, J. B., 1984. Sr-Pb-Nd isotopic evidence that both MORB and OIB sources contribute to oceanic island arc magmas in Fiji. *Earth Planet. Sci. Lett.* **68**, 443−58.

Girardeau, J. & Nicolas, A., 1981. The structures of two ophiolite massifs, Bay of Islands, Newfoundland: a model for the oceanic crust and upper mantle. *Tectonophysics* **77**, 1−34.

Green, D. H., Hibberson, W. O. & Jaques, A. L., 1979. Petrogenesis of mid-ocean ridge basalts. In McElhinny, M. W., ed., *The Earth: Its origin, structure and evolution:* London, Academic Press, 283−97.

Greenbaum, D., 1972. Magmatic processes at ocean ridges: evidence from the Troodos massif, Cyprus. *Nature Phys. Sci.* **238**, 18−21.

Hamelin, B. & Allegre, C. J., 1985. Large-scale regional units in the depleted upper mantle revealed by an isotope study of the South-West Indian Ridge. *Nature* **315**, 196−99.

——, Dupre, B. & Allegre, C. J., 1985. Pb-Sr-Nd isotopic data of Indian Ocean ridges: new evidence of large-scale mapping of mantle heterogeneities. *Earth Planet. Sci. Lett.* **76**, 288−98.

Hamlyn, P. R. & Bonatti, E., 1980. Petrology of mantle-derived ultramafics from the Owen fracture zone, Nothwest Indian Ocean: Implications for the nature of the oceanic upper mantle. *Earth Planet. Sci. Lett.* **48**, 65−79.

Hawkesworth, C. J., O'Nions, R. K., Pankhurst, R. J., Hamilton, P. J. & Evensen, N. M., 1977. A geochemical study of island-arc and back-arc tholeiites from the Scotia Sea. *Earth Planet. Sci. Lett.* **36**, 253−62.

——, —— & Arculus, R. J., 1979. Nd and Sr isotope geochemistry of island arc volcanics, Grenada, Lesser Antilles. *Earth Planet. Sci. Lett.* **45**, 237−48.

Hegner, E. & Tatsumoto, M., 1989. Pb, Sr, and Nd Isotopes in Seamount Basalts from the Juan de Fuca Ridge and Kodiak-Bowie Seamount Chain, Northeast Pacific. *J. Geophys. Res.* **94**, 17839−46.

Hekinian, R., Thompson, G. & Bideau, D., 1989. Axial and off-axial heterogeneity of basaltic rocks from the East Pacific Rise at 12°35'N-12°51'N and 11°26'N-11°30'N. *J. Geophys. Res.* **94**, 17437−63.

Ishii, T., 1985. Dredged samples from the Ogasawara fore-arc seamount or "Ogasawara Paleoland"-"fore-arc ophiolite". In *Nasu et al. (eds) Formation of Active Ocean Margins* 307−42.

Ishiwatari, A., 1985. Alpine ophiolites: product of low-degree mantle melting in a Mesozoic transcurrent rift zone. *Earth Planet. Sci. Lett.* **76**, 93−108.

Ito, E., White, W. M. & Gopel, C., 1987. The O, Sr, Nd and Pb isotope geochemistry of MORB. *Chem. Geol.* **62**,

IUGS Subcommission on the Systematics of Igneous Rocks, 1973. Classification and nomenclature of Plutonic rocks: Recommendations. *Neues Jahrb. Miner. Monatsh.* **4**, 149−64.

Jackson, E. D., 1971. The origin of ultramafic rocks by cumulus processes. *Fortschr. Miner.* **48**, 128−74.

——, Green, H. W. & Moores, E. M., 1975. The Vourinos ophiolite, Greece: cyclic units of lineated cumulates overlying harzburgite tectonite. *Geol. Soc. Am. Bull.* **86**, 390−98.

Jacobsen, S. B. & Wasserburg, G. J., 1979. Nd and Sr isotope study of the Bay of Islands ophiolite complex and the evolution of the source of Midocean Ridge Basalts. *J. Geophys. Res.* **84**, 7429−45.

Jaques, A. L. & Green, D. H., 1980. Anhydrous melting of peridotite at 0−15 Kb pressure and the Genesis of tholeiitic basalts. *Contr. Miner. Petrol.* **73**, 287−310.

Johnson, K. T., Dick, H. J. B. & Shimizu, N., 1990. Melting in the oceanic upper mantle: An ion microprobe study of diopsides in abyssal peridotites. *J. Geophys. Res.* **95**, 2661−78.

Johnston, M. R., 1981. Sheet O27 AC_Dun Mountain (1st ed.). Geological map of New Zealand, 1: 50000. Wellington. Department of Scientific and Industrial Research.

——, 1983. Sheet N28 BD_Red Hills (1st ed.). Geological map of New Zealand, 1: 50000. Wellington. Department of Scientific and Industrial Research.

Kagami, H., Okano, O., Sudo, H. & Honma, H., 1982. Isotopic analysis of Rb and Sr using a full-automatic thermal ionization mass spectrometer. *Papers of the Inst. of Thermal Spring Res., Okayama Univ.* **52**, 51−70.

——, Iwata, M., Sano, S. & Honma, H., 1987. Sr and Nd Isotopic Compositions and Rb, Sr, Sm and Nd Concentrations of Standard Samples. *Technical Rept. ISEI, Okayama Univ. Ser. B.* No. **4**.

Kay, R. W., Rubenstone, J. L. & Kay, S. M., 1986. Aleutian terranes from Nd isotopes. *Nature* **322**,

605−9.

Kelemen, P. B., 1986. Assimilation of ultramafic rock in subduction-related magmatic arcs. *J. Geology* **94**, 829−43.

——, 1990. Reaction between ultramafic rocks and fractionating basaltic magma 1. Phase relations, the origin of calk-alkaline magma series, and the formation of discordant dunite. *J. Petrology* **31**, 51−98.

——, Joyce, D. B., Webster, J. D. & Holloway, J. R., 1990. Reaction between ultramafic rock and fractionating magma 2. Experimental investigation of reaction between olivine tholeiite and harzburgite at 1150−1050℃ and 5kb. *J. Petrology* **31**, 99−134.

Kimbrough, D. L., Mattinson, J. M., Coombs, D. S., Landis, C. A., Pillai, D., Johnston, M. R. & Campbell, H.,. Uranium-lead isotopic ages from the Dun Mountain ophiolite belt and Brook Street terranes, South Island, New Zealand. submitted to *Geol. Soc. Am. Bull.*

Kornprobst, J., 1969. Le massif ultrabasique des Beni Bouchera (Rif Interne, Maroc): Etude des peridotites de haute temperature et de haute pression, et des pyroxenolites, a grenat ou sans grenat, qui leur sont associees. *Contr. Miner. Petrol.* **23**, 283−322.

Kuno, H., 1960. High-alumina basalt. *J. Petrology* **1**, 121−45.

Kurat, G., Palme, H., Spettel, B., Baddenhausen, H., Hofmeister, H., Palme, C. & Wanke, H., 1980. Geochemistry of ultramafic xenoliths from Kapfenstein, Austria Evidence for a variety of upper mantle process. *Geochim. Cosmochim. Acta* **44**, 45−60.

Kushiro, I., 1969. The system forsterite-diopside-silica with and without water at high pressure. *Am. J. Sci.* **267A**, 269−94.

——, 1973. Origin of some magmas in oceanic and circum-oceanic region. *Tectonophysics* **17**, 211−22.

Langmuir, C. H., Bender, J. F. Bence, A. E., Hanson, G. N. & Taylor, S. R., 1977. Petrogenesis of basalts from the FAMOUS area: Mid-Atlantic Ridge. *Earth Planet. Sci. Lett.* **36**, 133−56.

Lanphere, M. A., Coleman, R. G. & Hopson, C. A., 1981. Sr Isotopic Tracer Study of the Samail Ophiolite, Oman. *J. Geophys. Res.* **86**, 2709−20.

Lawver, L. A. & Dick, H. J. B., 1983. The American-Antarctic Ridge. *J. Geophys. Res.* **88**, 8193−202.

Leake, B. E., 1978. Nomenclature of amphiboles. *Miner. Mag.* **42**, 533−63.

LeRoex, A. P., Dick, H. J. B., Erlank, A. J., Reid, A. M., Frey, F. A. & Hart, S. R., 1983. Geochemistry, Mineralogy and Petrogenesis of Lavas erupted along the Southwest Indian Ridge between the Bouvet Triple Junction and 11 Degree East. *J. Petrology* **24**, 267−318.

——, ——, Gulen, L., Reid, A. M. & Erlank, A. J., 1987. Local and regional heterogeneity in MORB from the Mid-Atlantic Ridge between 54.5°S and 51°S: Evidence for geochemical enrichment. *Geochim. Cosmochim. Acta* **51**, 541−55.

Loney, R. A. & Himmelberg, G. R., 1989. The Kanuti Ophiolite, Alaska. *J. Geophys. Res.* **94**, 15869−900.

Lorand, J. P., 1987. Cu-Fe-Ni-S mineral assemblages in upper-mantle peridotites from the Table Mountain and Blow-Me-Down Mountain ophiolite massifs (Bay of Islands area, Newfoundland): Their relationships with fluids and silicate melts. *Lithos* **20**, 59−76.

Loubet, M., Shimizu, N. & Allegre, C. J., 1975. Rare Earth Elements in Alpine Peridotites. *Contr. Miner. Petrol.* **53**, 1−12.

Macdougall, J. D. & Lugmair, G. W., 1985. Extreme isotopic homogeneity among basalts from the southern East Pacific Rise: mantle or mixing effect ? *Nature* **313**, 209−11.

—— & ——, 1986. Sr and Nd isotopes in basalts from the East Pacific Rise: significance for mantle heterogeneity. *Earth Planet. Sci. Lett.* **77**, 273−84.

Machado, N., Ludden, J. N. & Brooks, C., 1982. Fine-scale isotopic heterogeneity in the sub-Atlantic mantle. *Nature* **295**, 226−8.

Mahoney, J. J., Natland, J. H., White, W. M., Poreda, R., Bloomer, S. H., Fisher, R. L. & Baxter, A. N., 1989. Isotopic and Geochemical Provinces of the Western Indian Ocean Spreading Center. *J. Geophys. Res.* **94**, 4033−52.

Malpas, J., 1978. Magma generation in the upper mantle, field evidence from ophiolite suites, and application to the generation of oceanic lithosphere. *Phil. Trans. R. Soc. Lond. A.* **288**, 527−46.

McCulloch, M. T., Gregory, R. T., Wasserburg, G. J. & Taylor, Jr. H. P., 1980. A neodymium, strontium, and oxygen isotopic study of the Cretaceus Samail ophiolite and implications for the petrogenesis and seawater-hydrothermal alteration of oceanic crust. *Earth Planet. Sci. Lett.* **46**, 201−11.

—— & ——, 1983. Nd-Sr isotopic study of primitive lavas from the Troodos ophiolite, Cyprus: Evidence for a subduction-related setting. *Geology* **11**, 727−31.

—— & Perfit, M. R., 1981. $^{143}Nd/^{144}Nd$, $^{87}Sr/^{86}Sr$ and trace element constraints on the petrogenesis of Aleutian island arc magmas. *Earth Planet. Sci. Lett.* **56**, 167−79.

Melson, W. G., Vallier, T. L., Wright, T. L., Byerly, G. & Nelen, J., 1976. Chemical diversity of abyssal volcanic glass erupted along Pacific, Atlantic, and Indian Ocean sea-floor spreading centers. *Geophysics of the Pacific Ocean Basin and its Margin* **19**, 351−67.

Melson, W. G. & O'Hearn, T., 1979. Basaltic glass erupted along the Mid-Atlantic Ridge between 0−37° N: Relationships between composition and latitude. *Deep Drilling Results in the Atlantic Ocean: Ocean Crust* 249−61.

Menzies, M. A., 1984. Chemical and isotopic heterogeneities in orogenic and ophiolitic peridotites. *Ophiolite and Oceanic Lithosphere* 231−240.

Mercier, J-C. C. & Nicolas, A., 1985. Textures and fabrics of upper-mantle peridotites as illustrated by xenoliths from basalts. *J. Petrology* **16**, 454−87.

Michael, P. J. & Bonatti, E., 1985. Peridotite composition from the North Atlantic: regional and tectonic variations and implications for partial melting. *Earth Planet. Sci. Lett.* **73**, 91−104.

——, Chase, R. L. & Allan, J. F., 1989. Petrologic and geologic variations along the Southern Explorer Ridge, Northeast Pacific Ocean. *J. Geophys. Res.* **94**, 13895−918.

Michard, A., Montigny, R. & Schlich, R., 1986. Geochemistry of the mantle beneath the Rodriguez Triple Junction and the South-East Indian Ridge. *Earth Planet. Sci. Lett.* **78**, 104−14.

Moores, E. M., 1970. Petrology and structure of the Vourinos ophiolitic complex of Northern Greece. *Geol. Soc. Am.* Special Pap. No. 118.

Nabelec, P. I. & Langmuir, C. H., 1986. The significance of unusual zoning in olivines from FAMOUS area basalt 527−1−1. *Contr. Miner. Petrol.* **93**, 1−8.

Natland, J. H., 1989. Partial melting of a lithologically heterogeneous mantle: inferences from crystallization histories of magnesian abyssal tholeiites from the Siqueiros Fracture Zone. Saunders, A. D. and Norry, M. J. (eds) *Magmatism in the Ocean Basins, Geological Society Special Publication No.* **42**, 41−70.

Nicolas, A., Boudier, F. & Bouchez, J. -L., 1980. Interpretation of peridotite structures from ophiolitic and oceanic environments. *Am. J. Sci.* **280-A**, 192−210.

—— & Prinzhofer, A., 1983. Cumulative or residual origin for the transition zone in ophiolites: structural evidence. *J. Petrology* **24**, 188−206.

—— & Dupuy, C., 1984. Origin of ophiolitic and oceanic lherzolites. *Tectonophysics* **110**, 177−87.

Nohara, M., Yuasa, M. and Murakami, F., 1990. Discussion on a possibility for the spreading of the Sumisu-Rift. *97th Ann. Meet. Geol. Soc. Japan (Abstruct)*

Nohda, S. & Wasserburg, G. J., 1981. Nd and Sr isotopic study of volcanic rocks from Japan. *Earth Planet. Sci. Lett.* **52**, 264−76.

O'Hara, M. J., 1968. Are ocean floor basalts primary magma? *Nature* **220**, 683−86.

——, 1977. Geochemical evolution during fractional crystallization of a periodically refilled magma chamber. *Nature* **266**, 503−07.

O'Nions, R. K. & Pankhurst, R. J., 1974. Petrogenetic significance of isotope and trace element variations in volcanic rocks from the Mid-Atlantic. *J. Petrology* **15**, 603−34.

——, Hamilton, P. J. & Evensen, N. M., 1977. Variation of $^{143}Nd/^{144}Nd$ and $^{87}Sr/^{86}Sr$ ratios in oceanic basalts. *Earth Planet. Sci. Lett.* **43**, 13−22.

Ozawa, K., 1988. Ultramafic tectonite of the Miyamori ophiolitic complex in the Kitakami Mountains, North-

east Japan: hydrous upper mantle in an island arc. *Contr. Miner. Petrol.* **99**, 159−75.

Pallister, J. S. & Hopson, C. A., 1981. Samail ophiolite plutonic suite: field relations, phase variation, cryptic variation and layering, and a model of a spreading ridge magma chamber. *J. Geophys. Res.* **86**, 2593−644.

Piccardo, G. B., Messiga, B. & Vannucci, R., 1988. The Zabargad peridotite-pyroxenite association: petrological constraints on its evolution. *Tectonophysics* **150**, 135−62.

Pinsent, R. H. & Hirst, D. M., 1977. The metamorphism of the Blue River ultramafic body, Cassiar, British Columbia, Canada. *J. Petrology* **18**, 567−94.

Press, S., Witt, G., Seck, H. A., Eonov, D. & Kovalenko, V. I., 1986. Spinel peridotite xenoliths from the Tariat Depression, Mongolia. 1: Major element chemistry and mineralogy of a primitive mantle xenolith suite. *Geochim. Cosmochim. Acta* **50**, 2587−99.

Presnall, D. C., Dixson, J. R., O'Donnell, T. H. & Dixson, S. A., 1979. Generaton of Mid-Ocean Ridge tholeiites. *J. Petrology* **20**, 3−35.

Price, R. C., Kennedy, A. K., Riggs-Sneeringer, M. & Frey, F. A., 1986. Geochemistry of basalts from the Indian Ocean triple junction: implications for the generation and evolution of Indian Ocean ridge basalts. *Earth Planet. Sci. Lett.* **78**, 379−96.

Prinz, M., Keil, K., Green, A., Reid, A. M., Bonatti, E. & Honnorez, J., 1976. Ultramafic and mafic dradge samples from the equatorial Mid-Atlantic Ridge and fracture zones. *J. Geophys. Res.* **81**, 4087−103.

Prinzhofer, A., Nicolas, A., Cassard, D., Moutte, J., Leblanc, M., Paris, J. P. & Rabinovitch, M., 1980. Structures in the New Caledonia peridotites-gabbros: implications for oceanic mantle and crust. *Tectonophysics* **69**, 85−112.

—— & Allegre, C. J., 1985. Residual peridotites and the mechanisms of partial melting. *Earth Planet. Sci. Lett.* **74**, 251−65.

——, Lewin, E. & Allegre, C. J., 1989. Stochastic melting of the marble cake mantle: evidence from local study of the East Pacific Rise at 12°50′N. *Earth Planet. Sci. Lett.* **92**, 189−206.

Quick, J. E., 1981a. Petrology and petrogenesis of the Trinity peridotite, an upper mantle diapir in the eastern Klamath Mountains, northern California. *J. Geophys. Res.* **86**, 11837−63.

——, 1981b. The origin and significance of large, tabular dunite bodies in the Trinity peridotite, northern California. *Contr. Miner. Petrol.* **78**, 413−22.

Reay, A. & Sipiera, P. P., 1987. Mantle xenoliths from the New Zealand region. *Mantle Xenoliths* 347−58.

Reisberg, L. & Zindler, A., 1986. Extreme isotopic variations in the upper mantle: evidence from Ronda. *Earth Planet. Sci. Lett.* **81**, 29−45.

Ringwood, A. E., 1975. *Composition and Petrology of the Earth's Mantle.* 618p. McGraw-Hill.

Roden, M. K., Hart, S. R., Frey, F. A. & Melson, W. G., 1984. Sr, Nd and Pb isotopic and REE geochemistry of St. Paul's Rocks: the matamorphic and metasomatic development of an alkali basalt mantle source. *Contr. Miner. Petrol.* **85**, 376−90.

Rhodes, J. M. & Dungan, M. A., 1979. The evolution of ocean-floor basaltic magmas. *Deep Drilling Results in the Atlantic Ocean: Ocean Crust* 262−272.

——, ——, Blanchard, D. P. & Long, P. E., 1979. Magma mixing at Mid-Ocean Ridges: evidence from basalts drilled near 22°N on the Mid-Atlntic Ridge. *Tectonophysics* **55**, 35−61.

——, Morgan, C. & Liias, R. A., 1990. Geochemistry of Axial Seamount lavas: magmatic relationship between the Cobb Hotspot and the Juan de Fuca Ridge. *J. Geophys. Res.* **95**, 12713−33.

Sato, H. & Tohara, T., 1985. Geochemical characteristics of back-arc basin basalt. In Nasu et al. (eds) *Formation of Active Ocean Margins* 399−410.

Schilling, J-G., 1973. Iceland mantle plume, geochemical evidence along Reykjanes Ridge. *Nature* **242**, 565−71.

Shaw, D. M., 1970. Trace element fractionation during anatexis. *Geochim. Cosmochim. Acta* **34**, 237−43.

Shaw, H. F., Chen, J. H., Saleeby, J. B. & Wasserburg, G. J., 1987. Nd-Sr-Pb systematics and age of the Kings River ophiolite, California: implications for depleted mantle evolution. *Contr. Miner. Petrol.* **96**,

281−90.

Shibata, T. & Thompson, G., 1986. Peridotites from the Mid-Atlantic Ridge at 43°N and their petrogenetic relation to abyssal tholeiites. *Contr. Miner. Petrol.* **93**, 144−59.

Shirey, S. B., Bender, J. F. & Langmuir, C. H., 1987. Three-component isotopic heterogeneity near the Oceanographer transform, Mid Atlantic Ridge. *Nature* **325**, 217−23.

Sinton J. M., 1977. Equilibration history of the basal alpine-type peridotite, Red Mountain, New Zealand. *J. Petrology* **18**, 216−46.

——, 1979. Petrology of (alpine-type) peridotites from site 395, DSDP Leg 45. *Initial Reports DSDP* **45**, 595−602.

——, 1980. Petrology and evolution of the Red Mountain ophiolite complex, New Zealand. *Am. J. Sci.* **280-A**, 296−328.

Smewing, J. D., Christensen, N. I., Bartholomew, I. D. & Browning, P., 1984. The structure of the oceanic upper mantle and lower crust as deduced from the northern section of the Oman ophiolite. *Ophiolites and Oceanic Lithosphere*

Song, Y. & Frey, F. A., 1989. Geochemistry of peridotite xenoliths in basalt from Hannuoba, Eastern China: Implications for subcontinental mantle heterogeneity. *Geochim. Cosmochim. Acta* **53**, 97−113.

Stolper, E., 1980. A phase diagram for Mid-ocean ridge basalts: Preliminary results and implications for petrogenesis. *Contr. Miner. Petrol.* **74**, 13−27.

Sun, S. S., 1982. Chemical composition and origin of the earth's primitive mantle. *Geochim. Cosmochim. Acta* **46**, 179−92.

—— & Jahn, B. M., 1975. Lead and strontium isotopes in post-glacial basalts from Iceland. *Nature* **255**, 527−30.

Takahashi, E., 1980. Thermal history of lherzolite xenoliths−1. Petrology of lherzolite xenoliths from the Ichinomegata crater, Oga peninsula, northeast Japan. *Geochim. Cosmochim. Acta* **44**, 1643−58.

Thirlwall, M. F. & Bluck, B. J., 1984. Sr-Nd isotope and chemical evidence that the Ballantrae 'ophiolite', SW Scotland, is polygenetic. *Ophiolite and Oceanic Lithosphere* 215−30.

—— & Graham, A. M., 1984. Evolution of high-Ca, high-Sr C-series basalts from Grenada, Lesser Antilles: the effects of intra-crustal contamination. *J. Geol. Soc. Lond.* **141**, 427−45.

Tormey, D. R., Grove, T. L. & Bryan, W. B., 1987. Experimental petrology of normal MORB near the Kane Fracture Zone: 22°−25°N, mid-Atlantic ridge. *Contr. Miner. Petrol.* **96**, 121−39.

Verma, S. P., Schilling, J. -G. & Waggoner, D. G., 1983. Neodymium isotopic evidence for Galapagos hotspot-spreading center system evolution. *Nature* **306**, 654−7.

Viereck, L. G., Flower, M. F. J., Hertogen, J., Schmincke, H. -U. & Jenner, G. A., 1984. The genesis and significance of N-MORB sub-types. *Contr. Miner. Petrol.* **102**, 112−26.

Volpe, A. M., Macdougall, J. D. & Hawkins, J. W., 1987. Mariana Trough basalts (MTB): trace element and Sr-Nd isotopic evidence for mixing between MORB-like and Arc-like melts. *Earth Planet. Sci. Lett.* **82**, 241−54.

von Drach, V., Marsh, B. D. & Wasserburg, G. J., 1986. Nd and Sr isotopes in the Aleutians: multi-component parenthood of island-arc magmas. *Contr. Miner. Petrol.* **92**, 13−34.

Walcott, R. I., 1969. Geology of the Red Hill Complex, Nelson, New Zealand. *Royal Soc. New Zealand Trans., Earth Sci.* **7**, 57−88.

Walker, D., Shibata, T. & Delong, S. E., 1979. Abyssal tholeiites from the Oceanographer Fracture Zone. *Contr. Miner. Petrol.* **70**, 111−25.

Waterhouse, J. B., 1964. Permian stratigraphy and faunas of New Zealand. *New Zealand Geological Survey bulletin (n.S.)* **72**.

Wells, P. R. A., 1977. Pyroxene thremometry in simple and complex systems. *Contr. Miner. Petrol.* **62**, 129−39.

White, W. M. & Hofmann, A. W., 1982. Sr and Nd isotope geochemistry of oceanic basalts and mantle evolution. *Nature* **296**, 821−5.

—— & Dupre, B., 1986. Sediment Subduction and Magma Genesis in the Lesser Antilles: Isotopic and Trace Element Constraints. *J. Geophys. Res.* **91**, 5927−41.

——, Hofmann, A. W. & Puchelt, H., 1987. Isotope geochemistry of Pacific Mid-Ocean Ridge basalt. *J. Geophys. Res.* **92**, 4881−93.

Whitford, D. J., White, W. M. & Jezek, P. A., 1981. Neodymium isotopic composition of Quaternary island arc lavas from Indonesia. *Geochim. Cosmochim. Acta* **45**, 989−95.

Wilkinson, J. F. G., 1982. The Genesis of Mid-Ocean Ridge Basalt. *Earth Sic. Rev.* **18**, 1−57.

Wood, D. A., Joron, J. -L., Treuil, M., Norry, M. & Tarney, J., 1979. Elemental and Sr Isotope Variations in Basic Lavas from Iceland and the Surrounding Ocean Floor. *Contr. Miner. Petrol.* **70**, 319−39.

——, Tarney, J. & Weaver, B. L., 1981. Trace element variations in Atlantic Ocean basalts and Proterozoic dykes from northwest Scotland: Their bearing upon the nature and geochemical evolution of the upper mantle. *Tectonophys.* **75**, 91−112.

Woodhead, J. D., Harmon, R. S. & Fraser, D. G., 1987. O, S, Sr, and Pb isotope variations in volcanic rocks from the Northern Mariana Islands: implications for crustal recycling in intra-oceanic arcs. *Earth Planet. Sci, Lett.* **83**, 39−52.

Yoder, H. S., Jr., 1976. Generation of basaltic magma. *National Academy of Sciences* Washington, D. C.

Zindler, A., Hart, S. R., Frey, F. A. & Jakobsson, S. P., 1979. Nd and Sr isotope ratios and Rare Earth Element Abundances in Reykjanes Peninsula basalts: Evidence for mantle heterogeneity beneath Iceland. *Earth Planet. Sci, Lett.* **45**, 249−62.

——, Staudigel, H. & Batiza, R., 1984. Isotope and trace element geochemistry of young Pacific seamounts: implications for the scale of upper mantle heterogeneity. *Earth Planet. Sci, Lett.* **70**, 175−95.

要　　旨

オフィオライトは，海洋地殻，地殻ーマントル境界部および最上部マントルの構成，ひいては海嶺性玄武岩の発生と成分変化の機構を直接的に明らかにするための，現時点における可能な最有力対象物である．本論文では，かつての海洋地殻からその下位のマントルに至る断面をよく保存し，かつ代表していると考えられるニュージーランド南島のダンマウンテン・オフィオライト中のレッドヒルズ超苦鉄質岩体とその構成岩石について，野外調査と岩石学的・鉱物学的研究，および主化学元素・微量元素の分析とストロンチウム同位体比（$^{87}Sr/^{86}Sr$）の測定を行い，岩体を構成する各岩類の由来とその相互の成因的関係について，次に列記する成果を得た．これらの岩石は，玄武岩マグマの活動に直接的に関わっており，これに基づいて，海嶺下におけるマグマの発生とその変化の機構を論じた．

(1)　レッドヒルズ超苦鉄質岩体は，下部のハルツバージャイトを主とする部分と，上部のダナイトを主とする部分からなっている．

a）岩体下部は，均質な岩相を示すハルツバージャイトを主体とし，上位には斜長石が含まれる部分があり，また，ハルツバージャイトに漸移する小規模なダナイトが伴われる．ハルツバージャイトは，ポーフィロクラスティック組織を示し，そのカンラン石は均質に Fo (100*Mg/(Mg+Fe))=91，スピネルの組成は Cr# (Cr/(Cr+Al))=0.2～0.6 である．カンラン石のモードと，共存する斜方輝石の Al_2O_3 量の間には，よい負の相関が認められ，また輝石温度計による平衡温度は約900℃である．ハルツバージャイト中の単斜輝石は軽希土側に極めて枯渇したパターンを示す．

b）岩体下部のハルツバージャイトは，そのテクトナイトに特有の組織，構成鉱物モード比と化学組織，および全岩化学組成から，溶融相を分離した，残留マントルであると考えられる．単斜輝石の希土類元素濃度から，このハルツバージャイトは，軽希土類元素に枯渇した，MORB のソースマントルから，12～20%程度の分別溶融物を分離した後の溶け残りである．さらに，ハルツバージャイト中のカンラン石の化学組成からは，共存する溶融物が12.5～15 wt% の MgO を持つピクライト質のものであったことを予想させる．

(2)　岩体上部は，厚さ約3㎞，主としてダナイトからなる．

a）ダナイト中には，しばしば単斜輝石と斜長石が不均質に含まれる．また，ブロック状岩塊ないしはフレーク状の岩片として，ハルツバージャイトも存在し，ダナイトに貫入される関係が認められる．ダナイトは，中～粗粒の等粒状組織を，ハルツバージャイトは中～粗粒の再結晶によるプロトグラニュラー組織を呈する．両岩相を構成するカンラン石の組成は，Fo=87～91，スピネルの Cr# は，0.2～0.6である．ダナイト中のカンラン石は，その Ca 量と累帯構造の有無に基づいて，2つのタイプが認められる．輝石温度計により推定される平衡温度は約1000℃である．岩体上部の岩石中の単斜輝石と斜長石の Sr 同位体比は，0.7019～0.7027である．

b）スピネルの産状と構成鉱物の化学組織から，ダナイトを主とする岩体上部，少なくともその一部は溶融相からのカンラン石集積物，すなわちマグマからの集積岩からなることが明らか

となった.

c）上部のダナイト中のハルツバージャイトがダナイトに貫入され，また，再結晶組織を示し，かつその輝石成分が分解していることは，ハルツバージャイトとマグマとの反応を示すものである．反応の存在，このハルツバージャイトの Al_2O_3 と CaO 含量が岩体下部の溶け残りマントルを代表するハルツバージャイトより低いこと，および，ダナイト中には Ca に関して累帯構造をもつものと，累帯構造をもたないものの2種類のカンラン石があることから，このダナイトの一部は，カンラン石が分別結晶作用の過程で取り去られた後のマグマと，溶け残りマントル物質であるハルツバージャイトとの反応の結果生じたものであると考えられる．

d）すなわち，ダナイトを主とする岩体上部は，マントル－地殻漸移帯であり，集積相としてのカンラン石と，反応によって生じたカンラン石の混合体のダナイト，および溶け残りマントルであるブロック状のハルツバージャイトから構成される．

(3) 本岩体の岩石の地質学的位置づけ（テクトニックセッティング）は以下のとおりである．

1）部分溶融の程度やマントルカンラン岩の化学的違いを鋭敏に反映するスピネルの Cr# は，0.6より低く，伊豆－小笠原弧などの前弧で採取されたペリドタイトのスピネルの値（Cr#＞0.5）とは異なり，現在の中央海嶺で採取されているペリドタイト中のスピネルの値と一致する．2）鉱物の Sr 同位体比は0.7019～0.7027の低い値で特徴付けられ，海嶺性玄武岩のものに一致する．この組成域は緑海（≧0.7028）や島弧（≧0.7029）の値とはあきらかに異なり，海嶺性玄武岩でもファン・デ・フカ海嶺や東太平洋海膨のような最も非調和性元素に枯渇した Sr 同位体組成を示すものに良く似る．

(4) レッドヒルズ岩体をモデルとすると，海嶺性玄武岩の初生マグマの組成は，カンラン石とマグマの間の Mg－Fe 分配係数を0.28とすると，MgO が12.5～15 wt% のピクライト質のものである．そのマグマがマントル最上部で10～15%のカンラン石を晶出，分別すると Fo_{87} 程度のカンラン石と平衡になり，Fo_{91} のカンラン石を含むハルツバージャイトとは非平衡となる．その結果，ダナイト中のハルツバージャイトの“食い残し”で示される反応，すなわちハルツバージャイト中の輝石成分がカンラン石と溶融物の分解する反応（一種の分解溶融）が起りうる．反応後のマグマの組成は，よりシリカに富むようなもの，すなわち石英ソレアイトのような組成を示すものであろう．このことは，海嶺性玄武岩に石英ソレアイトが多産することとも調和的である．